

HIGH TEMPERATURE BEHAVIOR OF POLYPROPYLENE
AND POLYPROPYLENE / GLASS COMPOSITES

By

Katherine Mary Herber Shipley

A THESIS

Submitted to
Michigan State University
in partial fulfillment of the requirements
for the degree of

MASTER OF SCIENCE

Chemical Engineering

2011

ABSTRACT

HIGH TEMPERATURE BEHAVIOR OF POLYPROPYLENE AND POLYPROPYLENE / GLASS COMPOSITES

By

Katherine Mary Herber Shipley

Solid state die drawing of polymer matrix composite materials offers an opportunity to make products that cannot be produced by any other method. This is done by heating a composite billet to a temperature just below the melting point and drawing it through a heated converging die by pulling from the downstream side. Since this is done at high temperatures, it is imperative to understand the behavior of the polymer and the composites at high temperature. Therefore, in this work, the stress-strain behavior of neat polypropylene and polypropylene composites with glass flake and glass bead fillers was studied at 23°C, 130°C, and 145°C. The onset of debonding was found to occur at a lower stress and strain for the composites tested at higher temperature, while the loss of reinforcement was slower at the elevated temperatures. The interfacial interaction between the filler and matrix was also determined to be greater at elevated temperatures. The presence of filler particles also changed the character of the stress-strain curves at higher temperatures. Specifically, the filler induced a sharper neck region in the composites at elevated temperature. Annealing for one hour at temperatures between 130°C and 145°C produced a secondary, lower melting temperature peak in the DSC curves, which increased in prominence with increasing temperature. This increase in prominence was greater for the composites than for the neat polymer. Finally, the onset of debonding was studied using transverse strain vs. stress curves for the two composites. The debonding stress decreased with increasing temperature for both materials, and it was determined that stress amplification at the interface is greater for the flake composite than for the bead composite.

Dedicated to my husband and my parents

ACKNOWLEDGEMENTS

First, I would like to thank my advisor, Dr. Jayaraman, for his guidance and support through the last six years. Without him, this work would not have been possible. I would also like to thank my committee members, Dr. Drzal and Dr. Lee from the Department of Chemical Engineering and Materials Science, and Dr. Liu from the Department of Mechanical Engineering, for helpful discussions and ideas for my research. I would like to thank my colleagues in the lab and office: John, Amit, Tanmay, Rahul, and Susan, for helpful discussions and camaraderie.

I would like to thank Mike Rich and Brian Rook of the Composite Materials and Structures Center at Michigan State University for advice on testing methods and material preparation methods. I would also like to thank the staff at the Center for Advanced Microscopy at Michigan State University, including Ewa Danielewicz, Abby Vanderberg, and Carol Flegler, for assistance with SEM sample preparation and necessary refreshers on the use of the SEM.

Finally, I would like to thank my family for all of the love and support they've given me, without which I would not have been able to complete this degree. I'd like to thank my parents, Steve and Cathy Herber, for encouraging me to follow my dream and believe in myself, and I'd like to thank my brothers, Scott, Brian, and Mark Herber, for making me tough enough to stick with it. I'd like to thank my godmother, Donna Schnepf, for prayers and encouragement to keep my head up no matter what. And finally, I'd like to thank my husband, Mike Shipley, who has loved me, supported me, encouraged me, inspired me, and empowered me. Thank you!

TABLE OF CONTENTS

LIST OF TABLES	vii
LIST OF FIGURES	viii
1. Introduction and Background	1
1.1. Problem Statement and Objectives	1
1.2. Background	2
2. Material Specifications and Procedures.....	14
2.1. Material Specifications.....	14
2.2. Procedures	14
2.2.1. Mechanical Testing.....	14
2.2.1.1. Sample Preparation	14
2.2.1.2. Testing Procedure	15
2.2.2. Differential Scanning Calorimetry (DSC).....	16
2.2.2.1. Sample Preparation	16
2.2.2.2. Testing Procedure	16
2.2.3. Scanning Electron Microscopy (SEM).....	17
2.2.3.1. Sample Preparation	17
2.2.3.2. Testing Procedure	17
3. The Effect of Elevated Temperature on Stress-Strain Behavior.....	21
and DSC Curves.....	21
3.1. Introduction	21
3.2. Experimental	23
3.2.1. Materials	23
3.2.2. Processing.....	23
3.2.3. Mechanical Testing.....	24
3.2.4. Differential Scanning Calorimetry (DSC).....	24
3.3. Results and Discussion.....	24
3.3.1. Temperature Effects on Stress-Strain Curves.....	24
3.3.2. Effect of Annealing on DSC Curves	30
3.4 Conclusions	32
4. Debonding Stress at Elevated Temperatures	54
4.1. Introduction	54
4.2. Experimental	56
4.2.1. Materials	56
4.2.2. Processing.....	56
4.2.3. Mechanical Testing.....	56
4.2.4. Differential Scanning Calorimetry (DSC).....	57

4.3 Results and Discussion.....	57
4.3.1. Debonding Stress Measurement	57
4.3.2. Stress Balance.....	58
4.4. Conclusions	64
5. Summary.....	75
APPENDICES	77
Appendix A – Calculation of residual stress in bead filled composites	78
Appendix B – SEM micrographs for samples quenched in the linear elastic regime at low strain rate.....	82
Appendix C – SEM micrographs for samples quenched at higher strain at varying strain rates .	89
REFERENCES	95

LIST OF TABLES

Table 1: Yield stress and yield strain at various temperatures for neat PP, glass flake composite, and glass bead composite.....	37
Table 2: Calculated interfacial interaction parameter, B, for flake composite and bead composite.....	38
Table 3: Average percent crystallinity of samples tested in DSC.	53
Table 4: Matrix modulus and applied stress for debonding at each testing temperature.....	68
Table 5: Percent crystallinity in each composite after holding at elevated temperature for 60 minutes.....	71
Table 6: Adhesive stresses in both composites and residual stress in the bead-filled composite at the instance of debonding.	72

LIST OF FIGURES

Figure 1: Schematic representation of die drawing.	13
Figure 2: SEM image of glass flake particles prior to compounding with PP.....	18
Figure 3: Schematic of DSC sample selection. The shaded region is the volume that was used for DSC testing.	19
Figure 4: Tensile bar schematic for SEM sample preparation. The shaded plane is the plane viewed with SEM.....	20
Figure 5: Temperature dependence of stress-strain curves for neat PP.....	34
Figure 6: Temperature dependence of stress-strain curves for glass flake composite.....	35
Figure 7: Temperature dependence of stress-strain curves for glass bead composite.....	36
Figure 8: Tensile bars after testing to a strain of 0.4. Left to right: neat PP, 23°C; neat PP, 130°C; neat PP, 145°C; flake composite, 23°C; flake composite, 130°C; flake composite, 145°C; bead composite, 23°C; bead composite, 130°C; bead composite, 145°C.....	39
Figure 9: Stress-strain curves for neat PP with stress scaled by yield stress to allow for comparison of the character of the curves.	40
Figure 10: Stress-strain curves for glass flake composite with stress scaled by yield stress to allow comparison of the character of the curves.	41
Figure 11: Stress-strain curves for glass bead composite with stress scaled by the yield stress to allow comparison of the character of the curves.	42
Figure 12: Flake composite and neat PP curves for tensile tests at 23°C with calculated fully bonded and fully debonded curves.	43
Figure 13: Bead composite and neat PP curves for tensile tests at 23°C with calculated fully bonded and fully debonded curves.	44
Figure 14: Flake composite and neat PP curves for tensile tests at 130°C with calculated fully bonded and fully debonded curves.	45
Figure 15: Bead composite and neat PP curves for tensile tests at 130°C with calculated fully bonded and fully debonded curves.	46

Figure 16: Flake composite and neat PP curves for tensile tests at 145°C with calculated fully bonded and fully debonded curves.	47
Figure 17: Bead composite and neat PP curves for tensile tests at 145°C with calculated fully bonded and fully debonded curves.	48
Figure 18: DSC melting curves for neat PP after holding at various temperatures.....	49
Figure 19: DSC melting curves for glass flake composite after holding at various temperatures.	50
Figure 20: DSC melting curves for glass bead composite after holding at various temperatures.	51
Figure 21: DSC melting curve for bead composite with a heating rate of 1°C/min.....	52
Figure 22: Example transverse strain vs. stress plots for 16vol% glass flake filled composite at each temperature. Markers indicate experimental data points while the straight lines are fitted to the data.	65
Figure 23: Example transverse strain vs. stress plots for the 19vol% glass bead composite at each temperature. Markers indicate experimental data points while the straight lines are fitted to the data.	66
Figure 24: Example axial strain vs. stress curves for the glass flake filled composite and the neat matrix PP at 145°C. The composite shows a kink in the curve, while the neat polymer exhibits no kink. Markers indicate experimental data points while the straight lines are fitted to the data....	67
Figure 25: DSC melting curve for glass flake composite after holding at 130°C and 145°C for 60 minutes.....	69
Figure 26: SEM micrograph of fracture surface of glass flake composite stretched to 0.3% strain at 0.2in/min at 130°C.....	70
Figure 27: Debonding stress as a function of adhesive stress for the flake-filled and bead-filled composites.....	73
Figure 28: Relationship among residual, adhesive, and debonding stresses for the bead-filled composite.....	74
Figure 29: Schematic of model system used for residual stress calculations for spherical fillers.	81
Figure 30: SEM image of a fracture surface of a glass flake-filled polypropylene composite that was stretched to 0.3% axial strain at 150°C.....	85
Figure 31: SEM image of a fracture surface of a glass bead-filled polypropylene composite that was stretched to 0.3% axial strain at 150°C.....	86

Figure 32: SEM image of a fracture surface of a glass flake composite sample stretched to 1% axial strain at 150°C..... 87

Figure 33: SEM images of a fracture surface of a glass bead composite sample stretched to 5% strain at 150°C at (a) low magnification, and (b) higher magnification. 88

Figure 34: SEM image of bead composite sample stretched to 5% strain at 0.2in/min at 150°C.90

Figure 35: SEM image of bead composite sample stretched to 5% strain at 5in/min at 150°C... 91

Figure 36: SEM image of bead composite sample stretched to 5% strain at 20in/min at 150°C. 92

Figure 37: 500x magnification SEM image of bead composite sample stretched to 5% strain at 0.2in/min at 150°C..... 93

Figure 38: 500x magnification SEM image of bead composite sample stretched to 5% strain at 20in/min at 150°C..... 94

1. Introduction and Background

1.1. Problem Statement and Objectives

With the environmental movement to go green and the current economic conditions, consumers are demanding more from less. Engineers and scientists are faced with the challenge of designing and producing goods from less material without sacrificing safety, style, or comfort. One manufacturing technique that has many possibilities in modern homes and workplaces is solid state die drawing of polymer composites, which allows the production of new materials that cannot be manufactured in any other way.

Solid state die drawing involves heating a prepared polymer billet to a temperature below the melting point to allow it to become a soft solid, and then pulling it from the downstream side through a heated converging die as illustrated in Figure 1. There are two regions of deformation. The first is the deformation that occurs within the die, and the second is the deformation that occurs due to neck propagation of the freely drawn billet (1). Inside the die, the polymer billet maintains the draw ratio of the die, whereas once the polymer has exited the die, it freely necks down, and the finished dimensions of the drawn sample are a function of the draw rate (1).

Solid state die drawing of composite materials allows the production of materials that exhibit lower density while maintaining the same, or even improved, mechanical properties of the undrawn material. It has long been known that drawing of neat semicrystalline polymers produced oriented polymers with improved mechanical properties, such as modulus and tensile strength (2; 3). When the semicrystalline polymer contains a particulate filler, the density of the drawn composite is lower than that of the composite before drawing due to debonding; however, the mechanical properties are the same or improved. Therefore, die drawing of a semicrystalline polymer matrix composite can be used to produce a product with low density that still maintains

an acceptable modulus and tensile strength to allow the product to be useful in many engineering applications.

This is achieved by three phenomena, the first of which is void initiation. Void initiation occurs by partial debonding of the filler particles, and is followed closely by void growth, which occurs with increasing axial strain. Void initiation and growth are responsible for lowering the density of the solid state die drawn material. Along with void initiation and growth, both the crystalline and amorphous regions of the polymer are oriented during die drawing. The orientation of the polymer leads to enhanced mechanical properties of the polymer matrix. This work focuses on void initiation and growth, as well as the effect of running die drawing tests at temperatures just below the melting point.

One objective of this work is to investigate the temperature dependence of the stress-strain curves of neat polypropylene and two polypropylene composites, one containing glass flakes and one containing glass beads. This is important because die drawing takes place at elevated temperatures just below the melting point of the polymer. Additionally, the differential scanning calorimetry (DSC) melting curves will be studied after holding for one hour at temperatures ranging from 130°C to 145°C. This will be done in order to investigate the crystallinity of the samples at the same conditions they would experience immediately prior to die drawing. Finally, debonding will be studied by measuring transverse strain during a tensile test at temperatures of 130°C, 135°C, 140°C, and 145°C for the glass flake composite and the glass bead composite. This will allow for determination of the effect of temperature on debonding as well as the effect of the filler shape.

1.2. Background

Success with solid state extrusion of neat polymers began in the 1970s with the discovery that processing neat high density polyethylene with large draw rates through a converging die in a capillary rheometer at temperatures just below the melting point induced high levels of polymer orientation. The polymer orientation improved the mechanical properties including tensile modulus and tensile strength (2; 3). The samples obtained from this method exhibited higher crystallinity, higher degree of crystal perfection, higher melting points, and more orientation in the formation direction than ever reported previously for high density polyethylene (4). These results led to attempts at solid state die drawing of composites. One such example is die drawing of short glass fiber reinforced polyoxymethylene (5; 6). Examination of the drawn composite indicated excessive voiding, and at higher draw speeds the composite exhibited macroscopic fracture just after exiting the die. Even samples that were successfully drawn at low draw rates exhibited poor mechanical properties due to debonding between the fibers and the matrix. Debonding occurs because the stress applied to the composite cannot be transmitted from the continuous polyoxymethylene phase to the dispersed glass fiber phase, and therefore the interfacial stress increases until the matrix debonds from the fiber (6). Debonding of the filler from the matrix lowers the effectiveness of the filler as reinforcement of the polymer.

Two important phenomena must be understood in order to make die drawing of composites a viable manufacturing method. The first is the behavior of composites at elevated temperature and the difference between composite behavior and neat polymer behavior at these temperatures. This includes the stress-strain response, as well as evolution of crystal structure at high temperature. The second is debonding of the polymer matrix from rigid inclusions of different shape at elevated temperatures. If these effects are understood and can be effectively controlled, the potential of die drawing to manufacture new materials can be realized.

The change in tensile modulus of neat polypropylene (PP) with temperature has been studied. Unequivocally, the tensile modulus has been found to decrease with increasing temperature (7; 8; 9). This makes sense due to the softening of the material as the temperature increases. However, Drozdov and Christiansen (10; 11) report that annealing the neat polypropylene at various temperatures and cooling to room temperature before testing has been shown to increase the tensile modulus. Greater improvement is seen as the annealing temperature is increased. Similarly, tests have shown that the yield stress decreases with increasing test temperature for neat PP (7; 8; 9; 12). Drozdov and Christiansen (13) have again shown that annealing and subsequent cooling to room temperature before testing increases the yield stress of the neat PP. Additionally, Seguela et al. (14) have shown that, not only does annealing the neat polymer increase the yield stress from that of the unannealed polymer, but it also makes the yield stress more sensitive to temperature when the two are tested in the same range of temperatures. While there is no extensive work carried out on the effect of temperature on the yield strain of neat polypropylene, examination of the experimental results of Bao and Tjong (7) suggests that the yield strain increases slightly with increasing temperature. However, Drozdov and Christiansen (15) have shown that the elongation ratio for yielding, which is somewhat analogous to the yield strain, decreases with increasing annealing temperature when the samples were cooled to room temperature before testing.

Besides affecting the stress-strain behavior of the polymer, heating, or specifically annealing, the neat polymer leads to changes in the crystallinity or crystal structure of the polymer as well. Polypropylene has a 3/1 helical structure when cooled from the melt (16). The helices form monoclinic α -crystals, hexagonal β -crystals, or orthorhombic γ -crystals, of which the α -crystals are the most thermodynamically stable (17; 18). The crystals form spherulites, or three-

dimensional, radial arrangements of crystal lamellae (19). When the melt is cooled rapidly, as in the case of injection molding, the helices may also form a smectic phase, in which the chains are ordered more in the longitudinal direction than in the transverse direction (16; 20).

Many studies have been done to investigate the effect of annealing on the microstructure of polymers (13; 21; 22; 23; 24; 25; 26; 27; 16). Most commonly, the crystallinity changes are detected by the presence of a secondary, lower melting temperature peak in the DSC heating curves (13; 21; 22; 24; 16) similar to that seen for polymer crystallized isothermally at temperatures near the melting point (28; 18).

It is generally agreed that annealing at temperatures between the crystallization temperature and the melting temperature allows increased mobility of the polymer chains (26; 16). This increased mobility allows the polymer chains to reorganize and rearrange when held at high temperature (21; 28; 24; 16). During this time, the smectic phase transforms gradually into α -crystals (16). Often, this rearrangement results in an increase in overall crystallinity (13; 21; 22; 24; 27; 16). The increase in crystallinity ranges from about 2% to 10% for 24 hours of annealing. It has also been shown to result in lamellar thickening (13; 21; 22; 23; 24; 25; 16; 28) and reduction of defects (21; 23; 16). Thickening and reordering of the crystals results in a state of lower free energy, which is thermodynamically preferred (21). The higher melting point peak has been shown to be unchanged by the annealing process, which indicates that annealing does not affect the more stable α -crystals (16). Studies have also shown that longer annealing times lead to greater increase in crystallinity (24; 27), but the greatest increase happens very rapidly, in approximately the first hour of annealing (27).

Addition of filler particles to a polymer matrix is also known to affect both the stress-strain behavior and the crystallinity. For example, Faulkner and Schmidt (29) found that the addition of

glass beads to polypropylene increased the tensile modulus but decreased the yield strength. Tsui et al. (30) found similar results with glass bead filled polyphenylene oxide, and also reported room temperature stress-strain curves with different character for the unfilled and filled polymer. Specifically, the unfilled polymer displayed a neck region before fracture, while the filled polymer displayed no neck region and only a gradual decrease in stress between the yield strain and fracture. The presence of a filler has also been shown to have an effect on the crystallinity and crystalline structure of a composite when compared with those of the neat polypropylene (31; 32; 33; 34; 35; 36). Yuan et al. (31), for example, found that addition of glass beads to a polypropylene matrix had a nucleating effect but decreased the overall crystallinity of the PP. In contrast, Arroyo and colleagues (32) found that short glass fibers were nucleators in PP, but that the overall crystallinity increased with increasing volume fraction of fibers. They also found that above 30vol%, glass fibers resulted in a decrease in the PP spherulite size. Finally, they discovered that glass fibers did not induce transcrystallinity in their samples. Transcrystallinity occurs when when crystal growth along a surface is restricted to a direction perpendicular to that surface (36). Not all surfaces produce transcrystallinity in PP, and the exact conditions that result in transcrystalline growth are not completely understood (36). Huson and McGill (33) have found that glass does not produce transcrystallinity in PP, but have concluded that the topography of the surface is key to whether or not transcrystals form. Specifically, they found that situations that result in the ability of PP chains to “prealign” led to transcrystallinity. This is in keeping with the work of Shaner and Corneliussen (35), who found that contact with a glass coverslip did not induce transcrystallinity unless there were cracks in the coverslip. In this case, transcrystals formed along the crack. A review of transcrystallinity by Quan et al. (36) points out

the ongoing debate about which materials may cause transcrystallinity and what conditions are favorable for the growth of transcrystals.

Aside from introducing differences in the stress-strain behavior and crystallinity from those of the neat polymer, inclusion of particulate fillers introduces the possibility of debonding when the composite samples are stretched. Debonding in composite materials has been the subject of many studies. Studies in polymer matrix composites have focused on debonding of spherical bead fillers through experiment (37; 38; 39; 40; 41; 42; 43; 44) and theoretical modeling (45; 46; 47; 48; 49; 50). Debonding of fiber fillers (51; 52; 53; 54) has also been studied. These studies have generally been done at room temperature, not near the melting point of the polymers. Debonding around spherical beads has been widely studied because the particles themselves cannot be oriented, making the composite isotropic. Gent and Park (37) worked with glass spheres in an elastomer matrix, and found that the stress required for debonding depended on the modulus of the elastomer as well as the size of the bead. Their work with multiple inclusions found that the debonding stress also decreased when the distance between two beads was decreased (37).

Dekkers and Heikens (38) studied crazing as a function of silane treatments that varied the adhesion. They found that, for well-adhered glass beads, crazes formed near the poles of the bead in the stretch direction, while for poorly-adhered glass beads, crazes formed between the poles and the equator of the beads. They proposed that the craze formation in the case of the poorly-adhered glass beads followed debonding of the matrix from the filler, which begins at the poles. The crazes subsequently form at the edges of the debonded region. They also found that the stress required for crazing was lower when the beads were not well-adhered to the matrix (55). Therefore, if debonding occurred before the crazes formed, and the stress at which crazing is

observed is lower for poorly adhering beads, the stress required for debonding must decrease with decreased adhesion between the filler and matrix.

Vollenberg, Heikens, and Ladan (39) found that, for bead shaped fillers, debonding is initiated at the poles of the particle in the direction of stretch, where interfacial stress is concentrated. The debonded region initially encompasses about 20° at each pole at a critical stress, hereinafter called the debonding stress. Zhuk et al. (47) found that as the stretching continued, the void grew and encompassed a greater portion of the bead, up to about 116° at each pole. Vollenberg et al. (39) used an energy balance between the potential energy in the matrix near the filler surface and the adhesive energy between the two phases to predict the debonding stress. This is given in Equation 1:

$$\frac{\sigma_d^2}{2E} |\Delta V_d| = W_A |\Delta S_d| \quad (1)$$

where σ_d is the local debonding stress, E is the matrix modulus, ΔV_d is the debonded volume, W_A is the work of adhesion between the matrix and filler, and ΔS_d is the debonded surface area. Particle shape can be taken into account with the expressions for ΔV_d and ΔS_d . Beads, for example, have $\Delta S_d/\Delta V_d$ of $6/R$, where R is the radius of the bead. If only a portion of the bead is debonded, the expression is modified to $6/R \sin \theta$, where θ is half of the debonded angle (39). Based on this energy balance, and confirmed with experimental results, Vollenberg et al. also established that larger beads require less stress and strain to debond than smaller beads (39). The larger particles debond more readily than the smaller particles because debonding of large particles creates more new surface area than debonding of small particles, and thus releases more energy (39; 45). In fact, composites with small beads may reach the macroscopic yield stress before the beads have debonded (39).

The energy balance of Vollenberg et al. does not take into account residual thermal stress in the composite that results from cooling from the melt during compounding and molding (39; 40; 56). It also does not take into account the stress concentration factor, a_s , which accounts for the increase in the local stress at the interface caused by the inability to transmit the applied stress across the interface. For spheres, the stress is concentrated most at the poles of the particle in the stress direction, and for a single sphere with no interaction or overlapping stress fields with other spheres, a_s has a value of 2 (37). According to Sudar et al (56), the debonding stress for spherical fillers is more accurately described by Equation 2:

$$\sigma_d = -C_1\sigma_T + C_2\sqrt{\frac{W_A E |\Delta S_d|}{|\Delta V_d|}} \quad (2)$$

where σ_T is the thermal residual stress and C_1 and C_2 are constants that depend on the material properties and also take into account the stress amplification factor, a_s .

Vratsanos and Farris focused their work on developing a model that could be used to predict the debonding stress of a composite under uniaxial tension (45; 46; 57). The model uses a linear elastic model for the matrix and assumes that changes in modulus as a function of applied stress are a result of an effective decrease in filler concentration caused by debonding. The model is given in Equation 3 for a composite containing spherical fillers in the absence of an external pressure imposed on the system (45; 46; 57):

$$\sigma_d = E_c \sqrt{\frac{12W_A}{R_p \frac{dE_c}{d\phi}}} \quad (3)$$

where σ_d is the debonding stress, E_c is the composite modulus, W_A is the work of adhesion, R_p is the radius of the particle and $dE_c/d\phi$ is the rate of change of composite modulus with filler volume fraction. This model was shown to work well for composites with an elastomer matrix (45; 46; 57), but did not work as well for more rigid matrices (58; 48; 59).

Specifically, Wong and Ait-kadi (59) were unable to fit the Farris model to glass bead filled high density polyethylene. The stress-strain behavior predicted by Farris' model deviates from the experimentally obtained curves, especially in the nonlinear elastic region. Based on this, Meddad and Fisa focused on developing a method to identify debonding from simple experiments, and found that at room temperature, the debonding detected from stress-strain curves might be obscured by strain softening of the matrix, and therefore not detectable from tensile tests alone. Also, results from tensile dilatometry are obscured by the dilational response of the matrix itself, which, along with the fact that the volume change due to debonding is very small, makes tensile dilatometry an undependable method for detecting debonding (60).

Dubnikova, Muravin, and Oshmyan (61) found that low concentrations of fillers resulted in debonding that was independent and complete at the initial stages of drawing, while above a critical concentration, debonding was correlated. This was a result of overlapping stress fields at higher filler concentrations. Sjogren and Berglund (62) found that debonding began at a very low stress (corresponding to 0.7% strain at room temperature), after which the matrix deformed plastically. If the strain was continued, the debonded portions formed voids that were nearly cylindrical in the direction of stretch. They also found that the stress and strain at the onset of debonding decrease with increasing volume fraction of glass beads. Data from Asp, Sjogren, and Berglund (63) agree with those of Meddad and Fisa (60) that debonding was complete before yielding occurred. In contrast, Pukanszky and Voros (40) concluded that debonding began near

the yield stress. Later work by Renner et al. (41) showed that, at filler loadings below 20%, debonding occurred at low stress, while at filler loadings above 20%, debonding occurred at the yield point. Sudar et al. (56) also found that the number of particles that debond was related to the stiffness of the polymer matrix. In fact, in stiff matrices most of the particles debonded, while in softer matrices less than 30% of the particles may have debonded. The growth of voids and final size of voids were also affected by the stiffness of the matrix, where stiffer matrices gave more voids with a smaller size and softer matrices gave fewer voids of a larger size.

For aligned short fiber reinforced polymers, when a tensile stress is applied to the composite in the direction of the fibers, the interfacial shear stress is the greatest at the fiber ends, which are the first to debond. Upon increasing the tensile stress, the debonded portion will increase along the length of the fiber from both ends. The growth of the voided regions continues until the fiber breaks or, if the fiber length is less than the critical value, the growth of the voided regions continues until the entire fiber is debonded (51). An important consideration for debonding of fibers from a polymer matrix is friction between the fiber and the polymer (52; 53; 54). Therefore, when testing for debonding in fiber composites, care must be taken to separate the force required for debonding from frictional forces (53). The fiber pull out method was shown to be most useful in obtaining both debonding stress and frictional components of the fiber pull out (54). With short fibers the effect of neighboring particles on stress concentration at the fiber ends is negligible; however, for aligned platelets the stress concentration at the ends of the platelet due to neighboring particles is much more significant (64).

Debonding clearly must be taken into account when dealing with stretching of composites, which occurs during die drawing. At room temperature, debonding has been experimentally detected by different methods. One method is to measure acoustic hits, or the high frequency

sound emitted when the filler debonds from the matrix. The range of deformation over which debonding occurs can be determined, but this method has not worked well for composites with a broad particle size distribution (41). Volume strain measurements have also been used by monitoring the slope of a volume strain versus elongation curve. When the slope increases, debonding has occurred (42; 65). The downside of this method is that the debonding produces a very small volume increase, and it could potentially be obscured by dilation of the polymer matrix (60). Microscopy has also been used to detect the onset of debonding, in which the sample has been stretched in tension while being observed with a light microscope (47; 43) or SEM (66). Finally, analysis of the stress-strain curve has been used to detect debonding (39). The stress-strain curve exhibits two linear portions of differing slope, giving a kink in the linear region of the curve. This kink indicates the onset of debonding. The potential problem with this method is that, at room temperature, the debonding stress might be obscured by strain softening of the matrix (58; 60). This method was chosen to evaluate the onset of debonding at high temperatures in this study. At elevated temperatures, the material is very soft, and low strain rates do not cause enough strain softening to obscure the kink in the stress-strain curve.

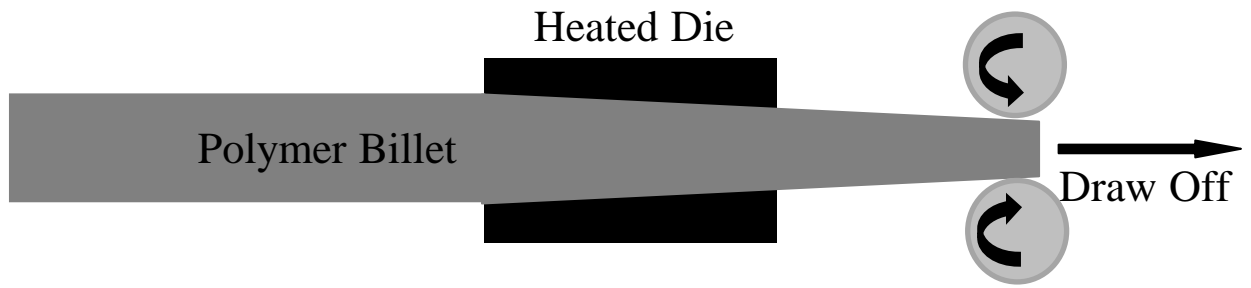


Figure 1: Schematic representation of die drawing.

2. Material Specifications and Procedures

2.1. Material Specifications

The matrix polymer used in this study is 5D37, a polypropylene homopolymer manufactured by Dow Chemical Company. 5D37 has a melting temperature of 166°C and a M_w of 249,400. It has a melt flow rate of 2.7 g/10 min and a polydispersity of 4. Two types of E-glass filler particles with different shapes were used in this study, neither of which contained any type of surface treatment to enhance adhesion with polypropylene. The spherical glass particles were solid spheres, 3000E, manufactured by Potter's Industries, Inc. They had a mean particle diameter of 35 μm . The glass flakes, REF-015, were manufactured by NGF Canada, Ltd., and had a mean particle length before compounding of 10.7 μm , a mean particle width of 6.0 μm , and a mean particle thickness of 5 μm , with a wide particle size distribution. An SEM image of the flake particles is shown in Figure 2. This figure shows the wide range of particle sizes and shapes present in the material. The aspect ratios of the glass flake particles before compounding ranged from 1 to 4, with a mode of 2. The polypropylene was compounded separately with the glass beads and glass flakes in a Farrel CP250 continuous mixer to obtain a filler volume fraction near 0.2 for each composite. Ash content tests indicated that the actual volume fraction of filler was 0.16 for the flake-filled composite and 0.19 for the bead-filled composite.

2.2. Procedures

2.2.1. Mechanical Testing

2.2.1.1. Sample Preparation

Neat polypropylene and the two composites were injection molded to form ASTM D638 Type 1 tensile bars for testing. These tensile bars have a gage area 12.5 mm wide and 3.0 mm thick. The melt temperature for each material was 204°C, and the mold temperature was 38°C.

The fill time was 1.3 seconds, with a packing time of 25 seconds. The packing pressure was 4.1 MPa. The tensile bars were used as received for tensile testing.

2.2.1.2. Testing Procedure

Mechanical tests were done in this work using a United Testing Systems model STM-20 tensile test frame. For a mechanical test at room temperature, the tensile bar was clamped between the grips of the mechanical testing frame and tested at a set crosshead speed to the desired final strain, as programmed into an appropriate template in the Datum 4.0 software from United Testing Systems. For a mechanical test at elevated temperature, the sample was placed in the lower grip of the tensile frame and held at the testing temperature for 60 minutes prior to testing. The top grip was tightened 10 minutes prior to testing. Once the full 60 minutes had elapsed, the test proceeded in the same way described for the room temperature test.

For greatest accuracy at low strains, extensometers must be used for strain measurements during tensile tests. In this study, both transverse and axial strains were measured, in different tests, using extensometers purchased from Epsilon Technology Corporation. The transverse extensometer was a high-temperature compensated extensometer, model 3575-025M-HT1, which is a strain gaged extensometer with a service temperature range from -40°C to 150°C, and a variable gage length, ranging from 0 to 25 mm. The axial extensometer was a model 3542-050M-035-ST, which is a strain gaged extensometer with a service temperature range from -40°C to 100°C and a gage length of 50 mm. This extensometer was used for measurement of modulus at temperatures up to 145°C, which is acceptable because the test duration is very short and the extensometer provided a better measurement of strain than the crosshead position. Whichever extensometer was to be used was placed on the tensile bar for the last 10 minutes of holding at the test temperature before testing took place. It is also important to note that the use

of extensometers is only applicable at low strains. At higher strains, above about 3% strain, the extensometers give very good agreement with the strain calculated from crosshead position. Additionally, the extensometers have a limited range of motion, after which their strain readings are erroneous. And finally, at strains above about 5%, the axial extensometer causes the sample to yield where it is attached while above about 10% strain, the transverse extensometer falls off of the sample, possibly damaging the extensometer. For these reasons, tensile tests that were run to the yield point and beyond were done without extensometers.

In testing soft materials, such as those tested in this study at elevated temperatures, there are often several data points at the beginning of a tensile test which are not indicative of the actual properties of the material (67). If such points exist, a toe correction must be applied to the data before any further calculations are done or any properties are obtained according to ASTM D638 (67). To make a toe correction, a straight line is drawn through the linear portion of the curve and extrapolated to the strain axis. The point of intersection with the strain axis becomes the point of zero strain, and the strain axis is adjusted accordingly. The stress axis is not affected by the toe correction.

2.2.2. Differential Scanning Calorimetry (DSC)

2.2.2.1. Sample Preparation

To prepare samples for DSC, tensile bars were scored with a razor blade along the lines shown on the front surface in Figure 3, immersed in liquid nitrogen for 10 minutes, and fractured along the score marks. Samples of approximately 10 mg were then cut from the fracture surface, represented by the shaded volume shown in Figure 3, and sealed in aluminum pans for DSC testing on a TA Instruments Q10 DSC.

2.2.2.2. Testing Procedure

To mimic the conditions of the sample at the time of the tensile test, DSC experiments were done in a TA Instruments DSC Q10 with a 60 minute isothermal step at temperatures corresponding to those of the tensile tests. The samples were heated at 10°C/min to the holding temperature, 130, 135, 140, or 145°C, held for 60 minutes at that temperature, and then heated at 1°C/min to 200°C. The entire DSC test was done with a nitrogen purge of 50 mL/min.

2.2.3. Scanning Electron Microscopy (SEM)

2.2.3.1. Sample Preparation

Samples that were to be viewed in SEM were sprayed with a compressed coolant for 15 seconds while still in the tensile frame to prevent relaxation after removal from the frame. The samples were then removed from the tensile frame and allowed to come to room temperature. The tensile bars were scored with a razor blade along the lines shown on the front surface of Figure 4 and immersed in liquid nitrogen for 10 minutes. The samples were removed from the liquid nitrogen and fractured along the score marks. The fractured samples were then mounted on SEM stubs and sputter coated with osmium to make the sample conductive and to eliminate charging during imaging. The shaded plane in Figure 4 indicates the surface that was viewed in the SEM.

2.2.3.2. Testing Procedure

The prepared samples were viewed on a JEOL JSM-6400 SEM using an accelerating voltage of 10kV. The stigmator coils were carefully adjusted prior to each session in order to remove astigmatism from the images. Care was taken to avoid images too close to the edges of the sample, which may have been altered during scoring and fracturing of the sample. For each sample viewed, multiple images were gathered, at varying magnifications, to ensure that an accurate portrayal of the sample was obtained.

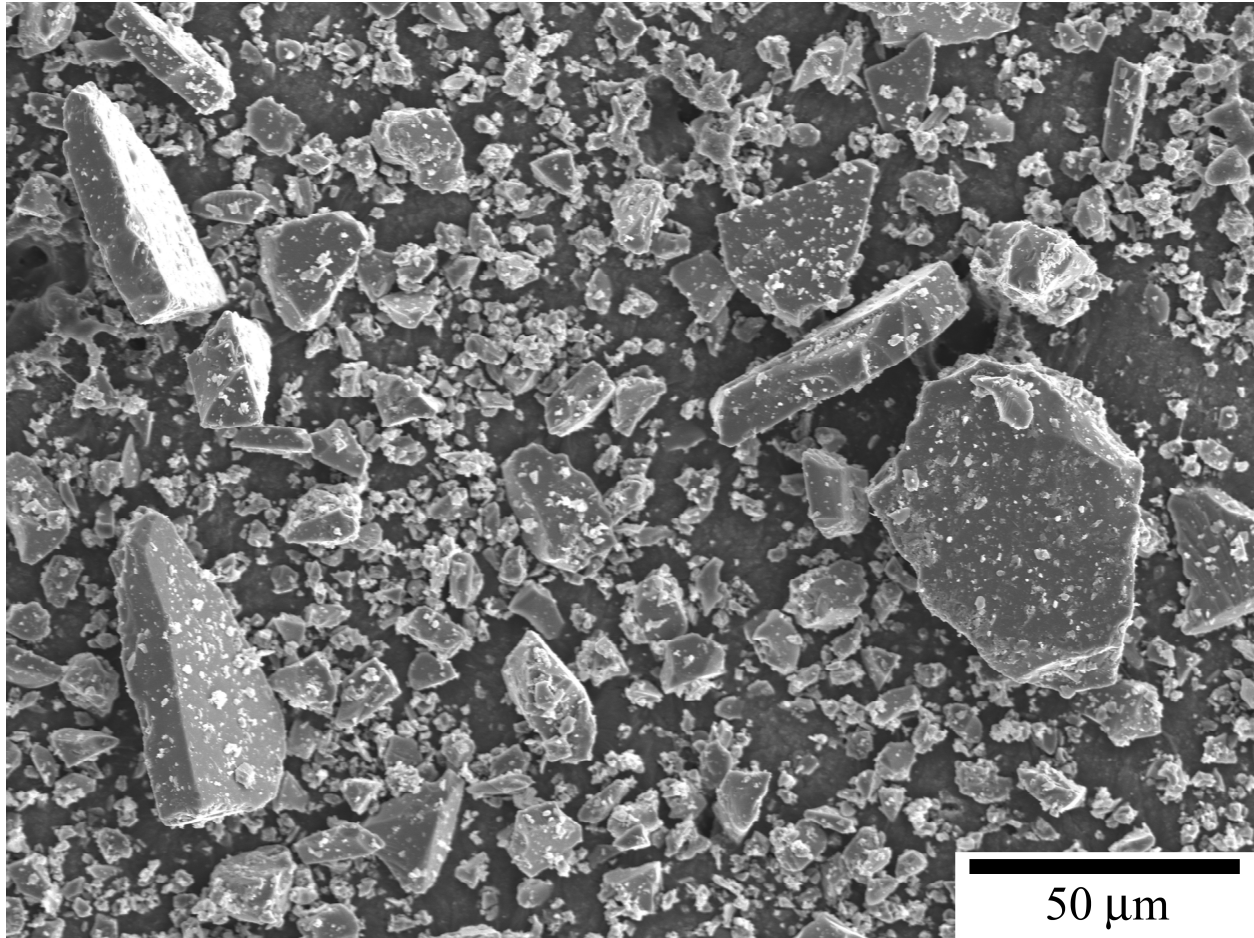


Figure 2: SEM image of glass flake particles prior to compounding with PP.

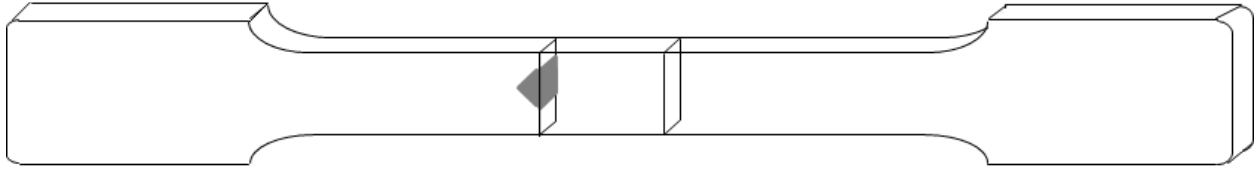


Figure 3: Schematic of DSC sample selection. The shaded region is the volume that was used for DSC testing.

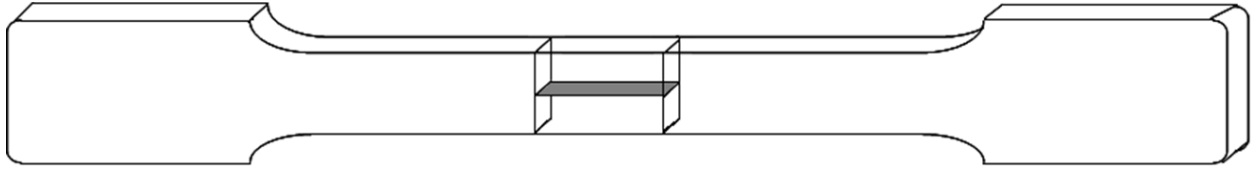


Figure 4: Tensile bar schematic for SEM sample preparation. The shaded plane is the plane viewed with SEM.

3. The Effect of Elevated Temperature on Stress-Strain Behavior and DSC Curves

3.1. Introduction

The stress-strain behavior of a polymer or polymer composite can be described by five regions on the stress strain curve. The first region is the linear elastic region, where the stress is proportional to the strain, and the slope of the line is the Young's modulus of the material (67). Following the linear elastic region is the nonlinear elastic region, where the increase in stress becomes less and less with increasing strain (67). The maximum on the stress-strain curve is the yield point, beyond which plastic deformation occurs (68). Following the yield point is the neck region, where the stress decreases with increasing strain, and a neck can be observed in the tested specimen (69). After necking is the neck propagation region, where continued strain causes very little change in the stress of the sample. In this region, fresh material is being drawn into the necked region of the sample (68).

Polymer behavior is affected by temperature. Even within the region between a polymer's glass transition temperature and melting temperature, behavior can vary widely. Particularly, mechanical properties such as tensile modulus and yield stress decrease with increasing testing temperature (7). Temperature has also been shown to play a role in determining yield strain (70) and in the overall character of the stress-strain curve (8; 9; 12). Specifically, changes in temperature bring about changes in the yield and neck propagation areas of the stress-strain curves (9; 12).

Additionally, annealing has been shown to affect the mechanical properties of polymers. In tensile tests at room temperature, the elastic modulus of isotactic polypropylene was improved by annealing, and annealing at higher temperatures led to greater modulus improvement (10; 11). In similar tests, the yield strain has been found to decrease with annealing temperature (15).

Annealing has also been found to increase the yield stress of polypropylene and affect the behavior in the post-yield region by decreasing the strain hardening rate (14). Annealing also affects the temperature sensitivity of the yield behavior of polypropylene; for annealed samples, the yield stress is more sensitive to increased temperature than for unannealed samples (14).

Annealing affects the mechanical properties of polymers because it affects the crystallinity and crystal structure of the polymers. The effect of annealing on the microstructure of polymers has been studied by many research groups; specifically, a large number of studies have been conducted on annealed polypropylene (13; 21; 22; 23; 24; 25; 26; 27; 16). Crystallinity changes are frequently identified by the presence of a lower melting temperature shoulder in the DSC heating curves (13; 21; 22; 24; 16) similar to that seen for polymer crystallized isothermally at temperatures near the melting point (28; 18).

It is generally agreed the mobility of the polymer chains increases when the samples are annealed at temperatures between the crystallization temperature and the melting temperature (26; 16). This increased mobility allows the polymer chains to reorganize and rearrange (21; 28; 24; 16), which often results in an increase in overall crystallinity (13; 21; 22; 24; 27; 16). It has also been shown to lead to lamellar thickening (13; 21; 22; 23; 24; 25; 16; 28) and reduction of crystal defects (21; 23; 16). However, it is important to note that the secondary, lower melting temperature peak represents crystals that are smaller, thinner, and less stable than those represented by the main, higher melting temperature peak. The higher melting point peak has been shown to be unchanged by the annealing process, which indicates that annealing does not affect the more stable α -crystals (16). Studies have also shown that longer annealing times lead to more increase in crystallinity (24; 27), but the greatest increase happens very rapidly, in approximately the first hour of annealing (27).

It is also well established and expected that the presence of a filler will affect the stress-strain behavior of a polymer. Addition of a filler particle, such as talc (71) or glass beads (30) has been shown to increase the tensile modulus and decrease the effective yield stress and yield strain of the composite, as compared to the neat polymer. Filler particles have also been shown to change the character of the stress-strain curve in room temperature tensile tests (30).

Because die drawing is done at elevated temperatures, it is imperative to understand the behavior of the polymer composites tested at high temperatures after annealing at that same temperature, without cooling. This work was designed to mimic the processing conditions that the material faces in the die drawing process.

3.2. Experimental

3.2.1. Materials

The polymer used for this work was a polypropylene homopolymer (5D37) with a melting temperature of 166°C and a M_w of 249,400 manufactured by Dow Chemical Company. The spherical glass particles were solid E-glass spheres (3000E) manufactured by Potter's Industries, Inc. with a mean particle diameter of 35 microns. The glass flakes (REF-015) were made of E-glass by NGF Canada, Ltd. with a mean particle length before compounding of 10.7 μm , a mean particle width of 6.0 μm , and a mean particle thickness of 5 μm and a wide particle size distribution. The aspect ratios of the glass flake particles before compounding ranged from 1 to 4, with a mode of 2. Neither the glass beads nor glass flakes had surface treatment to enhance adhesion with polypropylene.

3.2.2. Processing

The polypropylene was compounded separately with the glass beads and glass flakes in a Farrel CP250 continuous mixer to obtain a filler volume fraction near 0.20 for each composite.

Ash content tests indicated that the actual volume fraction of filler was 0.16 for the flake filled composite, and 0.19 for the bead filled composite. The composites, as well as neat polypropylene, were then injection molded into ASTM D638 Type I tensile bars.

3.2.3. Mechanical Testing

Tensile tests were done on a UTS STM-20 tensile test frame equipped with a heating chamber. For room temperature (23°C) tests, the tensile bar was placed between the grips of the tensile frame and tested at an initial axial strain rate of $1 \times 10^{-3} \text{ s}^{-1}$ to the desired final strain of approximately 0.4. For higher temperature (130°C and 145°C) tests, the tensile bar was placed in the lower grip of the tensile frame for 60 minutes at the testing temperature. After 60 minutes had elapsed, the top grip of the tensile frame was tightened onto the sample, and the test was continued in the same manner as the room temperature test. A toe correction was done on the data from each test, which removed the first few data points, which are typically not an indication of actual material properties, and aligned the linear elastic portion of the curve with the origin [14]. A minimum of three mechanical tests were done for each set of test conditions. Values reported here are average values unless otherwise noted as example values.

3.2.4. Differential Scanning Calorimetry (DSC)

Samples of around 10mg were cut out of the gage area of an as-received tensile bar and sealed in aluminum pans for DSC testing on a TA Instruments Q10 DSC. The samples were heated at 10°C/min to a temperature of 130-145°C, held for 60 minutes at that temperature, and then heated at 1°C/min to 200°C. The entire DSC test was done with a nitrogen purge of 50mL/min.

3.3. Results and Discussion

3.3.1. Temperature Effects on Stress-Strain Curves

The temperature dependence of mechanical properties for the neat polymer and the glass flake and glass bead composites was investigated with tensile tests at 23°C, 130°C, and 145°C. Figure 5 shows the results for the neat polymer. Increasing the temperature decreases the tensile modulus and the yield stress, as expected. It also has the effect of broadening the yield region of the stress-strain curve to a small degree, which is responsible for a slight increase in the yield strain of the PP at higher temperatures. The overall appearance of the curves, however, remains similar at the higher temperatures.

The results of the tensile tests at the different temperatures on the glass flake composite and the glass bead composite are shown in Figure 6 and Figure 7, respectively. As with the neat PP, increasing the temperature from 23°C to 130°C and 145°C resulted in a decrease in tensile modulus and yield stress. It is also clearer for the composite curves than for the neat PP curves that increasing the temperature induces an increase in the yield strain. The yield behavior for the composites, as well as the neat PP, is summarized in Table 1 for the three temperatures tested.

Turcsanyi, Pukanszky, and Tudos (72) related the relative yield stress of the composite, σ_{yc}/σ_{ym} , where σ_{yc} is the composite yield stress and σ_{ym} is the matrix yield stress, to a constant B_{int} , which is related to the interfacial interaction between the filler and matrix. This is given by Equation 4 (72):

$$\frac{\sigma_{yc}}{\sigma_{ym}} = \frac{1-\phi}{1+2.5\phi} \exp(B_{int}\phi) \quad (4)$$

where ϕ is the volume fraction of the filler particles. This equation has been shown to apply to particulate composites where the filler shape was spherical, short fiber, or platy (72). This equation has been used widely to calculate B_{int} for a given composite system in order to characterize the strength of the interfacial interaction between the matrix and filler (73; 74; 75;

76; 77). Higher values of B_{int} indicate a greater interfacial interaction between the two phases. Using the values for the yield stress of the composites and the neat PP given in Table 1, values of B_{int} were calculated for the flake composite and the bead composite and are shown in Table 2. This shows that the interfacial interaction is fairly low at 23°C for both composites but increases significantly when the temperature is increased to 130°C or 145°C.

For the two composites, the most striking difference between the low temperature stress-strain curve and the higher temperature curves is the overall appearance of the curve. At 23°C, the curve quickly reaches a maximum then slowly decreases, while at the higher temperatures, there is a sharp neck region, followed by a level neck propagation region. This difference that appears in the stress-strain curves can also be seen by observing the tested specimens, as shown in Figure 8. In this figure, the neat polymer samples show a necked region at all three temperatures tested, while the composite samples exhibit no necked region for the samples tested at 23°C and a necked region for the samples tested at 130°C and 145°C. Figure 8 also shows that for neat PP, stress whitening is observed only at 23°C and not at 130°C or 145°C, while the two composites exhibit stress whitening at all three temperatures tested. The stress whitening is observed throughout the gauge area of the specimens tested at room temperature, while the composite samples tested at elevated temperatures exhibit stress whitening only in the necked region of the specimen. Stress whitening occurs due to crazing and voiding when a specimen is subjected to stress (78; 79; 80).

In order to better compare the changes in the character of the stress-strain curves at different temperatures, the stress was divided by the yield stress. This allowed all of the curves to be easily compared on the same stress scale without masking the character of the high temperature

curves. This is shown in Figure 9-Figure 11, for the neat PP, the glass flake composite, and the glass bead composite, respectively.

Comparison of these scaled curves amplifies the differences between the neat PP and the two composites. For the neat PP in Figure 9, the curves are very similar at all three temperatures tested, while for the glass flake composite in Figure 10 and the glass bead composite in Figure 11, the appearance of the sharp neck region is more prominent at 130°C and 145°C in contrast to the gentle slope of the curve for the test done at 23°C.

Comparison of the onset of the neck propagation region of Figure 9 with those in Figure 10 and Figure 11 highlights another difference between the neat PP and the two composite materials. For all three materials tested, where necking and neck propagation are observed, the neck propagation begins at a stress of around 70% of the yield stress. However, for the two composite materials, the strain at the onset of neck propagation is 0.16, while the onset of neck propagation in the neat PP is nearly twice that, 0.30.

It is also instructive to compare the stress-strain curves for the composite materials to those of the neat PP. These are shown in Figure 12 and Figure 13 for the flake and bead composites at 23°C, Figure 14 and Figure 15 for the flake and bead composites at 130°C, and Figure 16 and Figure 17 for the flake and bead composites at 145°C, respectively. These figures also contain curves for the fully bonded and fully debonded composites, which were calculated as described by Meddad and Fisa (58). For the bead composite, the fully bonded curve is calculated from the neat PP curve using the Kerner-Lewis equation, given in Equation 5:

$$E_{sc} = E_{sm} \frac{1 + AB\phi}{1 - B\phi} \quad (5)$$

Where E_{sc} is the composite secant modulus, E_{sm} is the matrix secant modulus, ϕ is the volume fraction of filler, and A and B are as given in Equation 6 and 7.

$$A = \frac{7 - 5\nu_m}{8 - 10\nu_m} \quad (6)$$

$$B = \frac{\frac{E_f}{E_m} - 1}{\frac{E_f}{E_m} + A} \quad (7)$$

In Equations 6 and 7, ν_m refers to the Poisson's ratio of the matrix and E_f and E_m refer to the modulus of the filler and matrix, respectively. For the fully debonded composite, the filler particles are replaced with voids ($E_f = 0$), and Equation 5 becomes Equation 8:

$$E_{sc} = E_{sm} \frac{1 - \phi}{1 - B_1 \phi} \quad (8)$$

Where B_1 becomes equal to $-1/A$. It can be seen from Figure 13, Figure 15, and Figure 17 that the curves calculated in this manner for the fully bonded bead composite fit the corresponding measured composite curves at low strains. However, for the glass flake composite, a modification to the Kerner-Lewis equation is necessary in order to adequately fit the calculated curves to the measured curves at low strains. For the flake composite, Sudduth's (81) concept of "sphericity (s)" is used to account for non-spherical particles in the composite. Sphericity is defined in Equation 9 (81):

$$s = \frac{2\alpha + 1}{3\alpha^{2/3}} \quad (9)$$

Where α is the particle aspect ratio. A new parameter, A' , replaces A in Equations 5 and 7. For $1 < \alpha < 3.7$, A' is given by Equation 10:

$$A' = A \cdot s^{3.378} \quad (10)$$

For the fully debonded flake composite, B_1 in Equation 8 becomes equal to $-1/A'$. An average aspect ratio of 3.7 gave the best fit of the calculated fully bonded curves to the experimental flake composite curves in Figure 12, Figure 14, and Figure 16.

Examination of Figure 12 and Figure 13 indicates that the experimental composite curves coincide with the calculated fully bonded curves the longest at 23°C, indicating the slowest onset of significant debonding at this temperature when compared to 130°C and 145°C. The composite curves in these figures also cross over the curve for the neat PP at a low strain, which indicates that the loss of the reinforcing effect of the filler happens most rapidly at this temperature. Finally, the composite curves in Figure 12 and Figure 13 also cross over the calculated fully debonded curves at a low strain, approximately equal to the yield strain of the composite curve. This indicates that significant void growth occurs in the composites tested at room temperature by the time the composite has reached yield.

Examination of Figure 14 and Figure 15 shows that the composite curves deviate from the calculated fully bonded curve at a lower strain at 130°C than at 23°C, so the onset of debonding occurs sooner at 130°C. The bead composite curve, in Figure 15, crosses the neat PP curve just after yield while the flake composite experiences more strain before losing the reinforcing effect of the filler. For both composites at 130°C, the composite curve crosses over the neat PP curve at a higher strain than at 23°C or 145°C. This indicates that the loss of reinforcement caused by debonding is slowest at 130°C of all three temperatures tested.

Examination of Figure 16 and Figure 17 indicates that the composite curves deviate from the calculated fully bonded curve very soon after the test starts, which indicates a very rapid onset of debonding at 145°C. The composite curves are only very slightly above the neat PP curves at any

given strain before they cross over, which occurs at fairly low strain before the composite yield point. This shows that at high temperature, the filler does not have much reinforcing effect at all.

By comparing Figure 12-Figure 17, it is clear that the loss of reinforcement occurs most rapidly at 23°C and most slowly at 130°C for both composites. Comparison of the flake composite curves in Figure 12, Figure 14, and Figure 16, with the corresponding bead composite curves at each temperature in Figure 13, Figure 15, and Figure 17 reveals that for a given temperature, the loss of reinforcement proceeds more slowly for the flake composite than for the bead composite. This is most evident at 130°C, but is also true at 23°C and 145°C.

3.3.2. Effect of Annealing on DSC Curves

In order to match the conditions of the tensile tested samples as closely as possible, DSC tests were done with a holding step at the tensile testing temperature. In these tests, the samples were heated at 10°C/min to the holding temperature, held for 60 minutes at that temperature, and then heated at 1°C/min through the melting point. The results of these tests are shown in Figure 18 for the neat PP, Figure 19 for the glass flake composite, and Figure 20 for the glass bead composite. For Figure 19 and Figure 20, the heat flow was adjusted to account for the fact that there were both polymer and glass in the sample. Therefore, the weight fraction of polymer was used to adjust the heat flow to be in watts per gram of polymer instead of watts per gram of sample. For comparison, an example DSC melting curve for the bead composite with no holding step is shown in Figure 21. The DSC melting curves for the neat PP and the flake composite with no holding step are similar in appearance to that shown for the bead composite in Figure 21.

All three materials show that after the holding step, a lower melting point peak appears in the DSC curve. Also in all three materials, this peak becomes more pronounced with increasing the holding temperature. All of the holding temperatures in this study were within the broad melting

range of the unannealed samples, so before the holding step, some of the smaller, thinner crystals in the samples had melted. So, as the holding temperature increased from 130°C to 145°C, a greater portion of the crystals in the samples melted prior to the holding step. During the holding step, the mobility of the polymer chains was increased due to the higher temperatures. Therefore, the polymer chains were able to rearrange during the holding step and form crystals of a size and thickness that would melt just above the holding temperature. The increase in prominence of the lower melting point peak in the DSC curves with increasing temperature indicates that the polymer chains become increasingly mobile as the temperature increases, and therefore more rearrangement is possible at higher temperatures. This additional rearrangement results in more crystal formation at higher holding temperatures, which produces the more prominent peaks.

Comparing the neat PP curves with those for the two composites shows that the increase in prominence of the lower melting point peak is greater for the composites than for the neat PP. In other words, as the holding temperature increases, the peaks become more prominent for all three materials, but this increase in prominence is greater for the composite samples. There is also virtually no difference in the DSC curves for the two composite samples, indicating that the shape of the particulate filler has no effect on the rearrangement of the polymer chains during annealing. Additionally, Figure 18 through Figure 20 show that increasing the holding temperature has no effect on the location of the higher melting point curve. This is in agreement with literature showing that annealing has no effect on the already very stable crystals that are responsible for the main melting peak in the DSC curve (16).

The DSC curves can also be used to determine the level of crystallinity in the sample by using Equation 11 (82):

$$\chi_c = \frac{\Delta H_f \cdot 100}{\Delta H_f^0 \cdot w_m} \quad (11)$$

Where χ_c is the total crystallinity, ΔH_f is the heat of fusion, ΔH_f^0 is the equilibrium heat of fusion of a 100% crystalline sample, and w_m is the mass fraction of polymer in the composite (82). The heat of fusion of 100% crystalline polypropylene was taken as 207 J/g (17). The mass fraction of polypropylene in the glass flake composite was 0.64, in the glass bead composite was 0.59, and in the neat PP was 1.0. Equation 11 was used to calculate the percent crystallinity in the neat PP, glass flake composite, and glass bead composite, both for unannealed samples and samples annealed at 130°C and 145°C. The results of this calculation are shown in Table 3. The standard deviation in these calculated values is 0.7% crystallinity. This standard deviation indicates that differences between samples of the same material annealed at 130°C and 145°C are insignificant. However, differences between annealed and unannealed samples of the same material are significant. This shows that annealing resulted in a slight decrease in the crystallinity of the neat polymer, while an increase in crystallinity was seen for the two composites. A decrease in crystallinity would be expected due to the fact that prior to annealing, a portion of the crystals in the samples had already melted. However, the presence of the secondary peak in the DSC curves indicates that recrystallization takes place during annealing. These results show that the presence of the fillers allows for greater levels of recrystallization during the annealing period in the composites than in the neat PP.

3.4 Conclusions

Comparison of stress-strain curves for the composites to those for neat PP and calculated fully bonded and fully debonded curves indicated that the onset of debonding occurred at a lower stress and strain for higher temperatures than for lower temperatures, but that the loss of

reinforcement proceeded more slowly at elevated temperatures, with the slowest progress seen at 130°C. This type of comparison also showed that the loss of reinforcement proceeded more slowly for the flake composite than for the bead composite when the two composites were compared at a given temperature. Additionally, interfacial interaction between the filler and matrix in both composites, characterized by the constant B_{int} , was shown to be much greater at the higher temperatures of 130°C and 145°C than at 23°C.

Temperature affected the behavior of neat PP samples differently than glass flake and glass bead composite samples. Although increasing temperature had the expected results of decreasing the modulus and yield stress and increasing the yield strain of all three materials tested, the overall character of the curves was affected differently for the neat PP than for the composites. The general shape of the stress strain curves was the same at 23°C, 130°C, and 145°C for the neat PP, with a broad neck region followed by a neck propagation region. However, for both composite samples at 23°C, no neck region was noticed, while at 130°C and 145°C, there was a very sharp neck region followed by the neck propagation region. The strain at the onset of the neck propagation region for the neat PP was nearly twice that for the two composites.

Additionally, DSC results showed that increasing the annealing temperature from 130°C to 145°C increased the prominence of the lower melting point peak. The increased prominence of this peak was greater for the two composite samples than for the neat PP. Calculation of the percent crystallinity from the DSC curves indicated that the presence of filler particles allowed for more recrystallization during annealing for the composites than for the neat PP.

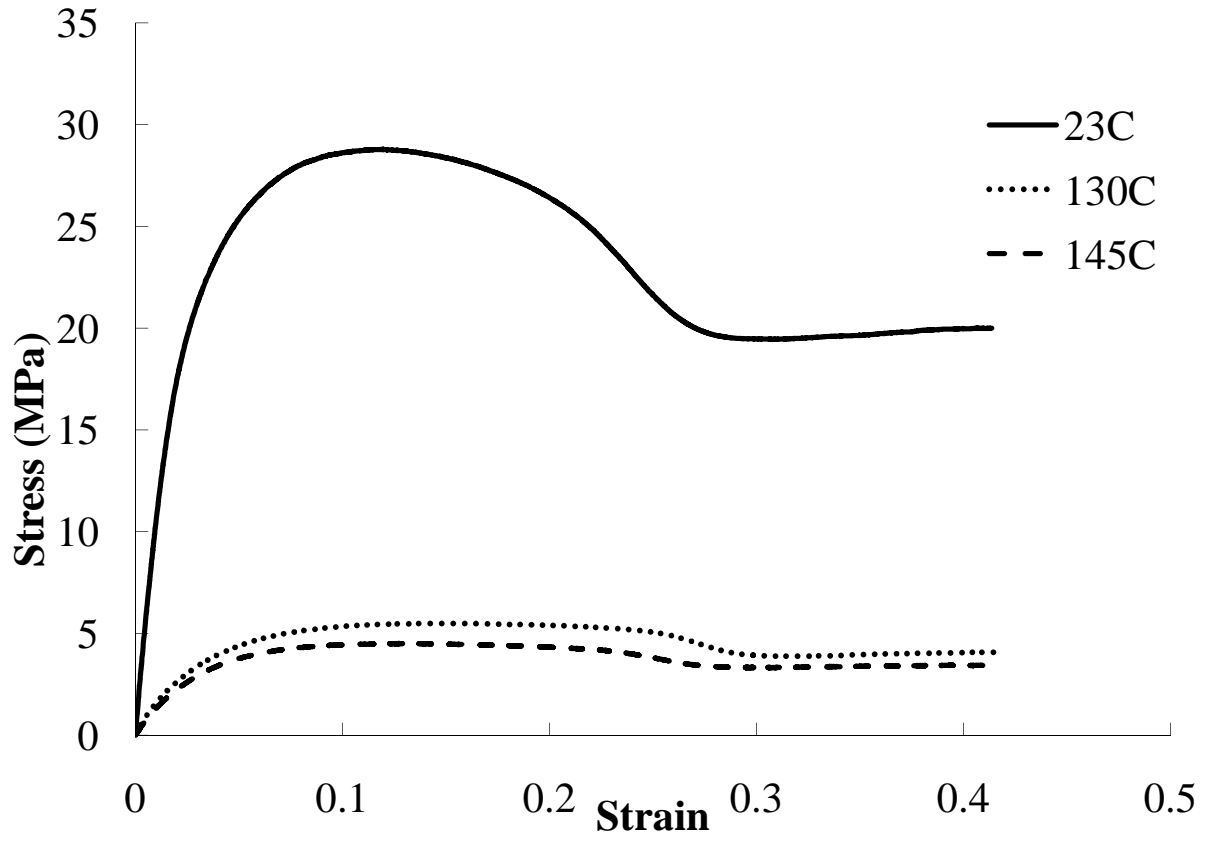


Figure 5: Temperature dependence of stress-strain curves for neat PP.

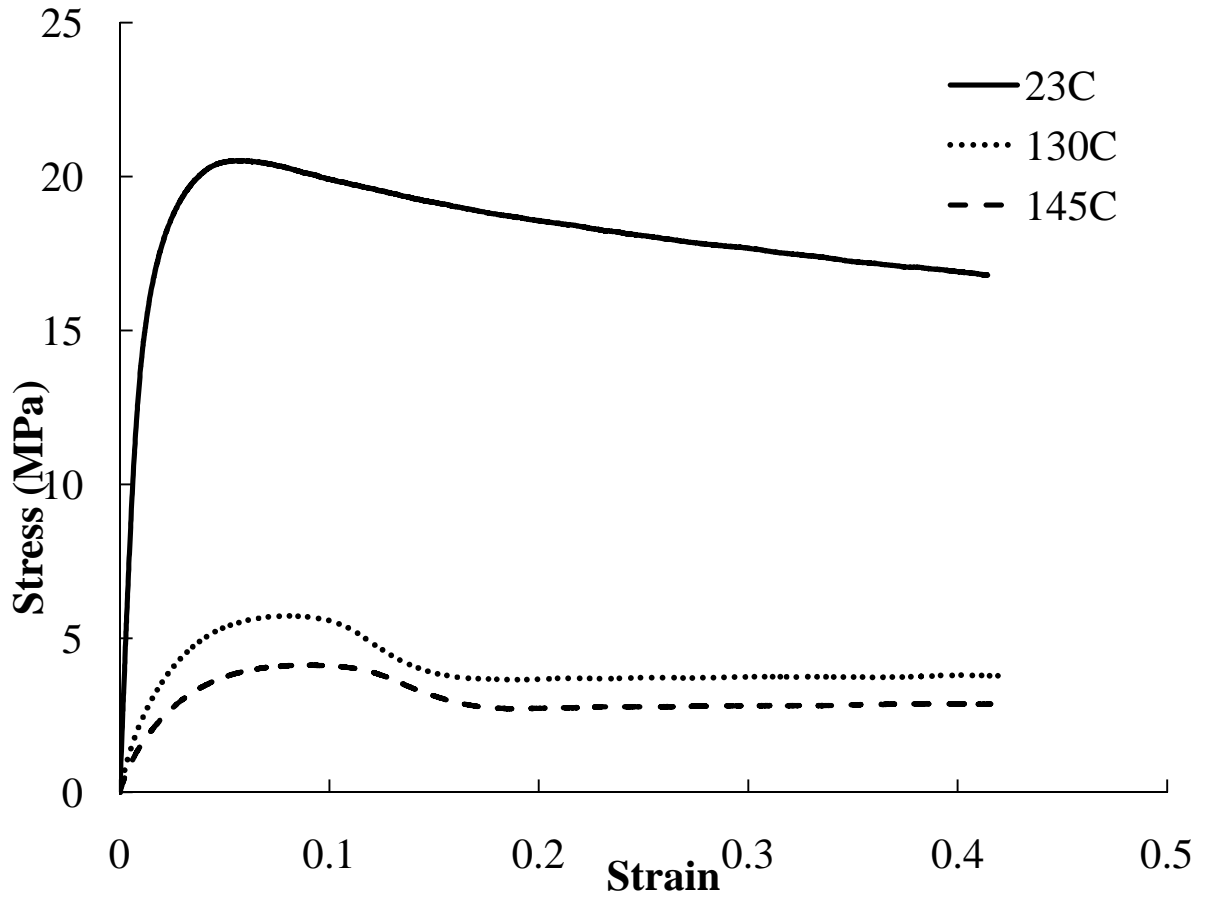


Figure 6: Temperature dependence of stress-strain curves for glass flake composite.

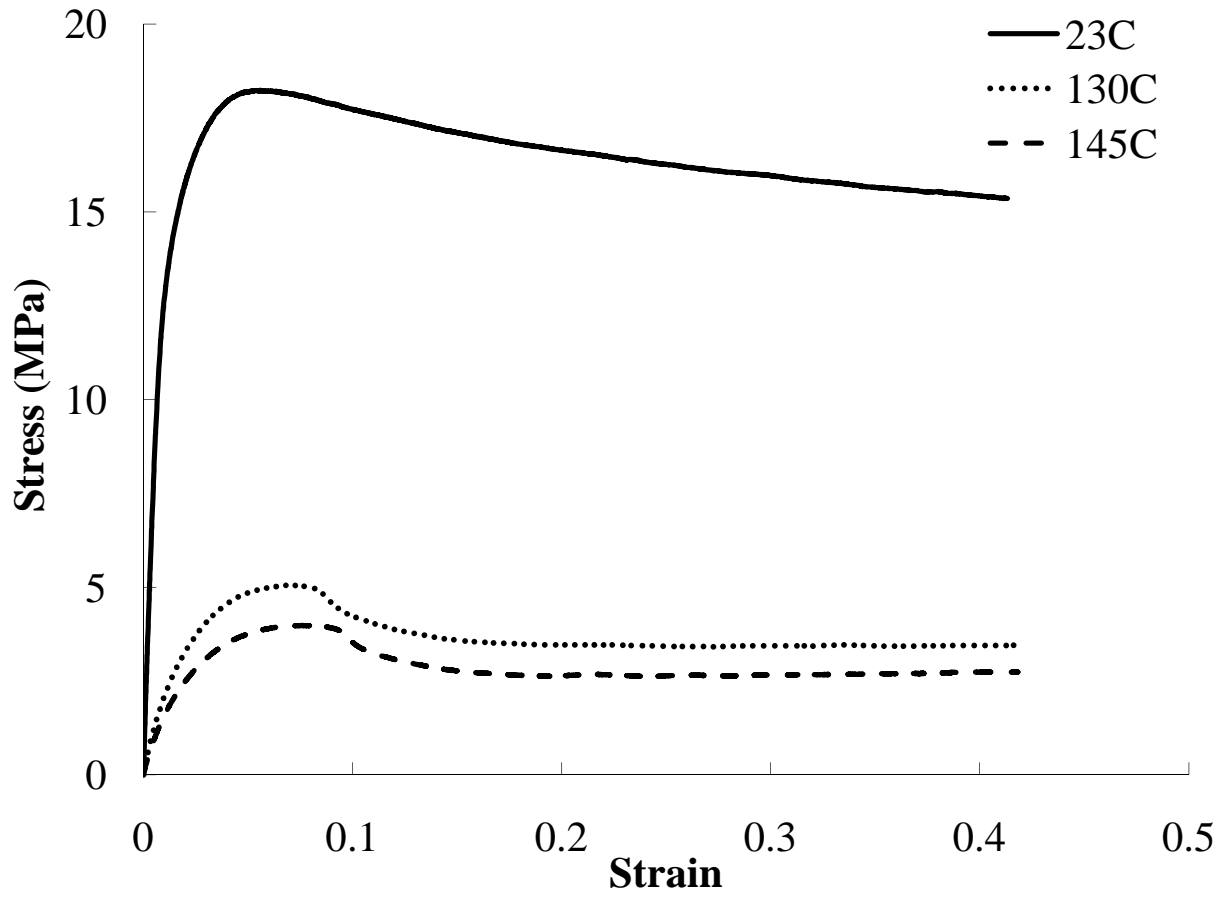


Figure 7: Temperature dependence of stress-strain curves for glass bead composite.

Table 1: Yield stress and yield strain at various temperatures for neat PP, glass flake composite, and glass bead composite.

Material	Temperature (°C)	Yield Stress (MPa)	Yield Strain (%)
Neat PP	23	29.6	11.9
	130	5.6	14.4
	145	4.3	12.6
Flake-filled	23	20.9	5.5
	130	5.5	8.1
	145	4.2	8.8
Bead-filled	23	18.1	5.6
	130	5.1	7.1
	145	4.0	7.5

Table 2: Calculated interfacial interaction parameter, B_{int} , for flake composite and bead composite.

Temperature (°C)	B_{int} , Flake Composite	B_{int} , Bead Composite
23	1.02	0.57
130	3.08	2.66
145	3.05	2.77

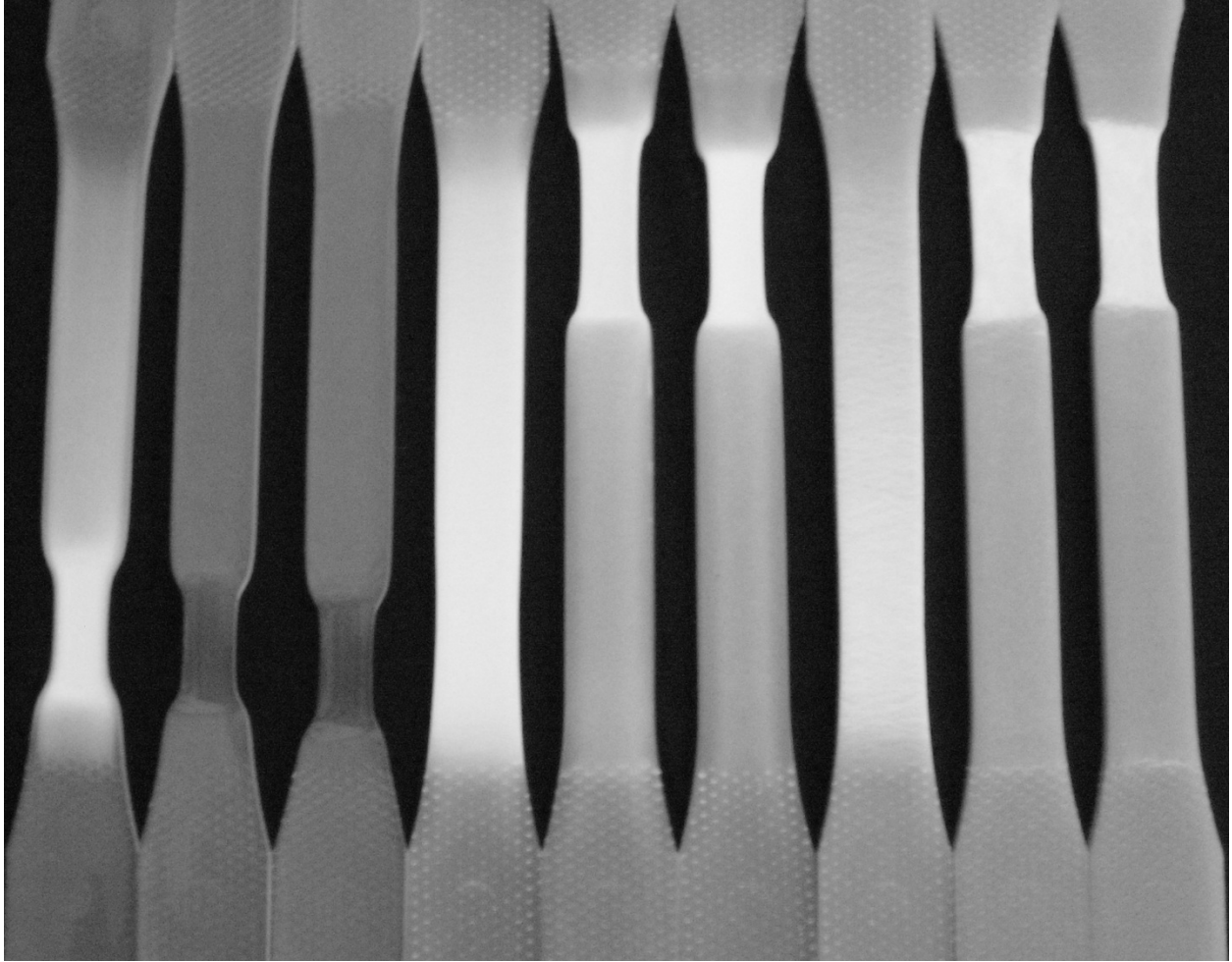


Figure 8: Tensile bars after testing to a strain of 0.4. Left to right: neat PP, 23°C; neat PP, 130°C; neat PP, 145°C; flake composite, 23°C; flake composite, 130°C; flake composite, 145°C; bead composite, 23°C; bead composite, 130°C; bead composite, 145°C.

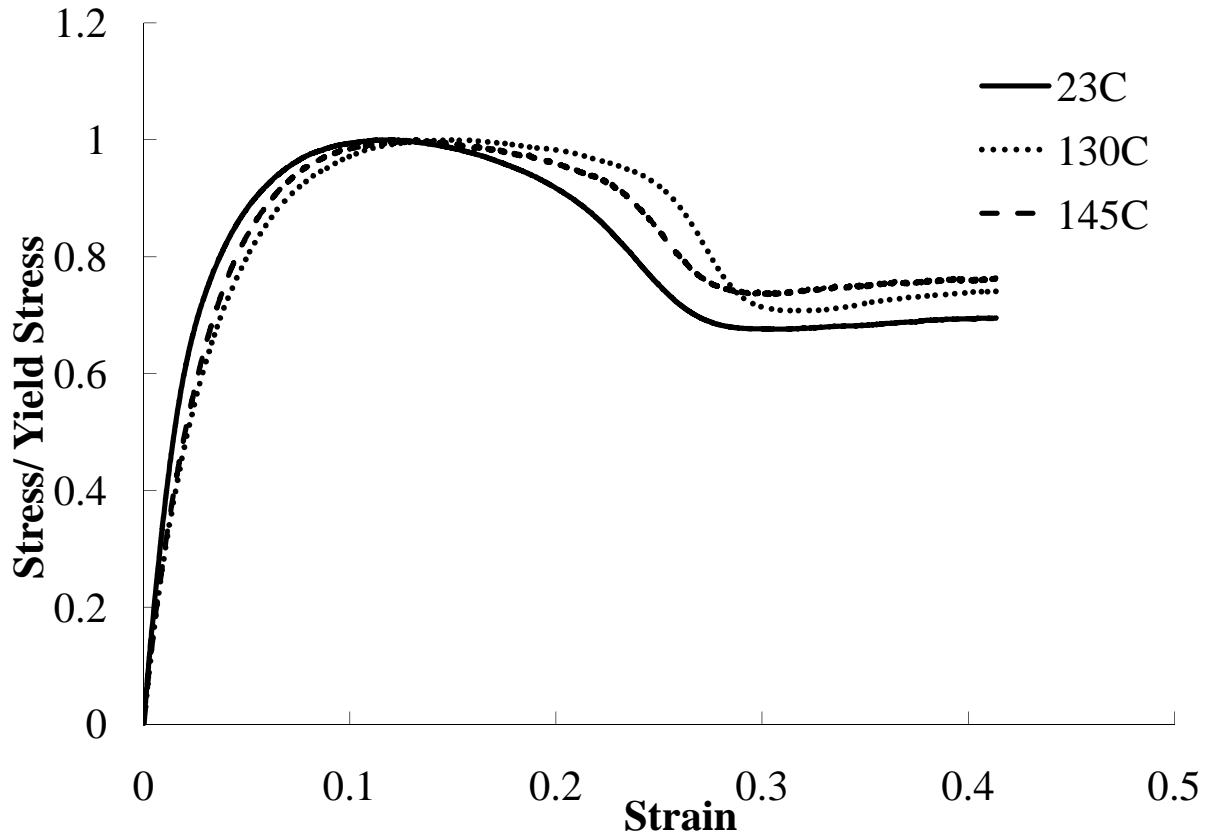


Figure 9: Stress-strain curves for neat PP with stress scaled by yield stress to allow for comparison of the character of the curves.

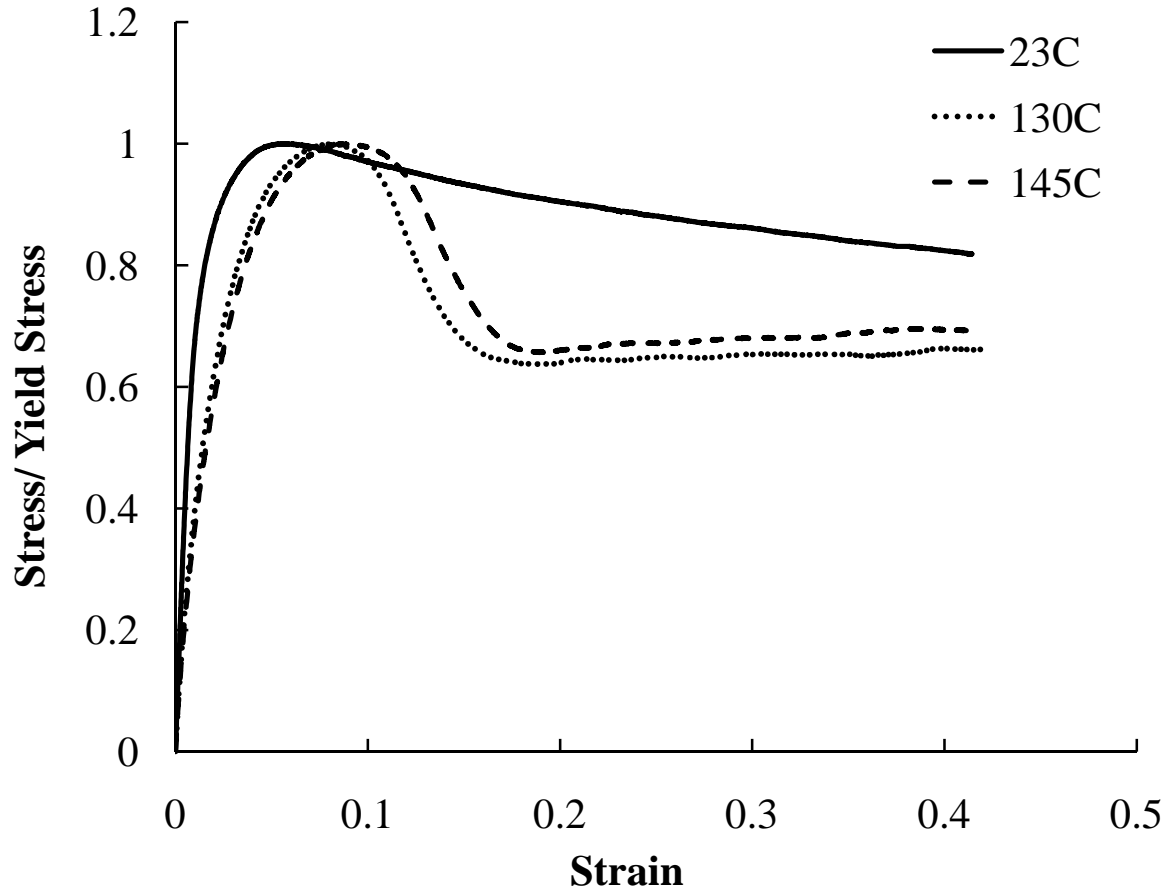


Figure 10: Stress-strain curves for glass flake composite with stress scaled by yield stress to allow comparison of the character of the curves.

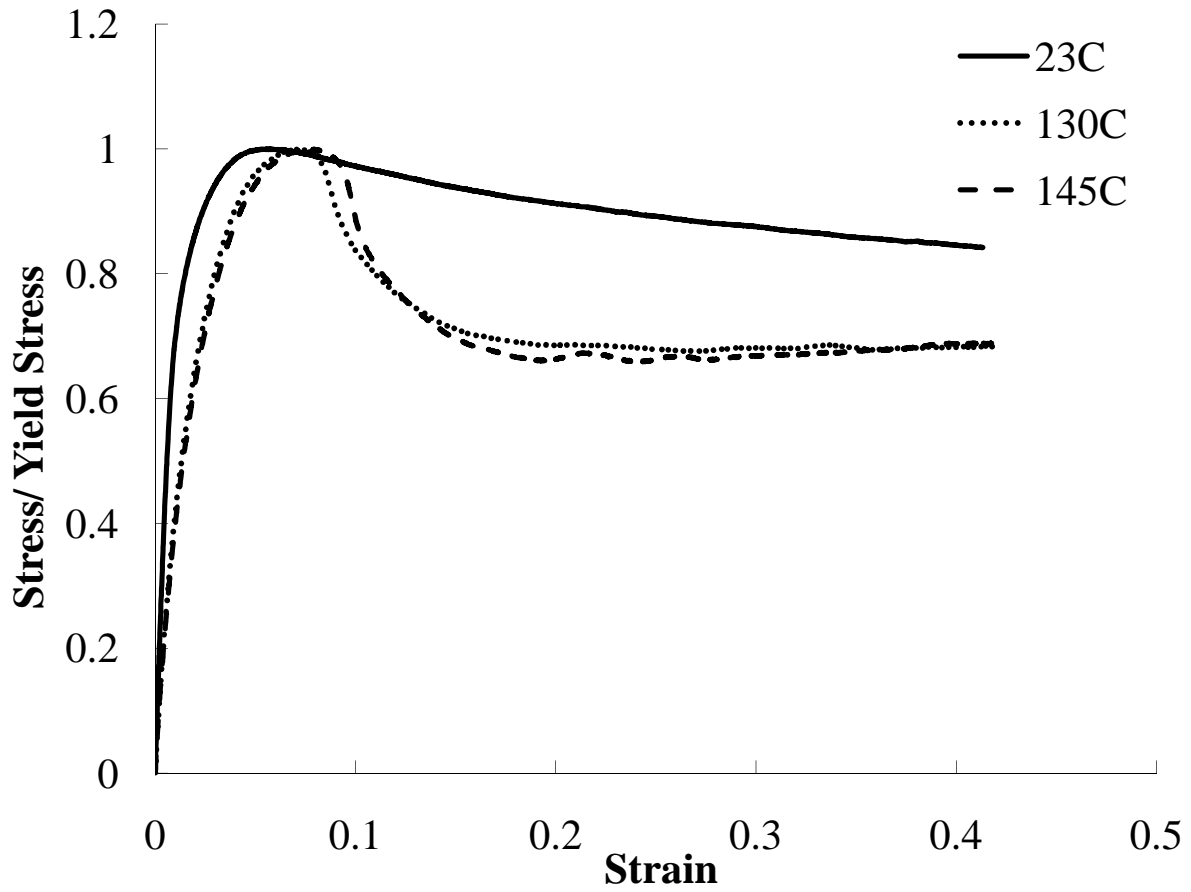


Figure 11: Stress-strain curves for glass bead composite with stress scaled by the yield stress to allow comparison of the character of the curves.

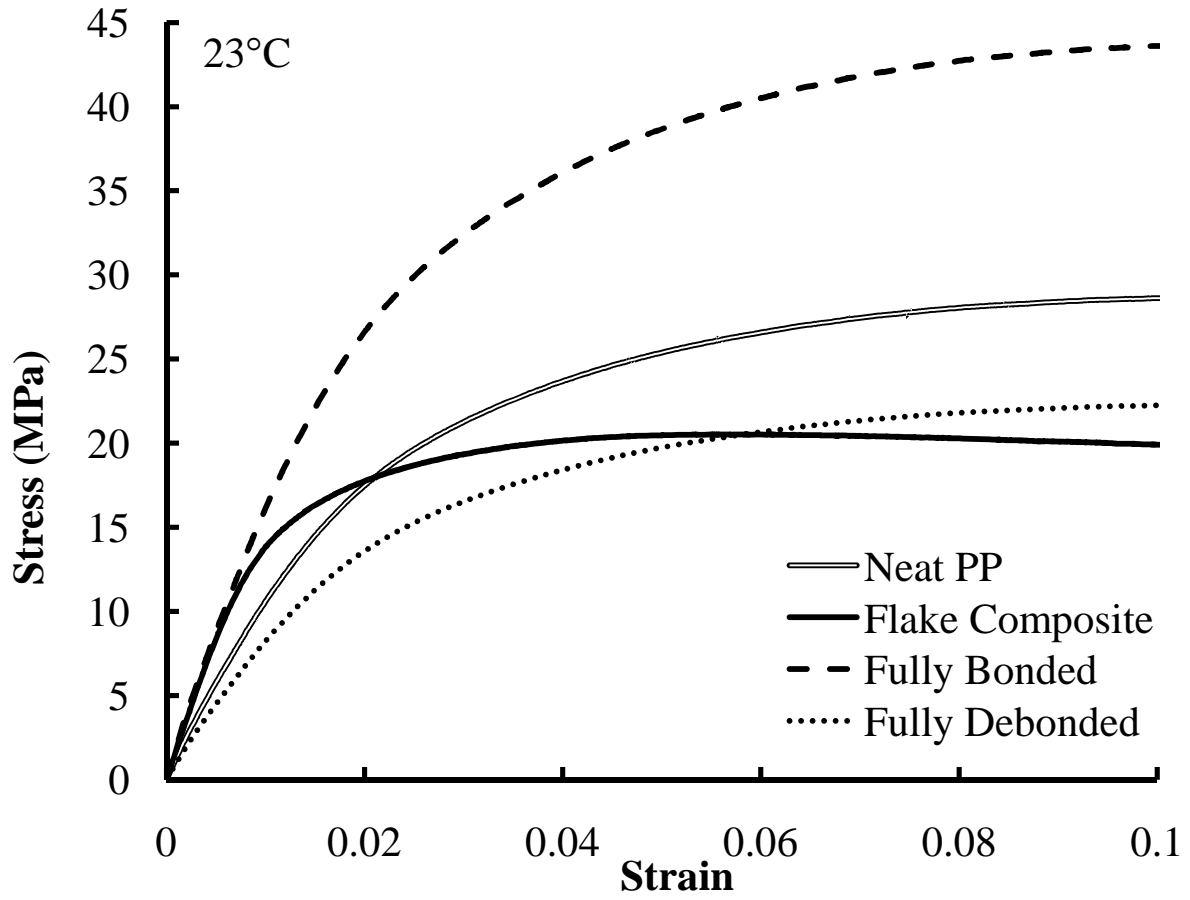


Figure 12: Flake composite and neat PP curves for tensile tests at 23°C with calculated fully bonded and fully debonded curves.

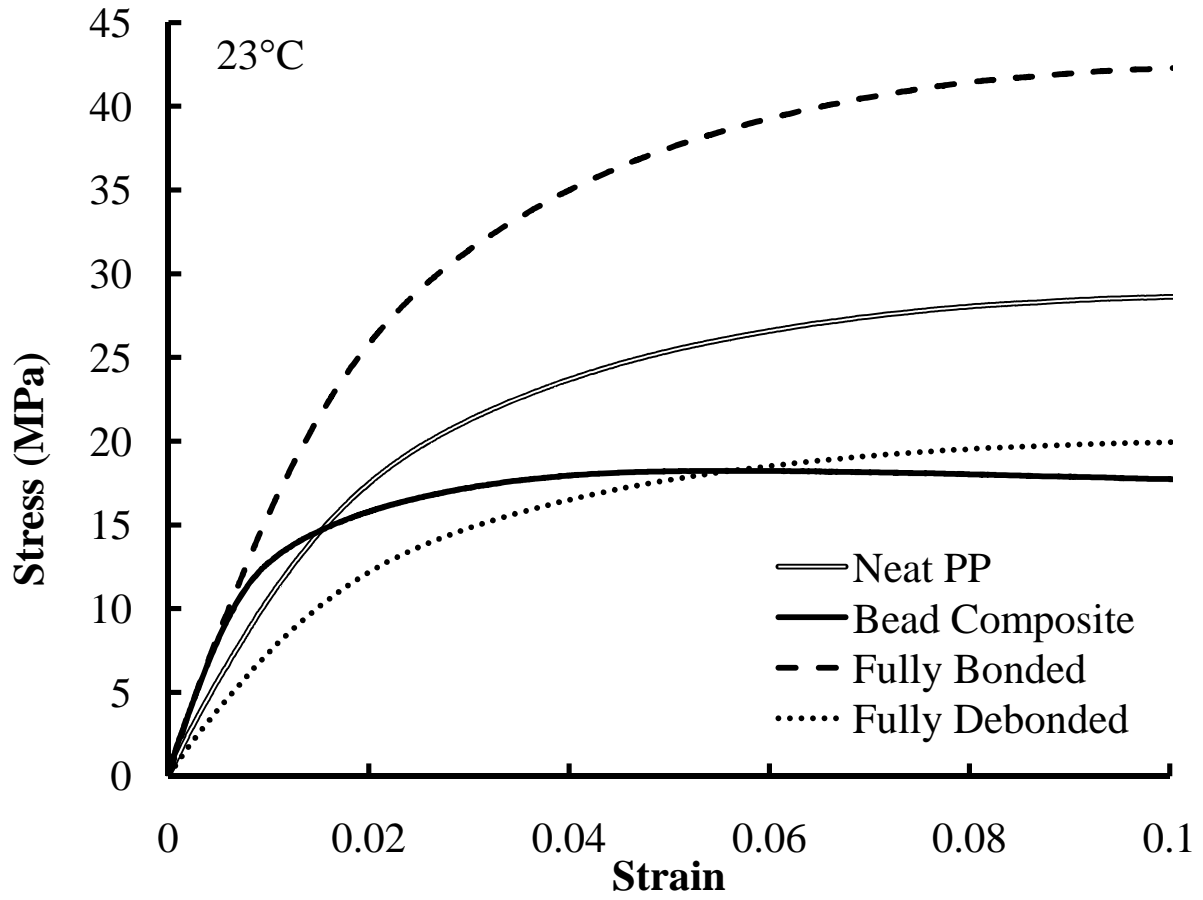


Figure 13: Bead composite and neat PP curves for tensile tests at 23°C with calculated fully bonded and fully debonded curves.

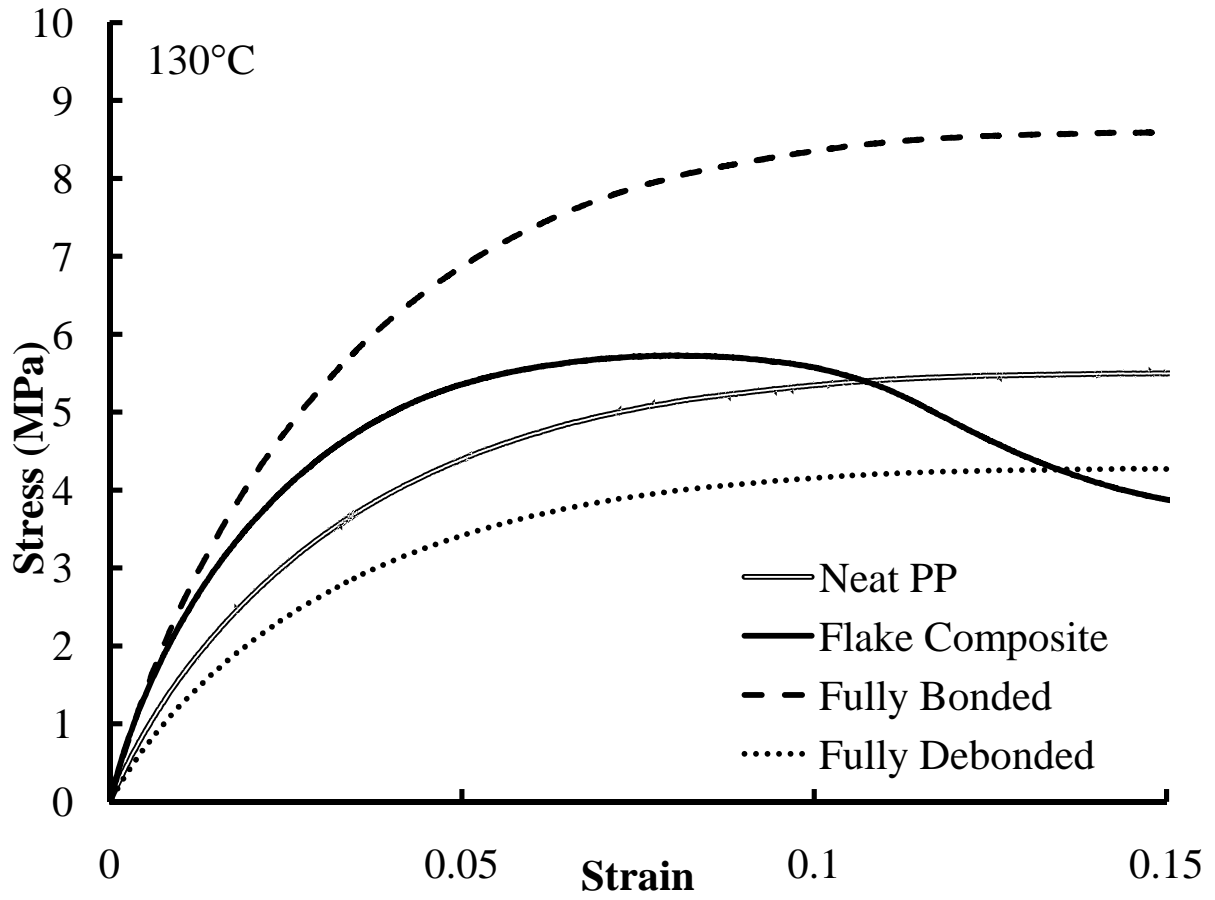


Figure 14: Flake composite and neat PP curves for tensile tests at 130°C with calculated fully bonded and fully debonded curves.

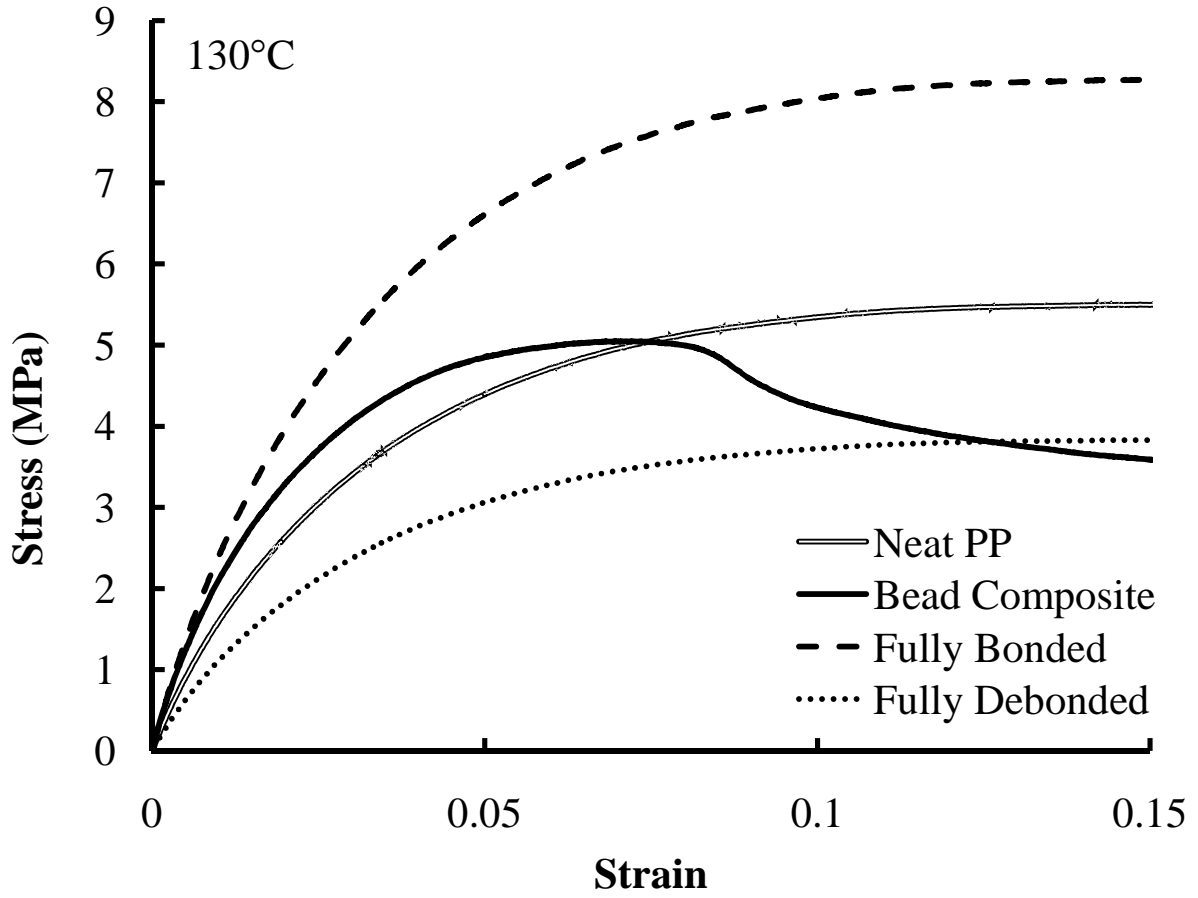


Figure 15: Bead composite and neat PP curves for tensile tests at 130°C with calculated fully bonded and fully debonded curves.

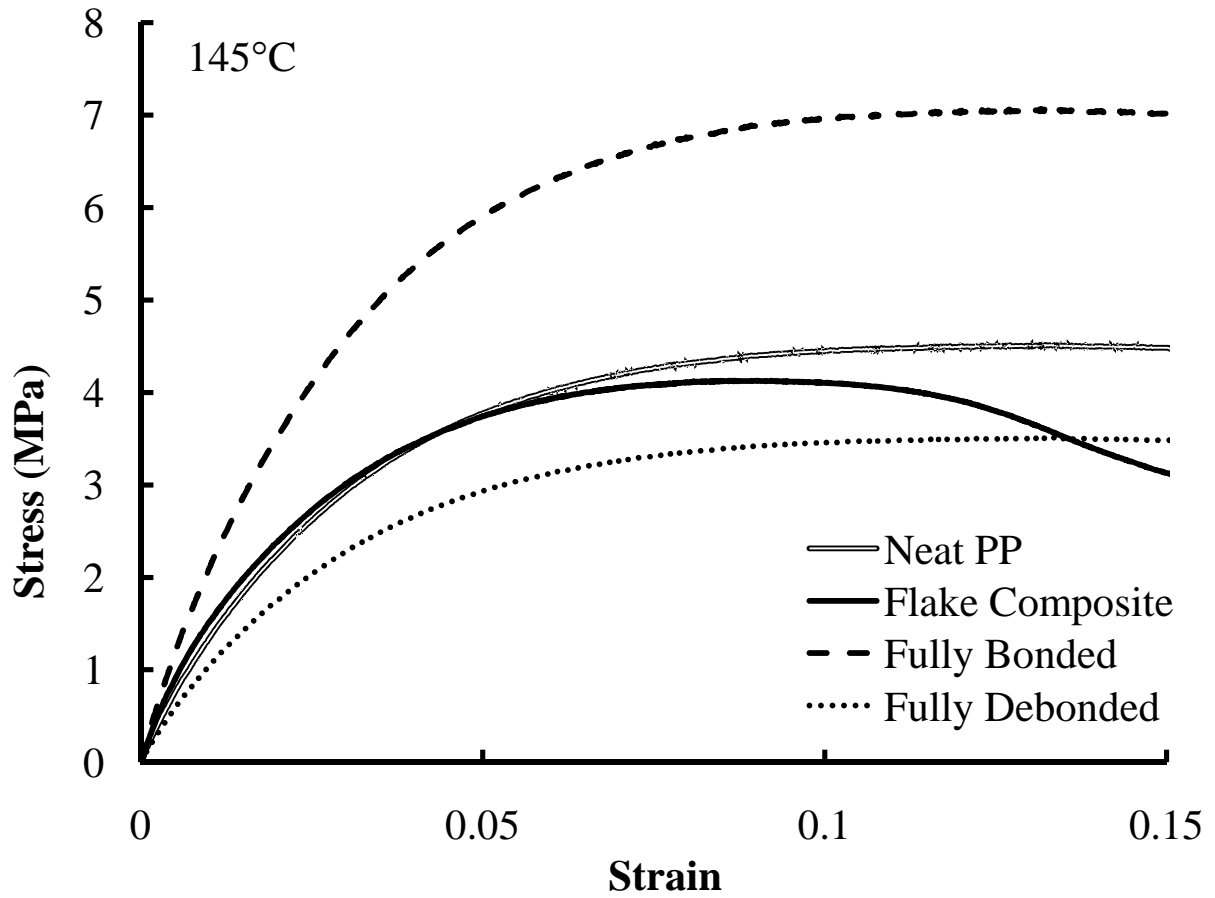


Figure 16: Flake composite and neat PP curves for tensile tests at 145°C with calculated fully bonded and fully debonded curves.

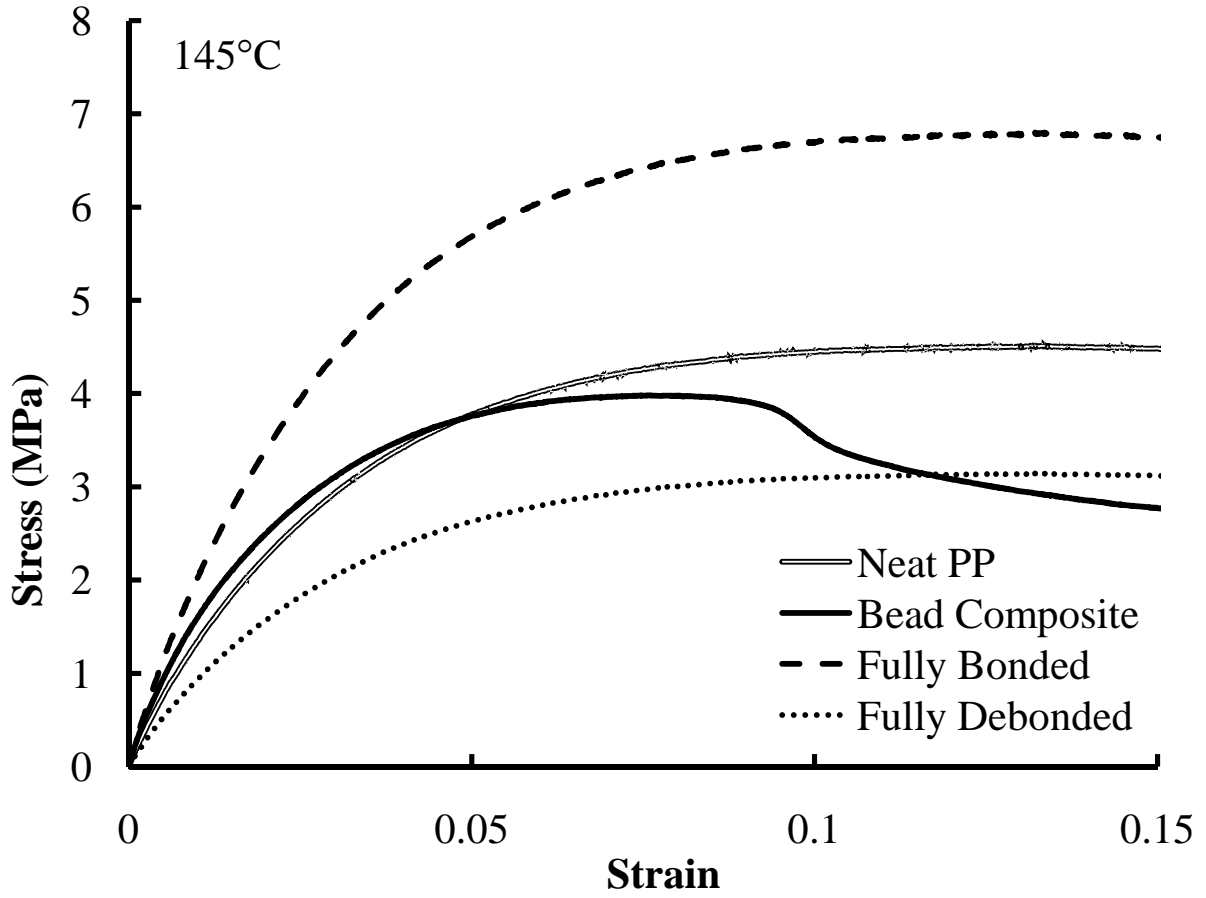


Figure 17: Bead composite and neat PP curves for tensile tests at 145°C with calculated fully bonded and fully debonded curves.

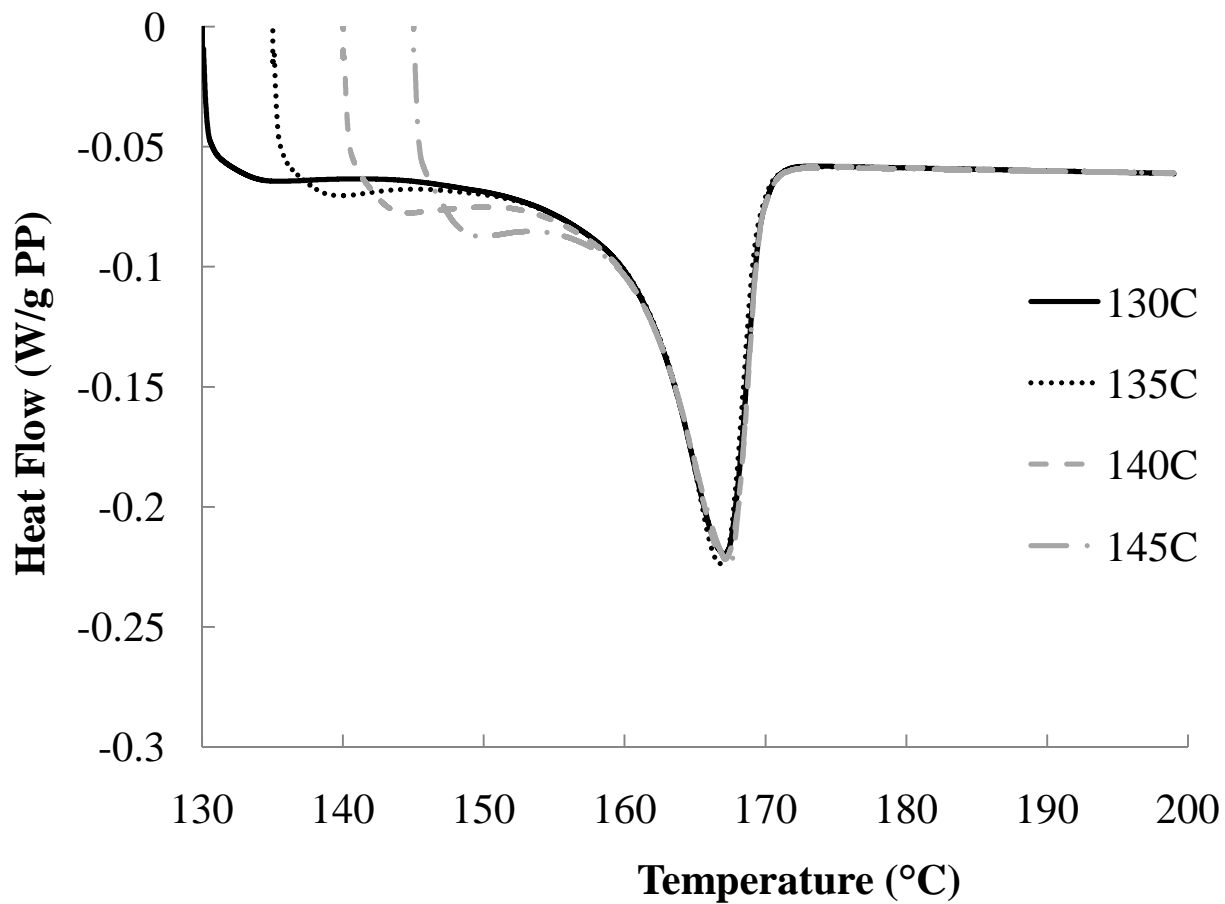


Figure 18: DSC melting curves for neat PP after holding at various temperatures.

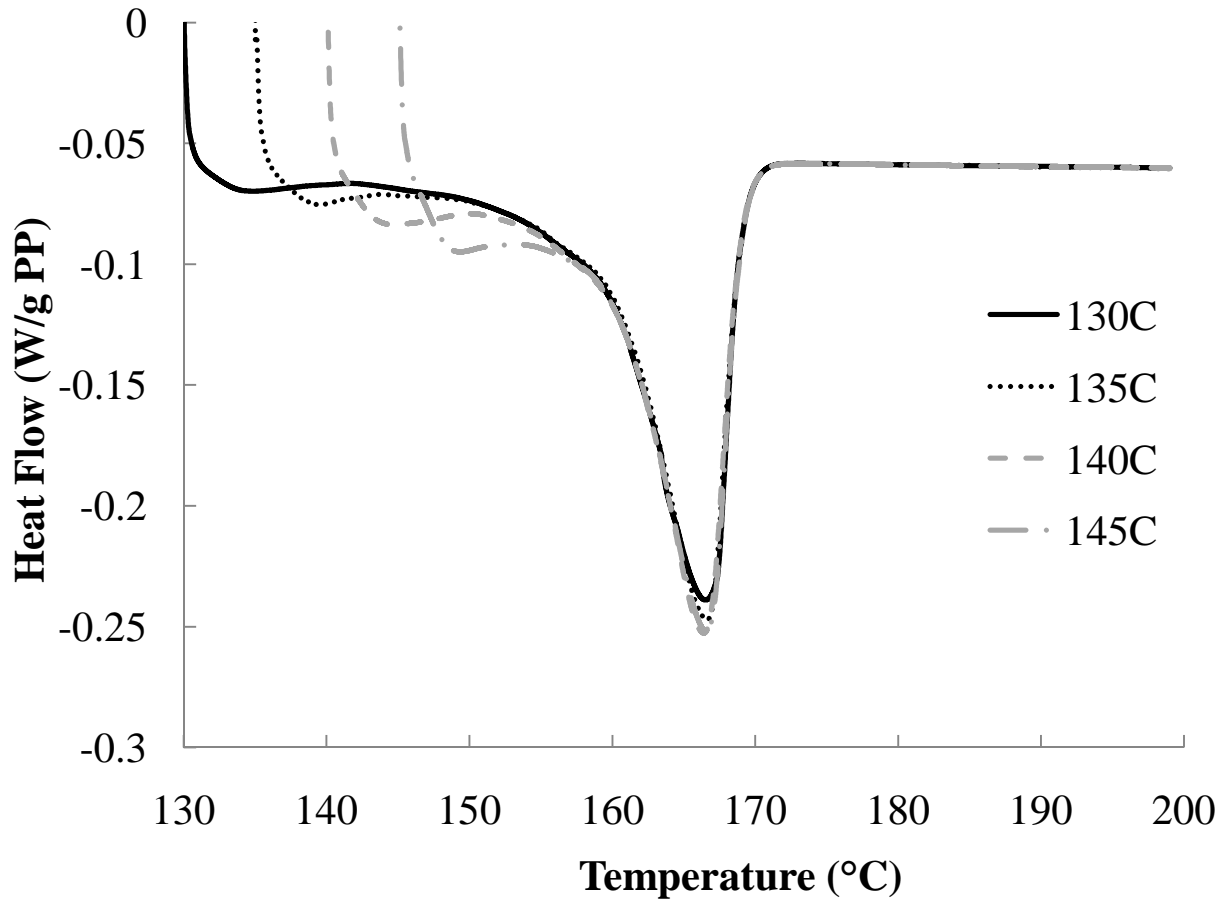


Figure 19: DSC melting curves for glass flake composite after holding at various temperatures.

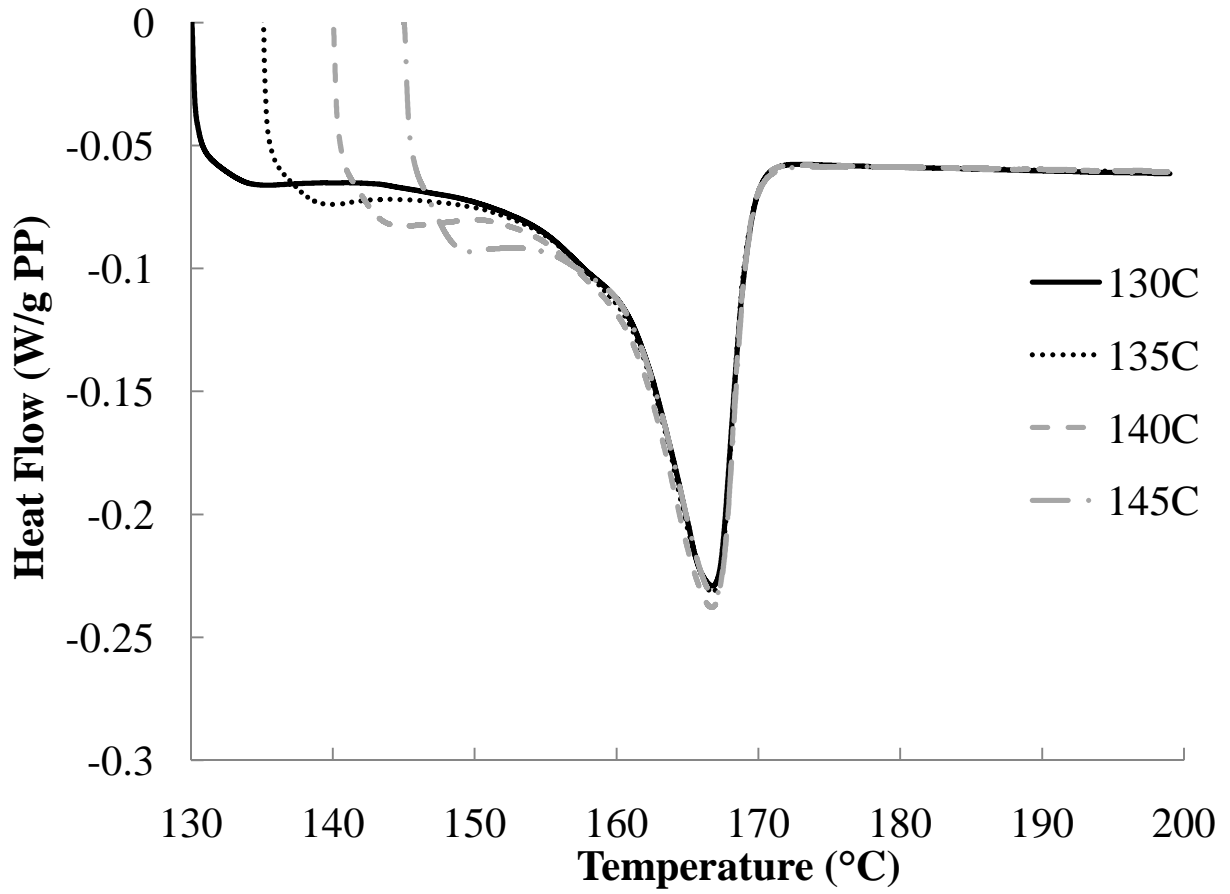


Figure 20: DSC melting curves for glass bead composite after holding at various temperatures.

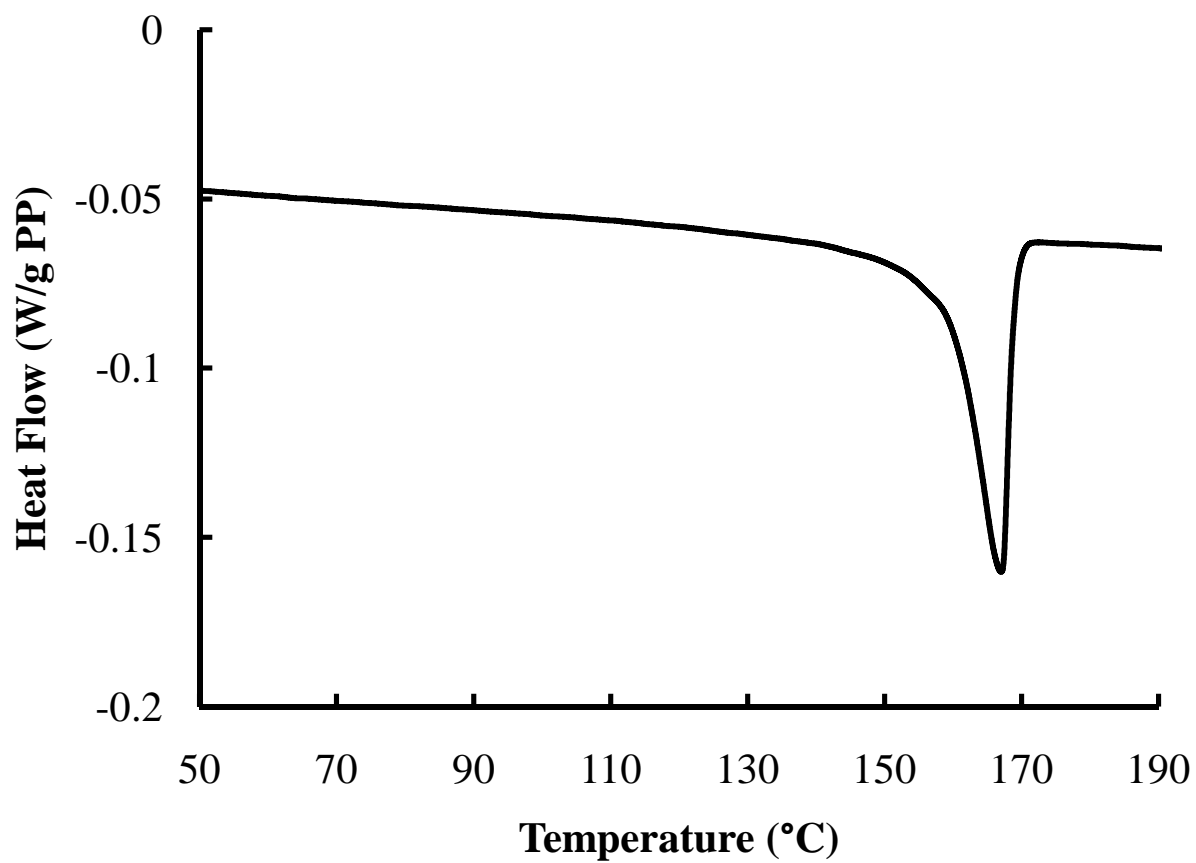


Figure 21: DSC melting curve for bead composite with a heating rate of 1°C/min.

Table 3: Average percent crystallinity of samples tested in DSC.

	Neat PP	Flake Composite	Bead Composite
Unannealed	43.2	44.5	43.7
130°C	42.2	46.6	48.4
145°C	41.0	47.0	48.6

4. Debonding Stress at Elevated Temperatures

4.1. Introduction

When a particulate composite is subjected to a tensile stress, there is a critical stress at which the interface between the matrix polymer and the particulate filler will fail, or debond. Debonding in polymer matrix composite materials has been the subject of many studies. Many of these studies have focused on debonding of spherical bead fillers through experimental studies (38; 39; 41; 37; 42; 43; 40; 44), and through development of theoretical models (47; 48; 49; 45; 46; 50). Fiber fillers (51) and aligned platelets (64) have also been studied to a lesser degree. These studies have generally been done at room temperature, not near the melting point of the polymers. Debonding around spherical beads has been widely studied because the particles themselves cannot be oriented, making the material isotropic. For bead shaped fillers, debonding is initiated at the poles of the particle in the direction of stretch, where interfacial stress is concentrated. For excellently adhering spheres, the debonded region initially encompasses an area of about 15° from each pole, while for poorly adhered spheres, debonding covers a region of about 60° from the pole (38; 50). As the stretching is continued, the void grows and encompasses a greater portion of the bead, up to about 60° from each pole (38; 39; 47; 37; 50). It has also been established that larger beads require less stress and strain to debond than smaller beads (39; 45; 46). The larger particles debond more readily than the smaller particles because debonding of large particles creates more new surface area than debonding of small particles, and thus releases more energy (39; 45). In fact, composites with small beads may reach the macroscopic yield stress before the beads have debonded (39), while debonding has been observed to occur well before yield for larger particles (41).

For aligned short fiber reinforced polymers, when a tensile stress is applied to the composite in the direction of the fibers, the interfacial shear stress is the greatest at the fiber ends, which are the first to debond. Upon increasing the tensile stress, the debonded portion will increase along the length of the fiber from both ends. The growth of the voided regions continues until the fiber breaks, or, if the fiber length is less than the critical value, the growth of the voided regions continues until the entire fiber is debonded (51). With short fibers the effect of neighboring particles on stress concentration at the fiber ends is negligible; however, for aligned platelets the stress concentration at the ends of the platelet due to neighboring particles is much more significant (64).

Debonding at elevated temperature must be taken into account for processes such as die drawing, in which the composite is stretched at elevated temperatures below the melting point. At room temperature, different methods have been used to experimentally detect debonding. One method is to measure acoustic hits, or the high frequency sound emitted when the filler debonds from the matrix. The range of deformation over which debonding occurs can be determined, but this method has not worked well for composites with a broad particle size distribution (41). Volume strain measurements have been used by monitoring the slope of a volume strain versus elongation curve. When the slope increases, debonding has occurred (42; 48; 60; 62). *In situ* tests have been done, in which the specimen is stretched in tension with observation by light microscope (43; 47) or scanning electron microscopy (SEM) (66). In these tests, the onset of debonding is observed visually. Finally, analysis of the stress-strain curve has been used to detect debonding (39). The stress-strain curve exhibits two linear portions of differing slope, giving a kink in the linear region of the curve, which indicates the onset of debonding. This method was

chosen to evaluate the onset of debonding at high temperatures in this study, using transverse strain rather than axial strain.

4.2. Experimental

4.2.1. Materials

The polymer used for this work was a polypropylene homopolymer (5D37) with a melting temperature of 166°C and a M_w of 249,400 manufactured by Dow Chemical Company. The spherical glass particles were solid E-glass spheres (3000E) manufactured by Potter's Industries, Inc. with a mean particle diameter of 35 microns. The glass flakes (REF-015) were made of E-glass by NGF Canada, Ltd. with a mean particle length before compounding of 10.7 μm , a mean particle width of 6.0 μm , and a mean particle thickness of 5 μm and a wide particle size distribution. The aspect ratios of the glass flake particles before compounding ranged from 1 to 4, with a mode of 2. Neither the glass beads nor glass flakes had surface treatment to enhance adhesion with polypropylene.

4.2.2. Processing

The polypropylene was compounded separately with the glass beads and glass flakes in a Farrel CP250 continuous mixer to obtain a filler volume fraction near 0.20 for each composite. Ash content tests indicated that the actual volume fraction of filler was 0.16 for the flake filled composite, and 0.19 for the bead filled composite. The composites, as well as neat polypropylene, were then injection molded into ASTM D638 Type I tensile bars.

4.2.3. Mechanical Testing

Tensile tests were done on a UTS STM-20 tensile test frame equipped with a heating chamber. To determine debonding stress, a high-temperature compensated transverse extensometer, model 3575-025M-HT1, from Epsilon Technology Corp. was used during the

tensile testing. To determine the tensile modulus of the matrix polymer, an axial extensometer, model 3542-050M-035-ST, from Epsilon Technology Corp was used. For either test, the tensile bars were loaded into the tensile frame and held at the test temperature for 60 minutes prior to testing. The appropriate extensometer was placed on the tensile bar for the last 10 minutes of holding at the test temperature. Tensile tests were then done at an axial strain rate of $1 \times 10^{-3} \text{ s}^{-1}$ to the desired final strain. A toe correction was done on the data from each test, which removed the first few data points which are typically not an indication of actual material properties (67). A minimum of three mechanical tests were done for each set of test conditions. Values reported here are average values unless otherwise noted as example values.

4.2.4. Differential Scanning Calorimetry (DSC)

Samples of around 10mg were cut out of the gauge area of an as-received tensile bar and sealed in aluminum pans for DSC testing on a TA Instruments Q10 DSC. The samples were heated at $10^\circ\text{C}/\text{min}$ to a temperature of $130\text{-}145^\circ\text{C}$, held for 60 minutes at that temperature, and then heated at $1^\circ\text{C}/\text{min}$ to 200°C . The entire DSC test was done with a nitrogen purge of $50\text{mL}/\text{min}$.

4.3 Results and Discussion

4.3.1. Debonding Stress Measurement

In order to determine the amount of applied stress required for debonding, mechanical tests were done with injection molded tensile bars of neat polypropylene, polypropylene filled with 19 vol% glass beads, and polypropylene filled with 16 vol% glass flakes at temperatures of 130, 135, 140, and 145°C at an axial strain rate of $1 \times 10^{-3} \text{ s}^{-1}$. Transverse strain vs. stress curves were obtained because the transverse extensometer was less damaging to the sample than the axial extensometer, and was less likely to cause anomalies in the strain vs. stress curves that were not

indicative of actual properties of the materials being tested. Example transverse strain vs. stress curves for the glass flake composite are shown for each temperature in Figure 22. The analogous curves for the glass bead composite are shown in Figure 23. For comparison, an example axial strain vs. stress curve for the glass flake composite at 145°C is shown in Figure 24, along with the corresponding curve for neat polypropylene. In the transverse strain vs. stress plots in Figure 22 and Figure 23, as well as the axial strain vs. stress plot for the composite in Figure 24, there are two linear portions of differing slope, creating a kink where the two linear portions intersect. The transverse strain vs. stress curve for 145°C in Figure 22 shows a kink at 0.166MPa, while the axial strain vs. stress curve for the composite in Figure 24 shows a kink at 0.165MPa, confirming that the kink occurs at a similar stress regardless of whether axial or transverse strain is measured. In contrast to the composite curves, the neat polypropylene curve in Figure 24 shows only one linear portion, and therefore no kink.

The average debonding stress (σ_d) identified for each composite at each temperature is given in Table 4, along with the matrix modulus (E_m) at each temperature. For both composites, the debonding stress decreases with increasing temperature, as expected due to a decreasing modulus.

4.3.2. Stress Balance

The applied tensile stress required for debonding, σ_d , needs only to be large enough to overcome the net stress that exists in the sample at the interface between the particle and matrix before stretching. The stress in the matrix at the interface determines when the interface fails, or debonding occurs. In these composites, the interfacial stresses in the matrix include adhesive stress (σ_A) and residual stress (σ_R). In both composites used in this study, the adhesive stress is compressive in the matrix, and the residual stress is tensile in the matrix, which is in agreement

with Harding et al. (43). Because the adhesive and residual stresses in the matrix act in opposite directions, the applied debonding stress need not necessarily be of the same order of magnitude as either the residual or adhesive stress individually.

Residual stress is a result of cooling the sample from the processing temperature to room temperature when the sample is molded, and can be caused by differences in the coefficient of thermal expansion or induced by crystallization that occurs as the material cools (83). The matrix and filler have different coefficients of thermal expansion, which results in differential contraction on cooling. The more rigid phase, in this case the glass particles, will dominate and will not allow the matrix to shrink as much as it would if unconstrained. This results in a tensile stress in the matrix. When the temperature increases above the glass transition temperature of the polymer, the thermal residual stress in the amorphous phase relaxes (84). However, because these tests have been run below the melting temperature of the composite, there are still crystalline domains. Therefore, the residual stress in the composite is primarily due to crystallization, and thermal stress in the amorphous phase is ignored. This assertion is backed up by DSC tests run after holding the composite samples at elevated temperatures from 130°C to 145°C. An example is shown in Figure 25, where the samples were held for 60 minutes at 130°C or 145°C during the test, and each curve exhibits a second, lower melting point peak. The appearance of a second peak in the DSC curves indicates that rearrangement of the polymer matrix takes place during the holding step. This rearrangement allows for the relaxation of thermal residual stresses, and also indicates that additional crystallization takes place during this step. The total crystallinity in the sample, which is responsible for the residual stress in the sample, has been calculated from Equation 12:

$$\chi_c = \frac{\Delta H_f \cdot 100}{\Delta H_f^0 \cdot w_m} \quad (12)$$

Where χ_c is the total crystallinity, ΔH_f is the heat of fusion, ΔH_f^0 is the equilibrium heat of fusion of a 100% crystalline sample, and w_m is the mass fraction of polymer in the composite (82). The heat of fusion of 100% crystalline polypropylene was taken as 207 J/g (17). The mass fraction of polypropylene in the glass flake composite was 0.64 and in the glass bead composite was 0.59.

The results of these tests, shown in Table 5, indicate that the crystallinity is nearly constant for both composites over the range of holding temperatures used in this study. The effect of viscoelastic relaxation is ignored in this case. The residual stress is calculated as described in Hsueh, and Hsueh and Becher for the bead filled composite (85; 86). The relevant equations are listed in Appendix A. The residual stress cannot be calculated from available equations for the flake filled composite.

There is also adhesive stress between the matrix and filler, which is acting in the opposite direction of the residual stress; compressive in the matrix in this case. The adhesive stress at the instance of debonding is calculated using an energy balance which has been developed for composites with spherical fillers (45; 46) and is given in Equation 13:

$$\sigma_A = \sqrt{E_m} f(\phi) \sqrt{\frac{2W_A |\Delta S_d|}{|\Delta V_d| \frac{df}{d\phi}}} \quad (13)$$

where σ_A is the elastic stress in the matrix that balances adhesion, E_m is the matrix modulus measured from tensile tests at elevated temperature on the neat matrix, ΔV_d is the debonded volume, W_A is the work of adhesion between the matrix and filler, taken as 0.050 J/m² (87), ΔS_d

is the debonded surface area, ϕ is the volume fraction of particles, and f is a function of the volume fraction and aspect ratio of particles. For the case of the glass beads, the Kerner-Lewis equation, as defined in Equations 5-7, was used for f , while for the glass flake composite, the Kerner-Lewis equation had to be modified using Sudduth's concept of "sphericity", defined in Equation 9 (81). In order to determine the average aspect ratio of debonded particles, SEM images were examined. The length and thickness of particles debonded from the matrix were measured, and the volume-weighted average aspect ratio was determined to be 5.4. For the flake composite, the Kerner-Lewis equation is given by Equation 14:

$$E_c = E_m \frac{1 + A' B' \phi}{1 - B' \phi} \quad (14)$$

Where E_c and E_m are the composite and matrix moduli, ϕ is the volume fraction of filler, and for an aspect ratio of 5.4, A' and B' are given by Equations 15 and 16:

$$A' = A \cdot 2.0492s^{4.637} \quad (15)$$

$$B' = \frac{\frac{E_f}{E_m} - 1}{\frac{E_f}{E_m} + A'} \quad (16)$$

Where A is as defined by Equation 6, s is as defined by Equation 9, and E_f is the filler modulus.

Inclusion of the factor $f (df/d\phi)^{-1/2}$ in Equation 13 accounts for the presence of multiple filler particles in a particle composite, which have overlapping stress fields. For the flake composite in this work, this factor has a value of 1.02, while for the bead composite, this factor has a value of 1.22. This indicates that the presence of multiple filler particles has much more effect on the calculated adhesive stress for the bead composite than for the flake composite.

Particle shape can be taken into account in Equation 13 with the expressions for ΔV_d and ΔS_d . Beads, for example, have $\Delta S_d/\Delta V_d$ of $6/(R \sin \theta_d)$ where R is the radius of the bead and θ_d is the debonding angle, while flakes have $\Delta S_d/\Delta V_d$ of $4(1/l + 1/w + 1/t)$, where l , w , and t are the length, width, and thickness of the particle. This reflects the fact that debonding occurs all around the flake particles. To calculate $\Delta S_d/\Delta V_d$ for the two composites, the particle dimensions were determined from examination of SEM images containing debonded particles, such as that in Figure 26. The length and thickness of the particles could be measured using the scale bar in the image. However, the width dimension could only be estimated from visual examination of particles such as that in the lower right corner of Figure 26 where all three dimensions were visible, but the third dimension could not be measured because it was not in the plane of the image. Volume-weighted average dimensions were determined, which led to $\Delta S_d/\Delta V_d$ values of $5.9 \times 10^5 \text{ m}^{-1}$ for the flakes and $2.1 \times 10^5 \text{ m}^{-1}$ for the beads. While temperature is not explicitly present in Equation 13, the matrix modulus is dependent on temperature. As expected, tensile tests on neat matrix have shown that increasing the temperature causes the matrix modulus to decrease, as shown in Table 4. The work of adhesion may also be dependent on temperature, but is expected to be a much weaker function of temperature.

The calculated adhesive and residual stresses for the bead filled composite are shown in Table 6. The adhesive and residual stresses are of the same order of magnitude, while the debonding stress, shown in Table 4, is an order of magnitude less. The calculated adhesive stress for the flake filled composite, also shown in Table 6, is of the same order of magnitude as that for the bead filled composite, but is higher due to a higher value of $\Delta S_d/\Delta V_d$. As shown in Table 4, the debonding stress for the flake filled composite is also of the same order of magnitude as

that of the bead filled composite. The residual stress is expected to be of the same order of magnitude for the two composites as well.

Stress amplification around the particles and geometric and material properties of the components of the composite must be taken into account in the stress balance across the interface (40; 44). Figure 27 shows the debonding stress as a function of adhesive stress for both composites. A straight line fit to the data for each composite gives an R^2 value of greater than 0.9 for each composite, indicating that the debonding stress is a fairly linear function of adhesive stress. The slope of the line for the bead filled composite is 0.14, while that of the flake filled composite is 0.12, indicating that the stress amplification at the interface of the particles is higher for the flake filled composite. Both lines have a negative intercept, which is associated with the presence of the tensile residual stress at the interface, and is in agreement with Harding et al (43). The line fit to the data for the bead filled composite has an intercept of -0.03, while that for the flake filled composite has an intercept of -0.11. This indicates that the residual stress plays a greater role in debonding in the flake filled composite than in the bead filled composite. This can be explained by the fact that flake particles are oriented to a great degree in the direction of stretch, so the residual stress at the interface is in the same direction as the direction of stretch. In contrast, the bead particles are not able to be oriented, so the total residual stress at the interface would have to be resolved into components to determine the residual stress in the direction of stretch (43).

The ratio of debonding stress to adhesive stress is plotted in Figure 28 as a function of the ratio of residual stress to adhesive stress. This figure clearly shows that the ratio of debonding stress to adhesive stress is invariant with the ratio of residual stress to adhesive stress. Figure 28 also highlights the fact that the debonding stress is an order of magnitude lower than either the

residual stress or adhesive stress. This figure demonstrates both the fact that the applied stress is amplified at the interface between the matrix and filler, and that the debonding stress is a greater function of adhesive stress than residual stress.

4.4. Conclusions

The onset of debonding in both composites was identified by a kink in transverse strain vs. stress curves from tensile tests. Adhesive stress in the two composites was an order of magnitude larger than the stress required for debonding, indicating that there is residual stress in the composites, even at elevated temperatures. Residual stress calculations for the glass bead composite confirm that the residual stress is of the same order of magnitude as the adhesive stress. Comparison of the debonding stress to the adhesive stress for the two composites indicates that the residual stress must be greater for the flake filled composite, and that the stress amplification at the particle-matrix interface is greater for the flake composite than for the bead composite.

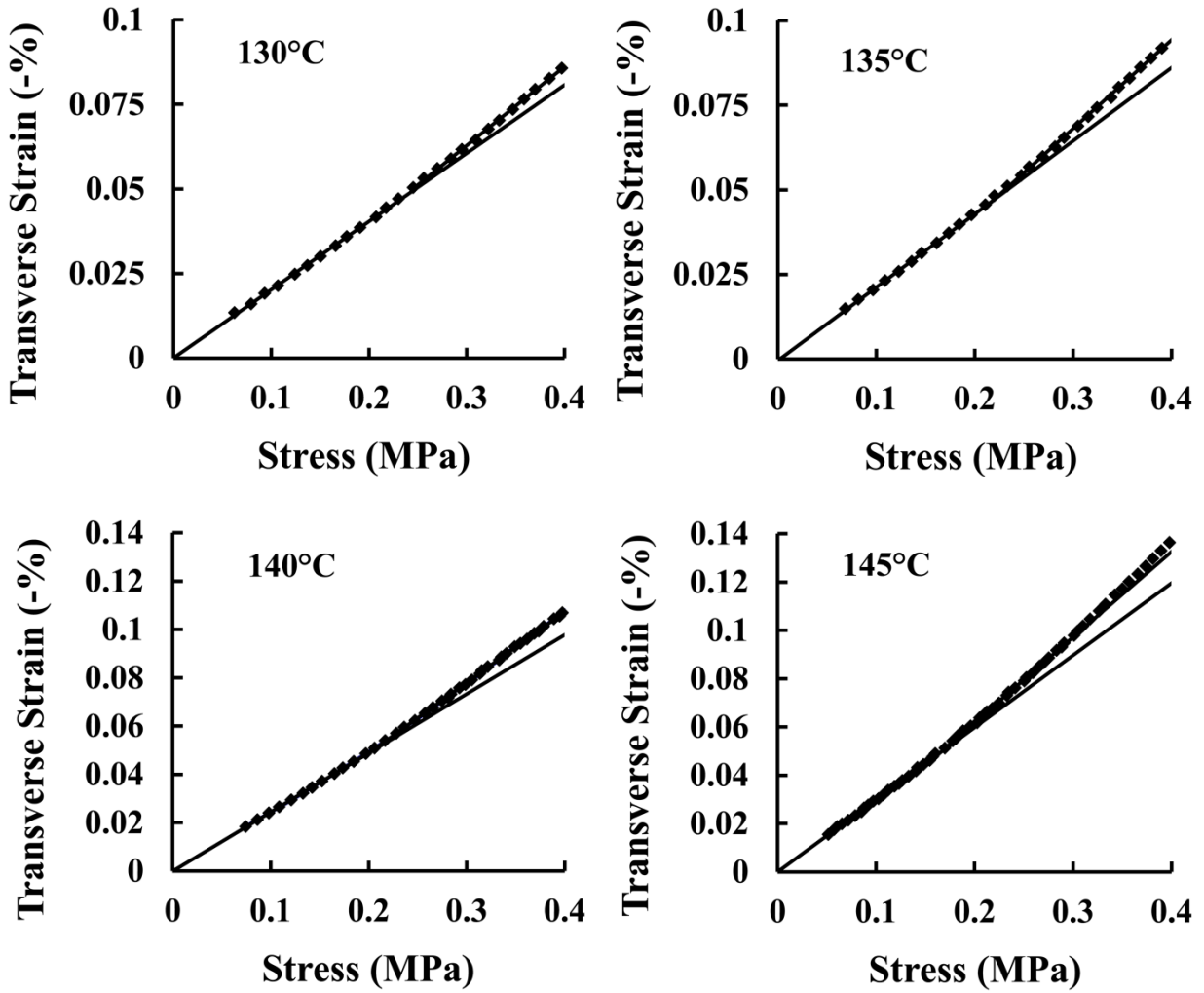


Figure 22: Example transverse strain vs. stress plots for 16vol% glass flake filled composite at each temperature. Markers indicate experimental data points while the straight lines are fitted to the data.

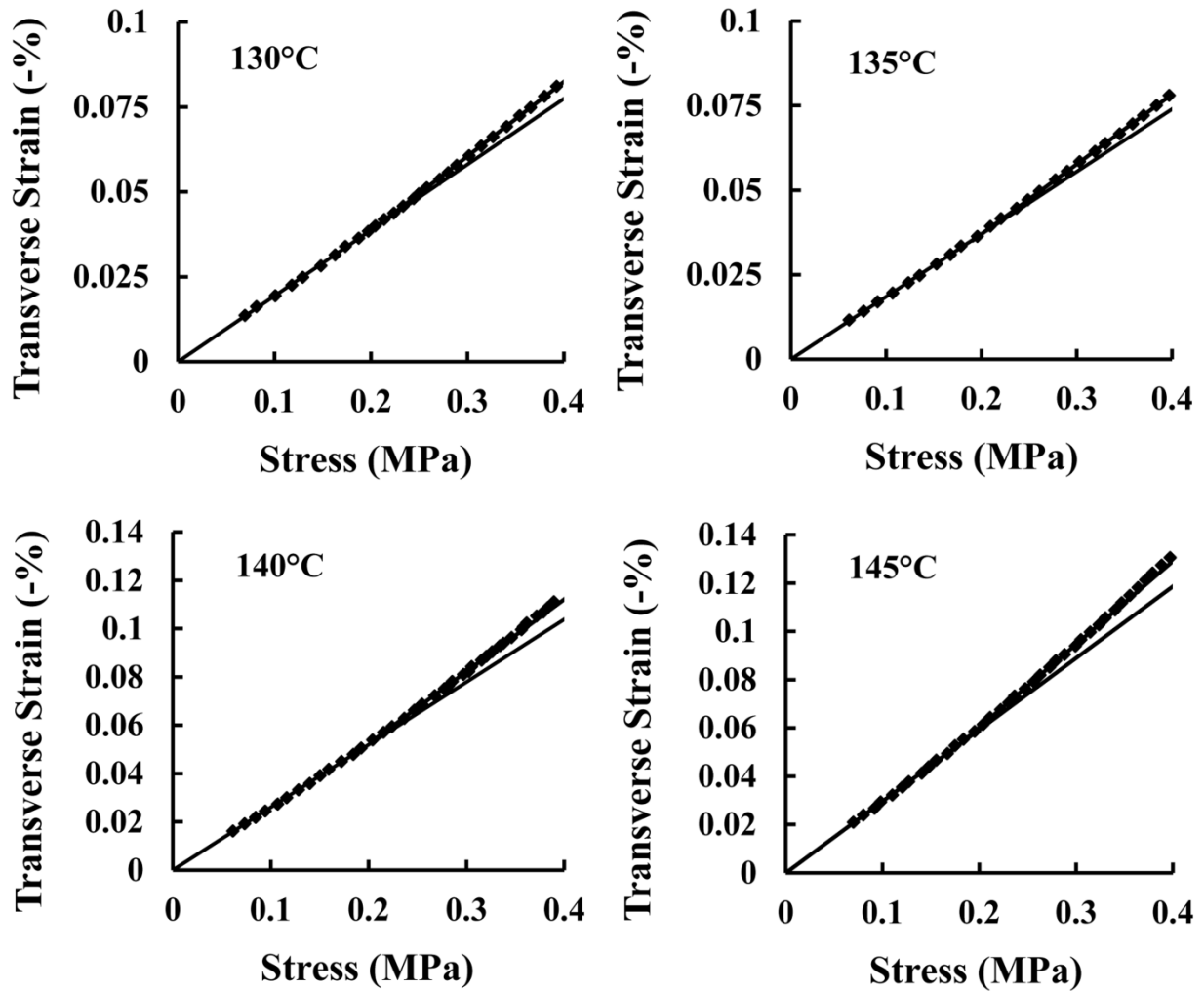


Figure 23: Example transverse strain vs. stress plots for the 19vol% glass bead composite at each temperature. Markers indicate experimental data points while the straight lines are fitted to the data.

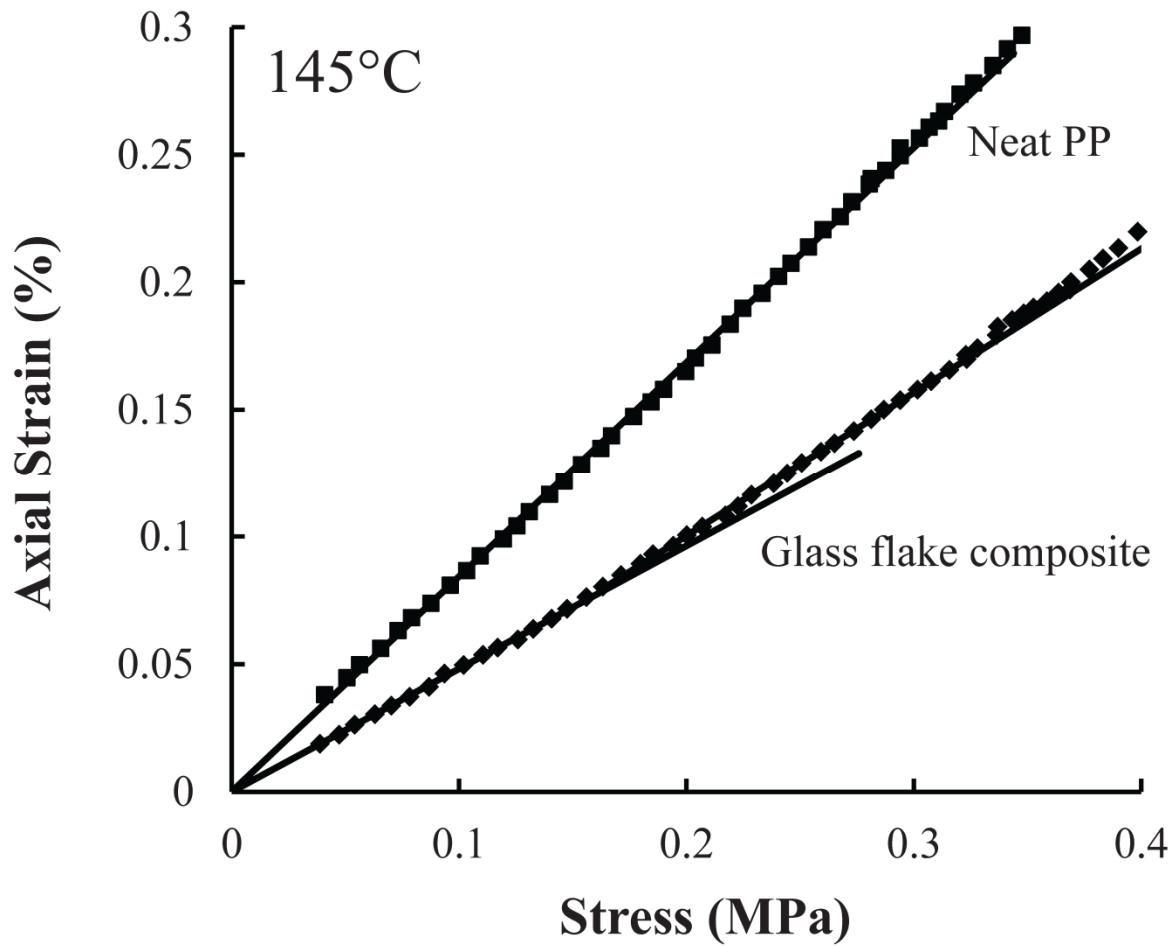


Figure 24: Example axial strain vs. stress curves for the glass flake filled composite and the neat matrix PP at 145°C. The composite shows a kink in the curve, while the neat polymer exhibits no kink. Markers indicate experimental data points while the straight lines are fitted to the data.

Table 4: Matrix modulus and applied stress for debonding at each testing temperature.

T (°C)	E _m (MPa)	σ _d (MPa)	
		Flake-filled	Bead-filled
130	226	0.216	0.224
135	198	0.189	0.201
140	177	0.161	0.187
145	140	0.150	0.169

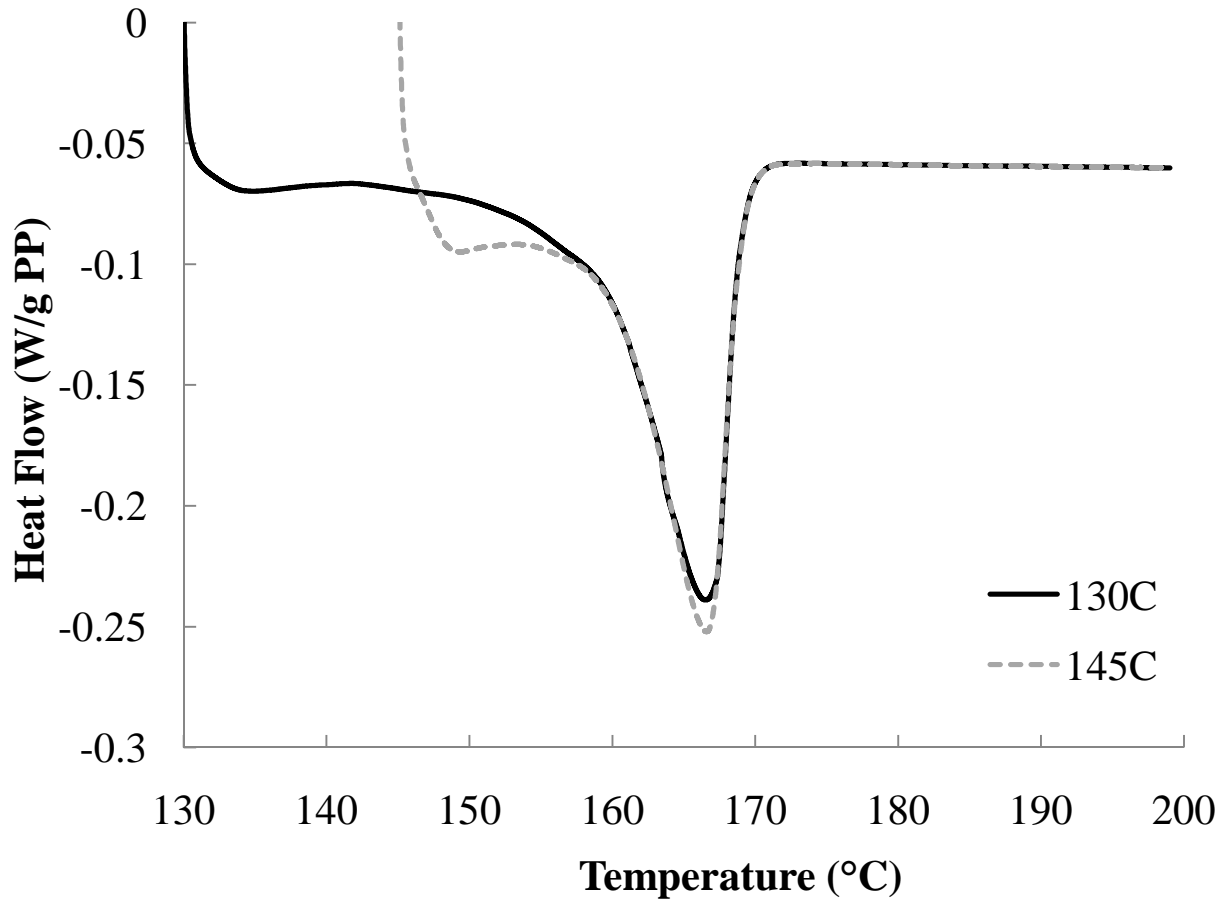


Figure 25: DSC melting curve for glass flake composite after holding at 130°C and 145°C for 60 minutes.

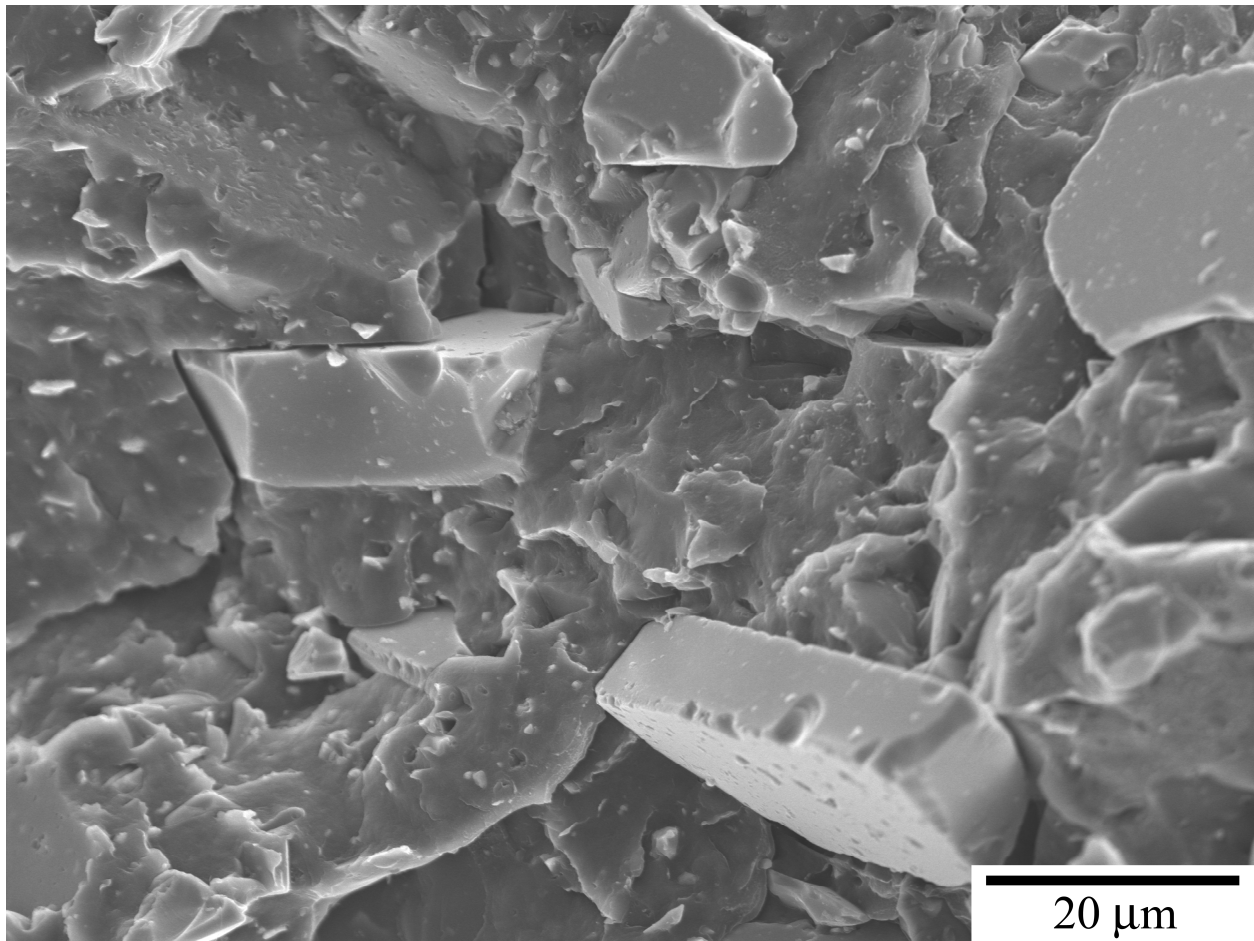


Figure 26: SEM micrograph of fracture surface of glass flake composite stretched to 0.3% strain at 0.2in/min at 130°C.

Table 5: Percent crystallinity in each composite after holding at elevated temperature for 60 minutes.

T (°C)	Crystallinity (%)	
	Flake-filled	Bead-filled
130	46.6	48.4
135	46.9	48.3
140	47.4	49.3
145	47.0	48.6

Table 6: Adhesive stresses in both composites and residual stress in the bead-filled composite at the instance of debonding.

T (°C)	Flake-filled		Bead-filled	
	σ_A (MPa)	σ_A (MPa)	σ_A (MPa)	σ_R (MPa)
130	2.62	1.66	1.66	3.34
135	2.46	1.56	1.56	2.92
140	2.23	1.47	1.47	2.66
145	2.07	1.31	1.31	2.08

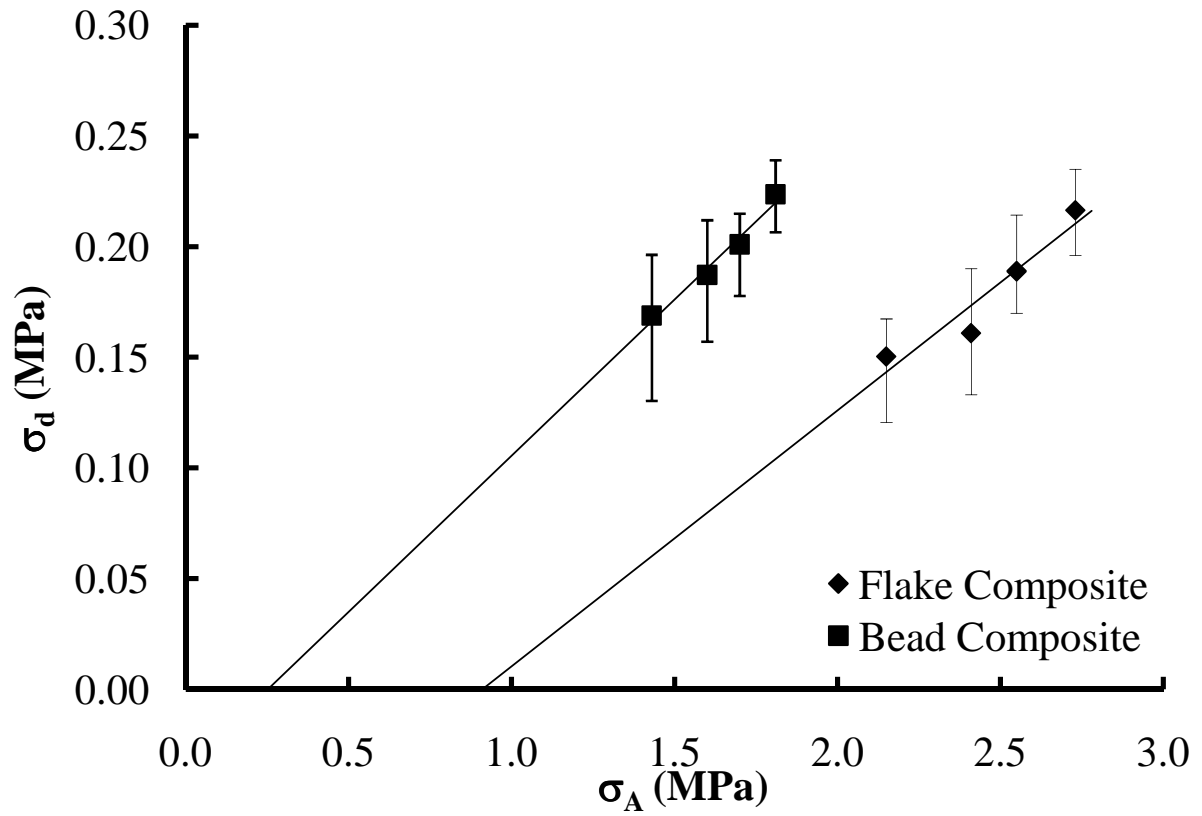


Figure 27: Debonding stress as a function of adhesive stress for the flake-filled and bead-filled composites.

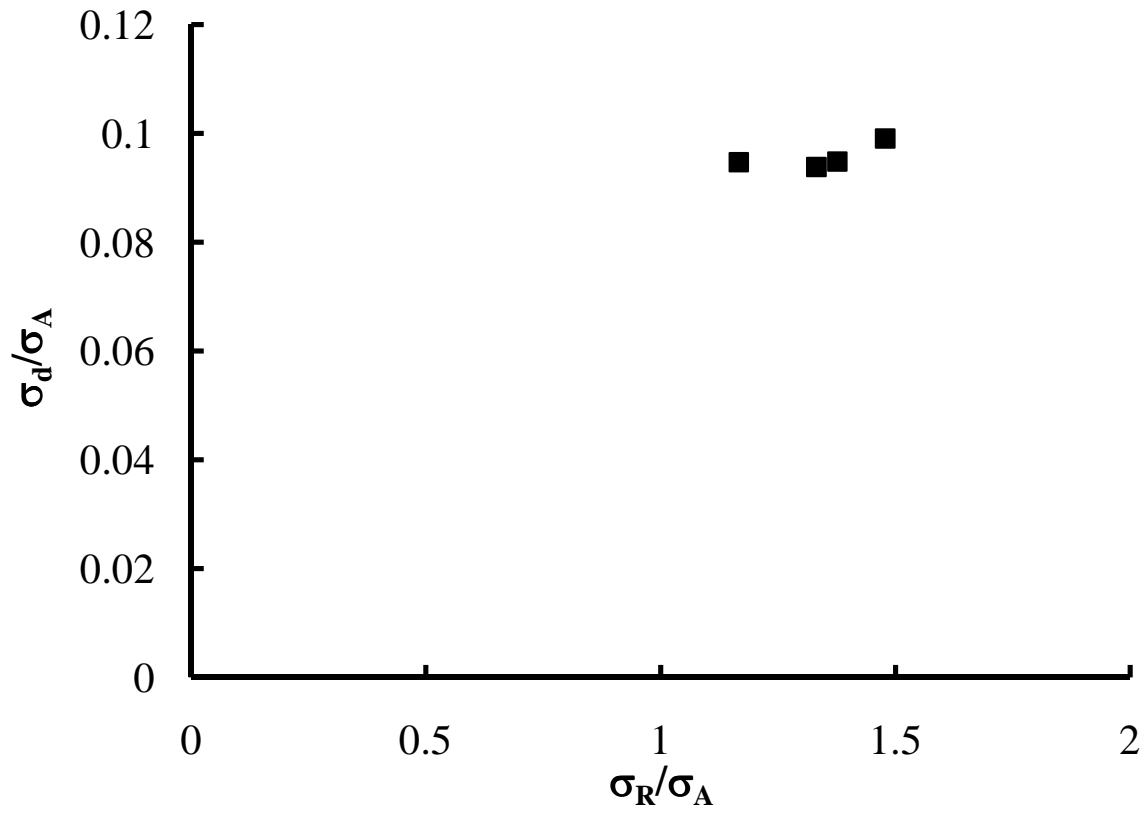


Figure 28: Relationship among residual, adhesive, and debonding stresses for the bead-filled composite.

5. Summary

One objective of this work was to investigate the temperature dependence of the stress-strain curves of neat polypropylene and two polypropylene composites, one containing glass flakes and one containing glass beads. This is important because die drawing takes place at elevated temperatures just below the melting point of the polymer. This was done by comparing stress-strain curves from tests done at 23°C, 130°C, and 145°C for the three materials. Comparison of stress-strain curves for the composites to those for neat PP and calculated fully bonded and fully debonded curves indicated that the onset of debonding occurs at a lower stress and strain for higher temperatures than for lower temperatures, but that the loss of reinforcement proceeds more slowly at elevated temperatures with the slowest progression seen at 130°C for both composites. This type of comparison also showed that the loss of reinforcement proceeded more slowly for the flake composite than for the bead composite when the two composites were compared at a given temperature. Additionally, interfacial interaction between the filler and matrix in both composites, characterized by the constant B_{int} , was shown to be much greater at the higher temperatures of 130°C and 145°C than at 23°C.

Temperature was also shown to affect the behavior of neat PP samples differently than glass flake and glass bead composite samples. Although increasing temperature had the expected results of decreasing the modulus and yield stress and increasing the yield strain of all three materials tested, the overall character of the curves was affected differently for the neat PP than for the composites. The general shape of the stress strain curves was the same at 23°C, 130°C, and 145°C for the neat PP, with a broad neck region followed by a neck propagation region. However, for both composite samples at 23°C, no neck region was noticed, while at 130°C and 145°C, there was a very sharp neck region followed by the neck propagation region. The strain at

the onset of the neck propagation region for the neat PP was nearly twice that for the two composites.

Additionally, DSC results showed that increasing the annealing temperature from 130°C to 145°C increased the prominence of the lower melting point peak. The increased prominence of this peak was greater for the two composite samples than for the neat PP. Calculation of the percent crystallinity from the DSC curves indicated that the presence of filler particles allowed for more recrystallization during annealing for the composites than for the neat PP.

Finally, debonding was studied by measuring transverse strain during tensile tests at temperatures of 130°C, 135°C, 140°C, and 145°C for the glass flake composite and the glass bead composite. This allowed for determination of the effect of temperature on debonding as well as the effect of the filler shape. The onset of debonding in both composites was identified by a kink in transverse strain vs. stress curves from tensile tests. Calculated adhesive stress in the two composites was an order of magnitude larger than the stress required for debonding, indicating that there is residual stress in the composites, even at elevated temperatures. Residual stress calculations for the glass bead composite confirm that the residual stress is of the same order of magnitude as the adhesive stress. Comparison of the debonding stress to the adhesive stress for the two composites indicates that the residual stress must be greater for the flake filled composite, and that the stress amplification at the particle-matrix interface is greater for the flake composite than for the bead composite.

APPENDICES

Appendix A – Calculation of residual stress in bead filled composites

Residual stresses in the matrix at the interface with a filler particle may be calculated with the following equations for a composite with spherical fillers, detailed in Hsueh (85), and Hsueh and Becher (86). A schematic representation of the model used for the equations is shown in Figure 29.

In a semicrystalline polymer, the residual stress has contributions from thermal shrinkage due to cooling a sample from its processing temperature to room temperature, as occurs during injection molding, and from crystalline shrinkage due to the formation of crystals. This is shown in Equation 17.

$$\sigma_R = \sigma_{R,thermal} + \sigma_{R,crystalline} \quad (17)$$

Where σ_R is the residual stress, $\sigma_{R,thermal}$ is the residual stress due to thermal shrinkage, and $\sigma_{R,crystalline}$ is the residual stress due to the formation of crystals. If the strain in the sample is caused by thermal shrinkage, it is given by Equation 18.

$$\varepsilon_m - \varepsilon_p = (\alpha_m - \alpha_p) \Delta T \quad (18)$$

Where ε is the strain, α is the coefficient of thermal expansion, ΔT is the temperature change over which the thermal shrinkage took place, and the subscripts m and p refer to the matrix and particle, respectively. If the strain in the sample is caused by crystal formation, it is given by Equation 19.

$$\varepsilon_m - \varepsilon_p = \frac{\chi}{3} \left(\frac{\rho_a}{\rho_c} - 1 \right) \quad (19)$$

Where χ is the crystalline fraction of the sample, ρ is the density, and the subscripts a and c refer to the amorphous and crystalline portions of the matrix, respectively. Although the quantity ρ_a/ρ_c is expected to change with temperature, this change is negligible over the range of temperatures used in this study (25). The values for the crystalline and amorphous densities are taken as 0.95 and 0.85, respectively (88).

For a composite with spherical fillers, the residual stress in the matrix at the interface ($r=a$) is given by Equation 20.

$$\sigma_R = -\frac{S}{2} \left(\frac{2\phi + 1}{1 - \phi} \right) \quad (20)$$

Where, ϕ is the volume fraction of the filler particles, given by Equation 21, and S is the mean normal stress inside the inclusion, and is given by Equation 22.

$$\phi = \left(\frac{a}{b} \right)^3 \quad (21)$$

where a is the radius of the particle, and b is the radius of the cell, as shown in Figure 29.

$$S = \frac{[\varepsilon_m - \varepsilon_p]}{\left(\frac{1}{3K_p} + \frac{1}{4G_m} \frac{1}{1-\phi} + \frac{1}{3K_m} \frac{\phi}{1-\phi} \right)} \quad (22)$$

Where K is the bulk modulus, as given in Equation 23, and G is the shear modulus, as given in Equation 24. In Equations 23 and 24, E is the tensile modulus, and ν is the Poisson's ratio.

$$K = \frac{E}{3(1-2\nu)} \quad (23)$$

$$G = \frac{E}{2(1+\nu)} \quad (24)$$

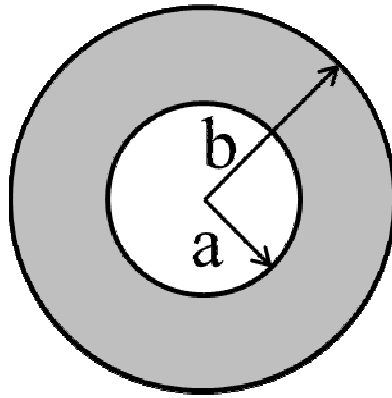


Figure 29: Schematic of model system used for residual stress calculations for spherical fillers.

Appendix B – SEM micrographs for samples quenched in the linear elastic regime at low strain rate

After testing in a tensile frame, the pattern of debonding around particulate fillers is notably different between bead filled composites and flake filled composites. Specifically, in flake filled composites, debonding occurs all around the particle, as shown in Figure 30, where a glass flake particle is debonded from the polypropylene matrix around all visible edges. This image is from a sample that was stretched to 0.3% axial strain at 150°C. Figure 30 also shows that the orientation of the flake particle does not affect the portion of the particle that debonds. Thus, regardless of the orientation, the debonded surface area to volume ratio, $\Delta S_d/\Delta V_d$, is the same. In this case, ΔS_d is equal to twice the particle's debonded surface area.

In comparison, in bead filled composites, debonding occurs at the poles of the particle in the stretch direction, as shown in Figure 31, where a glass bead is debonded from the polypropylene matrix at the horizontal poles of the particle, but remains bonded at the vertical poles of the particle. This image is from a sample that was stretched to 0.3% axial strain at 150°C. Figure 31 shows that the largest particle, in the center of the image, has a debonded region 40° from the pole. This is within reason from known values from room temperature tests (38).

Renner et al. (41) have stated that at room temperature, debonding cannot be seen in SEM images for samples that have not been stretched beyond the yield strain due to relaxation after removal from the test frame. Figure 30 and Figure 31 are well below the yield strain, yet debonding is clearly seen. This is likely due to the technique used after stretching, where the samples were quickly cooled to below room temperature before removing them from the test frame, which prevented relaxation.

Strikingly, this pattern persists even at higher levels of strain. Tensile tests were stopped at larger strains in order to determine how the morphology changed with increasing strain. Figure 32 shows a fracture surface of a glass flake composite sample that was stretched to 1% strain. In this image, the largest flakes are again debonded along planes at all angles relative to the stretch direction. Conversely, Figure 33 shows a glass bead composite sample which was stretched to 5% strain. Even when stretched to five times higher strain, the bead fillers are not debonded all around, which is in agreement with previous literature for bead filled composites at room temperature (38; 39; 47; 48; 50). Figure 33 shows that at 5% strain, the debonded region encompasses up to 50° from the pole.

Figure 30 and Figure 32 indicate that the extent of debonding, or debonded area, does not progress much with increasing strain from 0.3% to 1% for the flake filled composite, because the entire surface debonds initially. Figure 31 and Figure 33, however, show that the debonded area does increase for the bead filled composite with increasing strain from 0.3% to 5%, which agrees with published room temperature data (38; 39; 37; 47; 49). Figure 31 and Figure 33 also show an interesting phenomenon not previously discussed in literature. The bead filler particles do not always debond symmetrically. In some cases, both poles are debonded, while other particles show debonding at only one pole. This is observed in some SEM images from literature (60; 62; 66), specifically for strains well beyond the yield strain (62; 66). In some cases, debonding is observed at both poles of a spherical particle, but is clearly more pronounced at one pole (60), while other images in the literature (41; 47) show symmetric debonding around the spherical particles. This observation could be due to geometric irregularities of the spherical particles, which could act as stress concentrators. This asymmetry is not seen in the flake filled composite,

which could be due to the greater surface roughness observed for the flake filler, which could concentrate stress in more locations, thereby causing more of the surface area to debond.

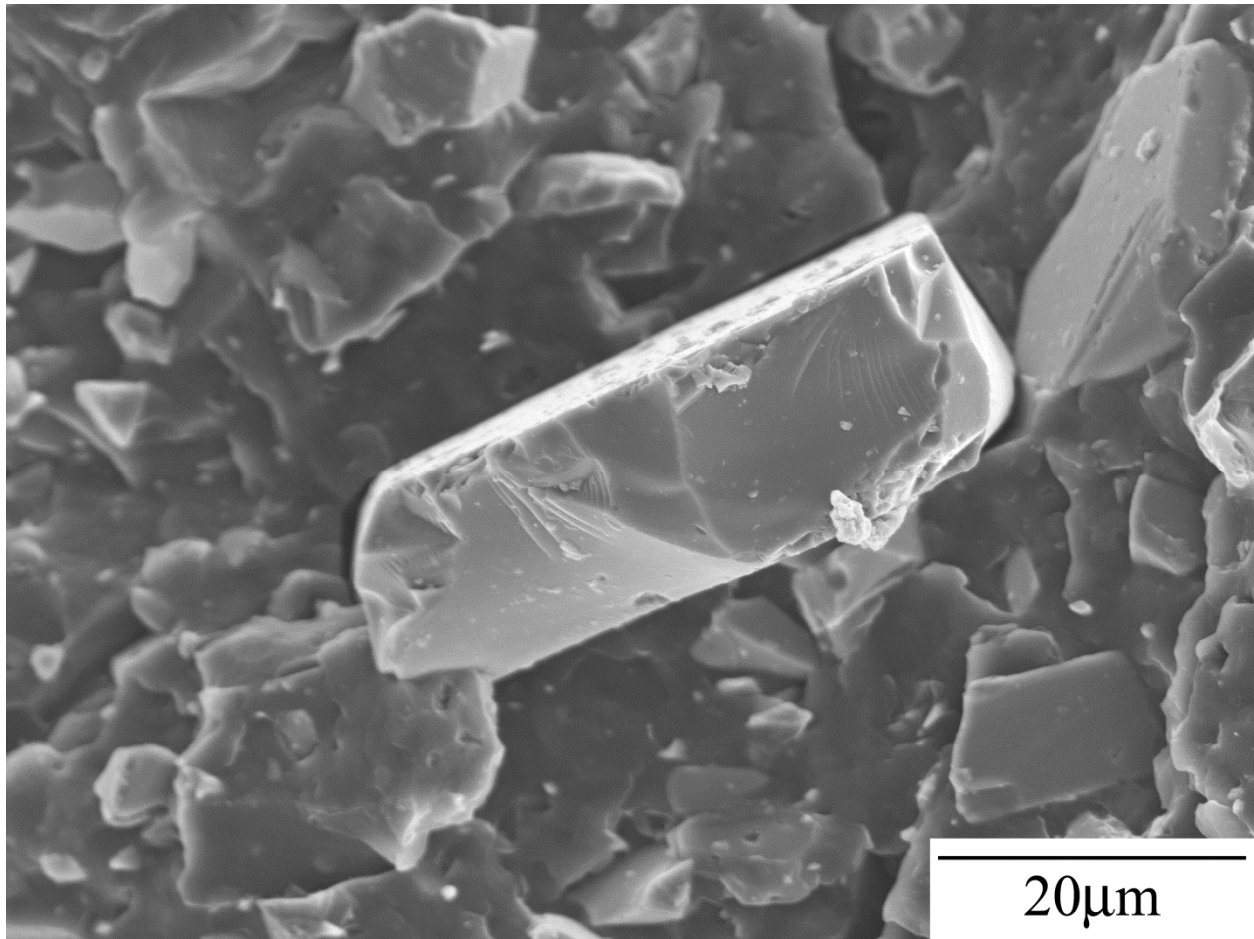


Figure 30: SEM image of a fracture surface of a glass flake-filled polypropylene composite that was stretched to 0.3% axial strain at 150°C.

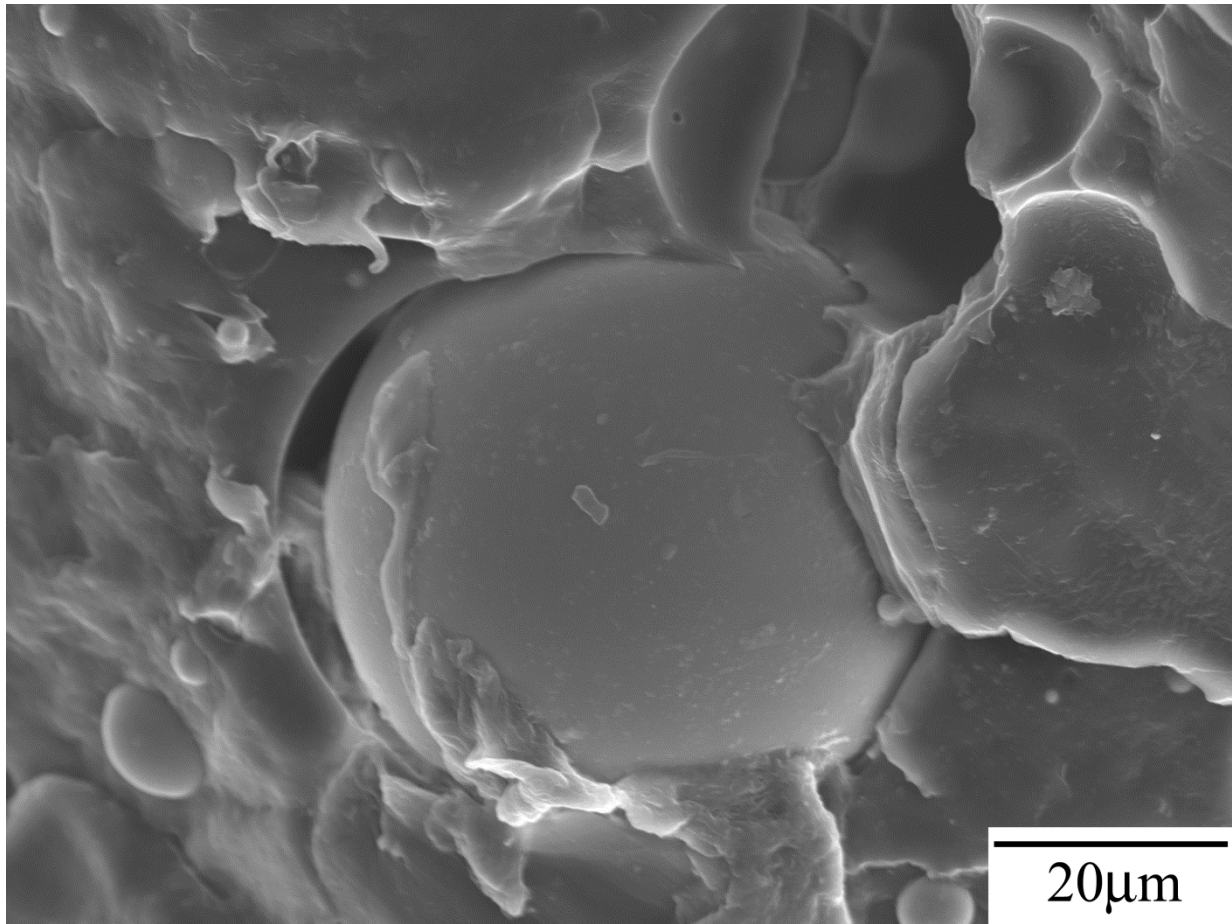


Figure 31: SEM image of a fracture surface of a glass bead-filled polypropylene composite that was stretched to 0.3% axial strain at 150°C.

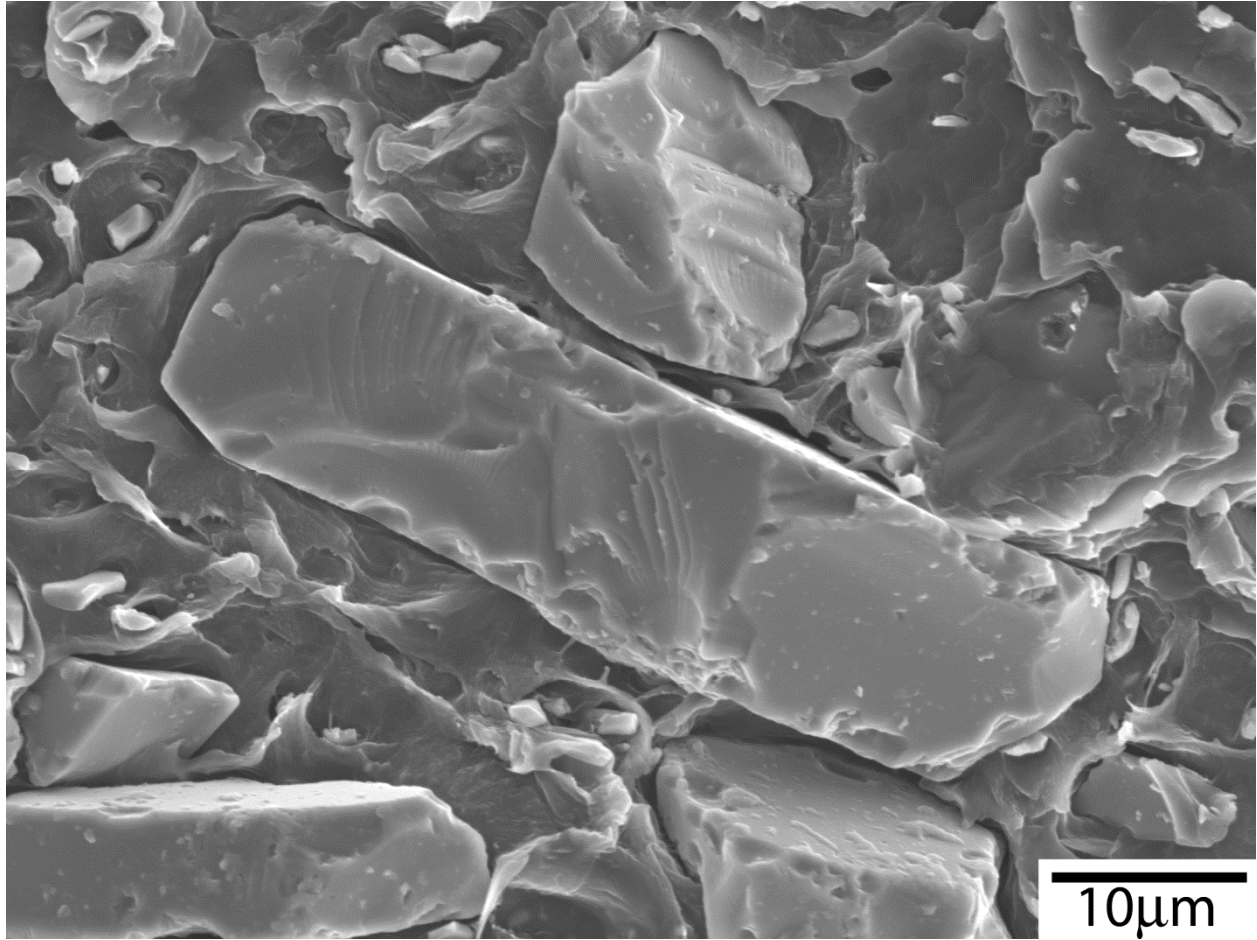


Figure 32: SEM image of a fracture surface of a glass flake composite sample stretched to 1% axial strain at 150°C.

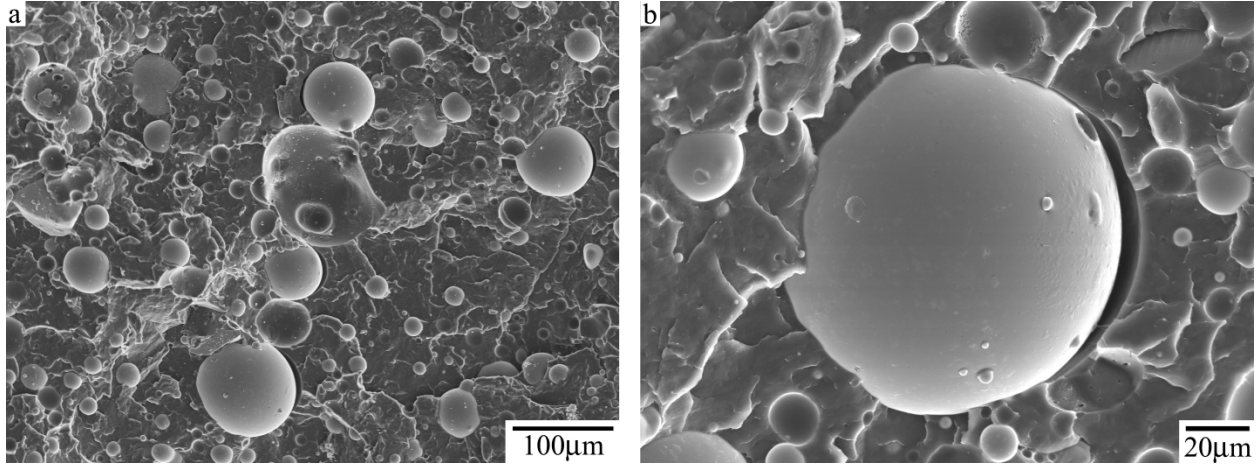


Figure 33: SEM images of a fracture surface of a glass bead composite sample stretched to 5% strain at 150°C at (a) low magnification, and (b) higher magnification.

Appendix C – SEM micrographs for samples quenched at higher strain at varying strain rates

A study was done on the effect of strain rate on voiding and void growth in the glass bead-filled composite. In this study, samples of the glass bead-filled composite were stretched at 150°C with crosshead speeds of 0.2 in/min, 5 in/min, and 20 in/min. For this composite, higher strain rates lead to more debonded particles than lower strain rates when compared at 5% strain. This is shown in Figure 34-Figure 36.

For the glass bead composite, samples stretched at 0.2 in/min not only show fewer debonded particles at 5% strain than those stretched at 20 in/min, the voids are also smaller at the lower strain rate. This shows that higher strain rates lead to more void growth at the same strain than lower strain rates. This is shown by comparison of Figure 37 and Figure 38.

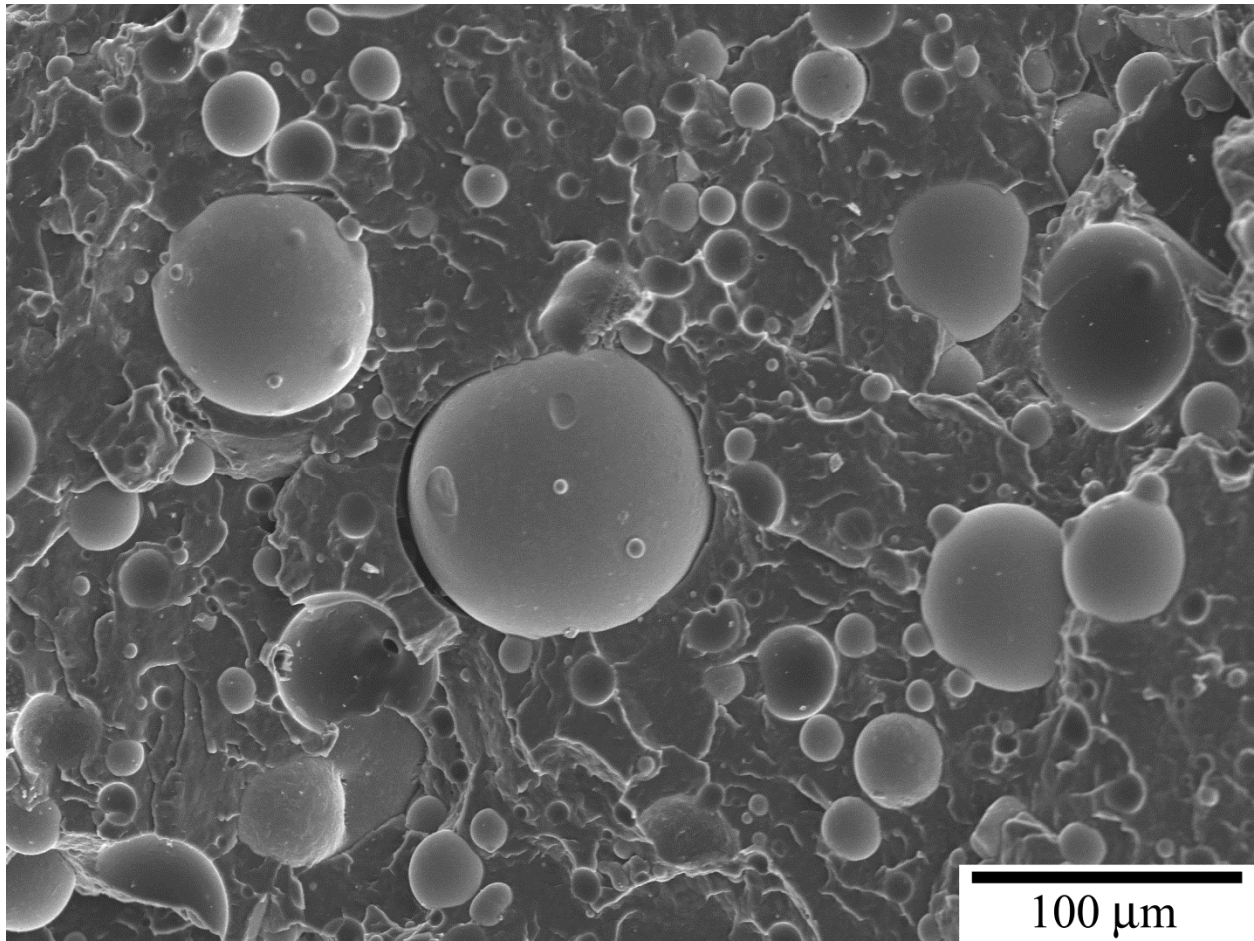


Figure 34: SEM image of bead composite sample stretched to 5% strain at 0.2in/min at 150°C.

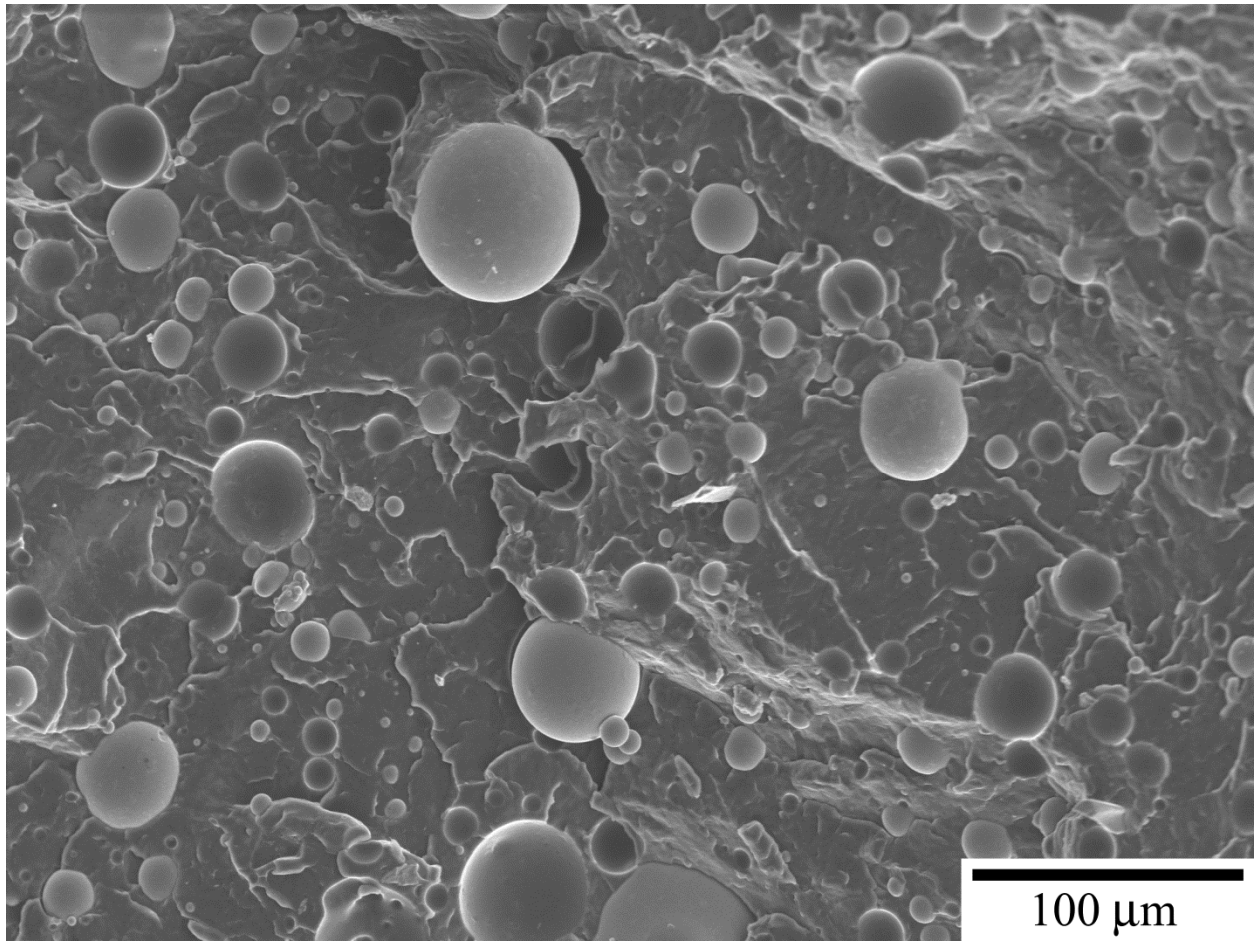


Figure 35: SEM image of bead composite sample stretched to 5% strain at 5in/min at 150°C.

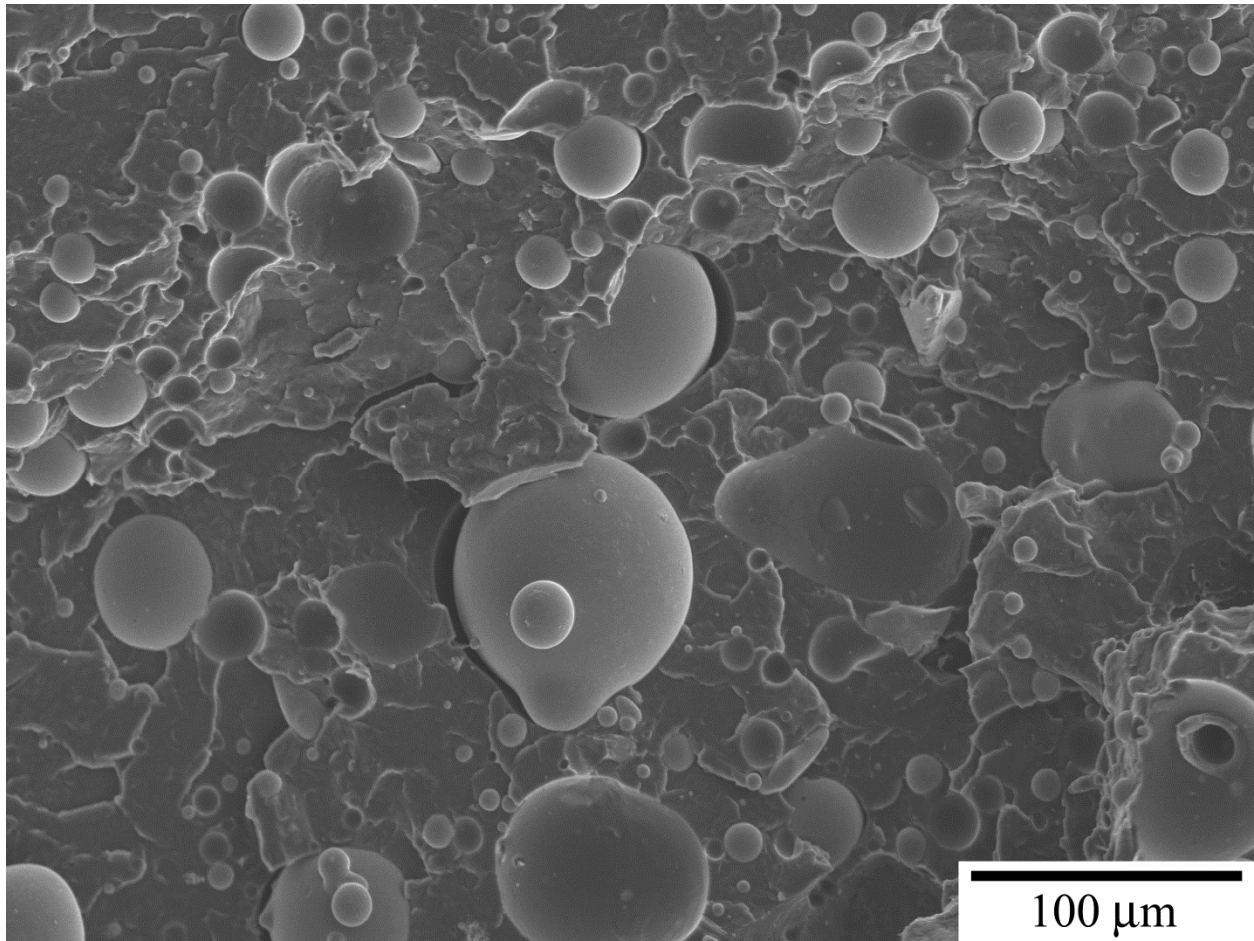


Figure 36: SEM image of bead composite sample stretched to 5% strain at 20in/min at 150°C.

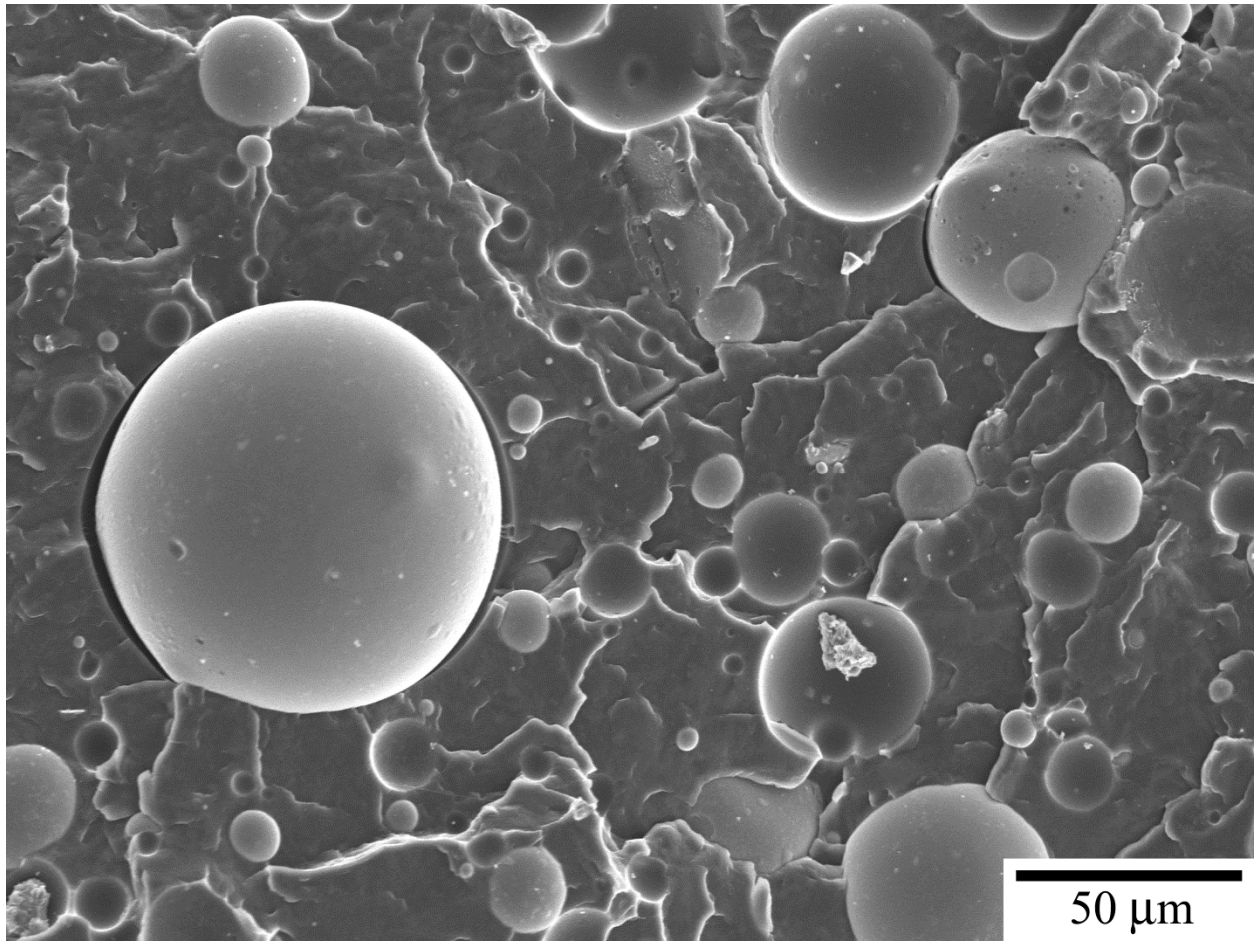


Figure 37: 500x magnification SEM image of bead composite sample stretched to 5% strain at 0.2in/min at 150°C.

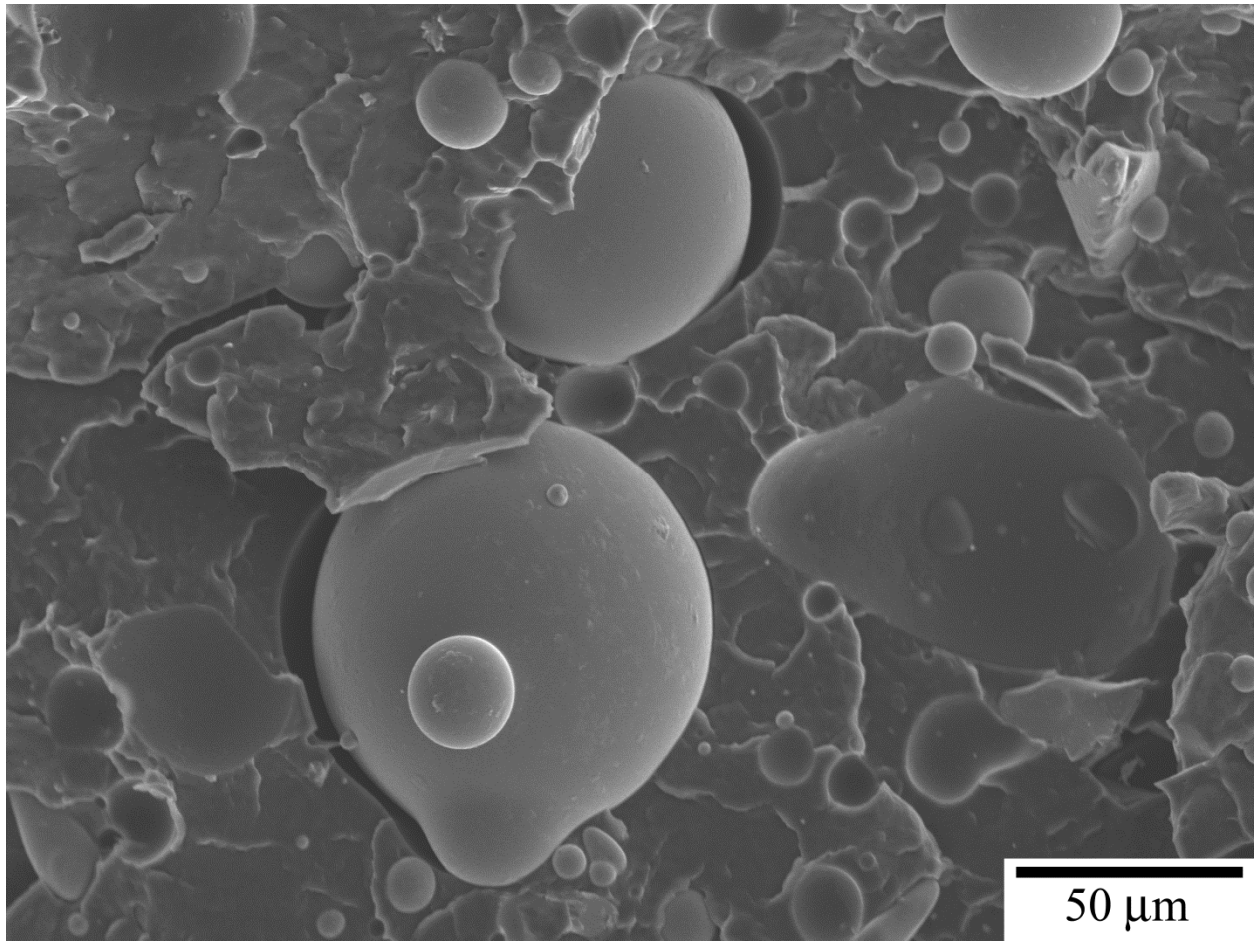


Figure 38: 500x magnification SEM image of bead composite sample stretched to 5% strain at 20in/min at 150°C.

REFERENCES

REFERENCES

1. **Ward, I M, Taraiya, A K and Coates, P D.** Solid State Extrusion and Die Drawing. [ed.] I M Ward, P D Coates and M M Dumoulin. *Solid State Processing of Polymers*. Munich : Hanser Publishers, 2000, 9, pp. 328-367.
2. **Weeks, N E and Porter, R S.** Mechanical properties of ultra-oriented polyethylene. *Journal of Polymer Science: Polymer Physics Edition*. 1974, Vol. 12, pp. 635-643.
3. **Capiati, N J and Porter, R S.** Tensile Properties of Ultradrawn Polyethylene. *Journal of Polymer Science: Polymer Physics Edition*. 1975, Vol. 13, pp. 1177-1186.
4. **Southern, J H, et al., et al.** Unique polyethylene morphologies produced under extrusion conditions. *Die Makromolekulare Chemie*. 1972, Vol. 162, pp. 19-30.
5. **Hope, P S, Richardson, A and Ward, I M.** Manufacture of ultrahigh-modulus poly(oxymethylenes) by die drawing. *Journal of Applied Polymer Science*. 1981, Vol. 26, pp. 2879-2896.
6. —. The hydrostatic extrusion and die-drawing of glass-fiber-reinforced polyoxymethylene. *Polymer Engineering and Science*. 1982, Vol. 22, pp. 307-313.
7. **Bao, S P and Tjong, S C.** Mechanical behaviors of polypropylene/carbon nanotube nanocomposites: the effects of loading rate and temperature. *Materials Science and Engineering A*. 2008, Vol. 485, pp. 508-516.
8. **Amoedo, J and Lee, D.** Modeling the uniaxial rate and temperature dependent behavior of amorphous and semicrystalline polymers. *Polymer Engineering and Science*. 1992, Vol. 32, pp. 1055-1065.
9. **Rettenberger, S, et al., et al.** Uniaxial deformation behavior of different polypropylene cast films at temperatures near the melting point. *Rheologica Acta*. 2002, Vol. 41, pp. 332-336.
10. **Drozdov, A D and Christiansen, J deC.** Effect of high-temperature annealing on the elastoplastic response of isotactic polypropylene in loading-unloading tests. *Journal of Applied Polymer Science*. 2003, Vol. 90, pp. 186-196.
11. —. The effect of annealing on the elastoplastic and viscoelastic responses of isotactic polypropylene. *Computational Materials Science*. 2003, Vol. 27, pp. 403-422.
12. **Koike, Y and Cakmak, M.** Real time development of structure in partially molten state stretching of PP as detected by spectral birefringence technique. *Polymer*. 2003, Vol. 44, pp. 4249-4260.

13. **Drozdov, A and Christiansen, J deC.** The effect of annealing on the time-dependent behavior of isotactic polypropylene at finite strains. *Polymer*. 2002, Vol. 43, pp. 4745-4761.
14. **Seguela, R, et al., et al.** Plastic deformation of polypropylene in relation to crystalline structure. *Journal of Applied Polymer Science*. 1999, Vol. 71, pp. 1873-1885.
15. **Drozdov, A D and Christiansen, J deC.** The effect of annealing on the viscoplastic response of semicrystalline polymers at finite strains. *International Journal of Solids and Structures*. 2003, Vol. 40, pp. 1337-1367.
16. **Saengsuwan, Sayant.** Influence of annealing on microstructure and molecular orientation, thermal behaviour, mechanical properties and their correlations of uniaxially drawn iPP thin film. *e-Polymers*. 2008, 113.
17. **Tortorella, N and Beatty, C L.** Morphology and crystalline properties of impact-modified polypropylene blends. *Polymer Engineering and Science*. 2008, Vol. 48, pp. 1476-1486.
18. **Iijima, M and Strobl, G.** Isothermal crystallization and melting of isotactic polypropylene analyzed by time- and temperature-dependent small-angle x-ray scattering experiments. *Macromolecules*. 2000, Vol. 33, pp. 5204-5214.
19. **Aboulfaraj, M, et al., et al.** Spherulitic morphology of isotactic polypropylene investigated by scanning electron microscopy. *Polymer*. 1993, Vol. 34, pp. 4817-4825.
20. **Drozdov, A D and Christiansen, J deC.** The effect of annealing on the elastoplastic response of isotactic polypropylene. *European Polymer Journal*. 2003, Vol. 39, pp. 21-31.
21. **Hedesiu, C, et al., et al.** Effect of temperature and annealing on the phase composition, molecular mobility, and the thickness of domains in isotactic polypropylene studied by proton solid-state NMR, SAXS, and DSC. *Macromolecules*. 2007, Vol. 40, pp. 3977-3989.
22. **Mileva, D, Androsch, R and Radusch, H-J.** Effect of structure on light transmission in isotactic polypropylene and random propylene-1-butene copolymers. *Polymer Bulletin*. 2009, Vol. 62, pp. 561-571.
23. **Maiti, P, et al., et al.** Lamellar thickening in isotactic polypropylene with high tacticity crystallized at high temperature. *Macromolecules*. 2000, Vol. 33, pp. 9069-9075.
24. **Poussin, L, et al., et al.** Influence of thermal treatment on the structure of an isotactic polypropylene. *Polymer*. 1998, Vol. 39, pp. 4261-4265.
25. **Albrecht, T and Strobl, G.** Temperature-dependent crystalline-amorphous structures in isotactic polypropylene: small-angle x-ray scattering analysis of edge-bonded two-phase systems. *Macromolecules*. 1995, Vol. 28, pp. 5267-5273.

26. **Gu, F, et al., et al.** Second-order phase transition of high isotactic polypropylene at high temperature. *Polymer*. 2002, Vol. 43, pp. 1473-1481.
27. **Dudic, D, Djokovic, D and Kostoski, D.** The high temperature secondary crystallisation of aged isotactic polypropylene. *Polymer Testing*. 2004, Vol. 23, pp. 621-627.
28. **Al-Raheil, I A, Qudah, A M and Al-Share, M.** Isotactic polypropylene crystallized from the melt. 2. Thermal melting behavior. *Journal of Applied Polymer Science*. 1998, Vol. 67, pp. 1267-1271.
29. **Faulkner, D L and Schmidt, L R.** Glass bead filled polypropylene. Part 1: Rheological and Mechanical Properties. *Polymer Engineering and Science*. 1977, Vol. 17, pp. 657-665.
30. **Tsui, C P, Tang, C Y and Lee, T C.** Tensile properties and damage behaviors of glass-bead-filled modified polyphenylene oxide under large strain. *Polymer Composites*. 2001, Vol. 22, pp. 742-751.
31. **Yuan, Q, et al., et al.** Nonisothermal crystallization behavior of glass-bead-filled polypropylene. *Journal of Applied Polymer Science*. 2006, Vol. 102, pp. 2026-2033.
32. **Arroyo, M, Lopez-Manchado, M A and Avalos, F.** Crystallization kinetics of polypropylene: 2. Effect of the addition of short lass fibres. *Polymer*. 1997, Vol. 38, pp. 5587-5593.
33. **Huson, M G and McGill, W J.** Transcrystallinity in polypropylene. *Journal of Polymer Science: Polymer Chemistry Edition*. 1984, Vol. 22, pp. 3571-3580.
34. **Varga, J and Karger-Kocsis, J.** Interfacial morphologies in carbon fibre-reinforced polypropylene microcomposites. *Polymer*. 1995, Vol. 36, pp. 4877-4881.
35. **Shaner, J R and Corneliussen, R D.** Transcrystalline growth at an internal surface. *Journal of Polymer Science Part A-2: Polymer Physics*. 1972, Vol. 10, pp. 1611-1613.
36. **Quan, H, et al., et al.** On transcrystallinity in semi-crystalline polymer composites. *Composites Science and Technology*. 2005, Vol. 65, pp. 999-1021.
37. **Gent, A N and Park, B.** Failure processes in elastomers at or near a rigid spherical inclusion. *Journal of Materials Science*. 1984, Vol. 19, pp. 1947-1956.
38. **Dekkers, M E J and Heikens, D.** The effect of interfacial adhesion on the mechanism for craze formation in polystyrene-glass bead composites. *Journal of Materials Science*. 1983, Vol. 18, pp. 3281-3287.
39. **Vollenberg, P, Heikens, D and Ladan, H C B.** Experimental determination of thermal and adhesion stress in particle filled thermoplasts. *Polymer Composites*. 1988, Vol. 9, pp. 382-388.

40. **Pukanszky, B and Voros, G.** Mechanism of interfacial interactions in particulate filled composites. *Composite Interfaces*. 1993, Vol. 1, pp. 411-427.
41. **Renner, K, et al., et al.** Analysis of the debonding process in polypropylene model composites. *European Polymer Journal*. 2005, Vol. 41, pp. 2520-2529.
42. **Pukanszky, B, et al., et al.** Micromechanical deformations in particulate filled thermoplastics: volume strain measurements. *Journal of Materials Science*. 1994, Vol. 29, pp. 2350-2358.
43. **Harding, P H, et al., et al.** Measurement of residual stress effects by means of single-particle composite tests. *Journal of Adhesion Science and Technology*. 1998, Vol. 12, pp. 497-506.
44. **Pukanszky, B and Voros, G.** Stress distribution around inclusions, interaction, and mechanical properties of particulate-filled composites. *Polymer Composites*. 1996, Vol. 17, pp. 384-392.
45. **Vratsanos, L A and Farris, R J.** A predictive model for the mechanical behavior of particulate composites. Part 1: Model derivation. *Polymer Engineering and Science*. 1993, Vol. 33, pp. 1458-1465.
46. —. A predictive model for the mechanical behavior of particulate composites. Part 2: Comparison of model predictions to literature data. *Polymer Engineering and Science*. 1993, Vol. 33, pp. 1466-1474.
47. **Zhuk, A V, et al., et al.** Debonding microprocesses and interfacial strength in particle-filled polymer materials. *Journal of Materials Science*. 1993, Vol. 28, pp. 4595-4606.
48. **Meddad, A and Fisa, B.** Filler matrix debonding in glass bead-filled polystyrene. *Journal of Materials Science*. 1997, Vol. 32, pp. 1177-1185.
49. **Gent, A N and Hwang, Y -C.** Internal failures in model elastomeric composites. *Journal of Materials Science*. 1990, Vol. 25, pp. 4981-4986.
50. **Ghassemieh, E.** Micro-mechanical analysis of bonding failure in a particle-filled composite. *Composites Science and Technology*. 2002, Vol. 62, pp. 67-82.
51. **McCrum, N G, Buckley, C P and Bucknall, C B.** *Principles of Polymer Engineering*. Oxford : Oxford University Press, 1997.
52. **Piggott, M R.** Debonding and friction at fibre-polymer interfaces. 1: Criteria for failure and sliding. *Composites Science and Technology*. 1987, Vol. 30, pp. 295-306.

53. **Piggott, M R and Dai, S R.** Debonding and friction at fibre-polymer interfaces. 2: Macroscopic model experiments. *Composites Science and Technology*. 1988, Vol. 31, pp. 15-24.
54. **Piggott, M R.** Failure processes in the fibre-polymer interphase. *Composites Science and Technology*. 1991, Vol. 42, pp. 57-76.
55. **Dekkers, M E J and Heikens, D.** The effect of interfacial adhesion on the tensile behavior of polystyrene-glass-bead composites. *Journal of Applied Polymer Science*. 1983, Vol. 28, pp. 3809-3815.
56. **Sudar, A, et al., et al.** The mechanism and kinetics of void formation and growth in particulate filled PE composites. *eXPRESS Polymer Letters*. 2007, Vol. 1, pp. 763-772.
57. **Anderson, L L and Farris, R J.** A predictive model for the mechanical behavior of particulate composites. *Polymer Engineering and Science*. 1988, Vol. 28, pp. 522-528.
58. **Meddad, A and Fisa, B.** A model for filler-matrix debonding in glass-bead-filled viscoelastic polymers. *Journal of Applied Polymer Science*. 1997, Vol. 65, pp. 2031-2024.
59. **Wong, F C and Ait-kadi, A.** Mechanical behavior of particulate composites: experiments and micromechanical predictions. *Journal of Applied Polymer Science*. 1995, Vol. 55, pp. 263-278.
60. **Meddad, A and Fisa, B.** Stress-strain behavior and tensile dilatometry of glass bead-filled polypropylene and polyamide 6. *Journal of Applied Polymer Science*. 1997, Vol. 64, pp. 653-665.
61. **Dubnikova, I L, Muravin, D K and Oshmyan, V G.** Debonding and fracture of particulate-filled isotactic polypropylene. *Polymer Engineering and Science*. 1997, Vol. 37, pp. 1301-1313.
62. **Sjogren, B A and Berglund, L A.** Failure mechanisms in polypropylene with glass beads. *Polymer Composites*. 1997, Vol. 18, pp. 1-8.
63. **Asp, L E, Sjogren, B A and Berglund, L A.** Prediction of failure initiation in polypropylene with glass beads. *Polymer Composites*. 1997, Vol. 18, pp. 9-15.
64. **Piggott, M R.** *Load Bearing Fibre Composites*. Oxford : Pergamon Press, 1980. Chapter 8.
65. **Naqui, S I and Robinson, I M.** Tensile dilatometric studies of deformation in polymeric materials and their composites. *Journal of Materials Science*. 1993, Vol. 28, pp. 1421-1429.
66. **Bai, S-L, et al., et al.** The role of the interfacial strength in glass bead filled HDPE. *Journal of Materials Science Letters*. 2000, Vol. 19, pp. 1587-1589.
67. **Standard, ASTM.** Standard test method for tensile properties of plastics. West Conshohocken, PA : ASTM International, 2010. ASTM D638-03.

68. **Callister, Jr., W D.** *Materials Science and Engineering: An Introduction*. Sixth. New York : John Wiley and Sons, 2003.
69. **University of Cambridge.** *Dissemination of IT for the Promotion of Materials Science (DoITPoMS)*. [Online] 2010. [Cited: August 18, 2011.] <http://www.doitpoms.ac.uk/tlplib/polymers/stress-strain.php>.
70. **Duan, Y, Saigal, A and Greif, R.** A uniform phenomenological constitutive model for glassy and semicrystalline polymers. *Polymer Engineering and Science*. 2001, Vol. 41, pp. 1322-1328.
71. **Zhou, Y, et al., et al.** Experimental study on thermal and mechanical behavior of polypropylene, talc/polypropylene and polypropylene/clay nanocomposites. *Materials Science and Engineering A*. 2005, Vol. 402, pp. 109-117.
72. **Turcsanyi, B, Pukanszky, B and Tudos, F.** Composition dependence of tensile yield stress in filled polymers. *Journal of Materials Science Letters*. 1988, Vol. 7, pp. 160-162.
73. **Pukanszky, B.** Influence of interface interaction on the ultimate tensile properties of polymer composites. *Composites*. 1990, Vol. 21, pp. 255-262.
74. **Liang, J-Z.** Toughening and reinforcing in rigid inorganic particulate filled poly(propylene): A review. *Journal of Applied Polymer Science*. 2002, Vol. 83, pp. 1547-1555.
75. **Kwok, K W, et al., et al.** Stiffness and toughness of polypropylene/glass bead composites. *Polymer Composites*. 2003, Vol. 24, pp. 53-59.
76. **Fu, S-Y, et al., et al.** Effects of particle size, particle/matrix interface adhesion and particle loading on mechanical properties of particulate-polymer composites. *Composites: Part B*. 2008, Vol. 39, pp. 933-961.
77. **Danyadi, L, Moczo, J and Pukanszky, B.** Effect of various surface modifications of wood flour on the properties of PP/wood composites. *Composites: Part A*. 2010, Vol. 41, pp. 199-206.
78. **ASM International.** *Characterization and Failure Analysis of Plastics*. Materials Park : ASM International, 2003. pp. 404-416. Fracture and Fractography.
79. **Liu, Y, et al., et al.** Characterization of stress-whitening of tensile yielded isotactic polypropylene. *Polymer*. 1997, Vol. 38, pp. 2797-2805.
80. **Pae, K D, et al., et al.** Healing of stress-whitening in polyethylene and polypropylene at or below room temperature. *Polymer Engineering and Science*. 2000, Vol. 40, pp. 1783-1795.

81. **Sudduth, R D.** Influence of nanoscale fibres and discs on intrinsic modulus and packing fraction of polymeric particulate composites and suspensions. *Materials Science and Technology*. 2003, Vol. 19, pp. 1181-1190.
82. **Goyal, R K, Negi, Y S and Tiwari, A N.** Preparation of high performance composites based on aluminum nitride/poly(ether-ether-ketone) and their properties. *European Polymer Journal*. 2005, Vol. 41, pp. 2034-2044.
83. **Jang, B Z, Uhlmann, D R and Vander Sande, J B.** Rubber-toughening in polypropylene. *Journal of Applied Polymer Science*. 1985, Vol. 30, pp. 2485-2504.
84. **Yu, X, et al., et al.** Structure and property of injection-molded polypropylene along the flow direction. *Polymer Engineering and Science*. 2009, Vol. 49, pp. 703-712.
85. **Hsueh, C-H.** Sintering behaviour of powder compacts with multiheterogeneities. *Journal of Materials Science*. 1986, Vol. 21, pp. 2067-2072.
86. **Hsueh, C-H and Becher, P F.** Residual thermal stresses in ceramic composites. Part 1: with ellipsoidal inclusions. *Materials Science and Engineering*. 1996, Vol. A212, pp. 22-28.
87. **Pisanova, E, Dutschk, V and Lauke, B.** Work of adhesion and local bond strength in glass fibre-thermoplastic polymer systems. *Journal of Adhesion Science and Technology*. 1998, Vol. 12, pp. 305-322.
88. **van Krevelen, D W.** *Properties of Polymers*. 4th. Amsterdam : Elsevier, 2009. pp. 79-84.
89. **Gent, A N.** Detachment of an elastic matrix from a rigid spherical inclusion. *Journal of Materials Science*. 1980, Vol. 15, pp. 2884-2888.
90. **Miller, A C and Berg, J C.** Unexpected behavior between polystyrene and untreated and silane-treated glass beads in filled polymeric composites. *Journal of Applied Polymer Science*. 2003, Vol. 89, pp. 521-526.
91. **Di Landro, L and Pegoraro, M.** Evaluation of residual stresses and adhesion in polymer composites. *Composites Part A*. 1996, Vol. 27A, pp. 847-853.